Study on the Effects of Matrix Properties on the Mechanical Properties of Carbon Fiber Reinforced Plastic Composites

Doctoral Thesis

By

YONGZHENG SHAO

Supervised by Prof. Toru FUJII

Prof. Kazuya OKUBO

Doshisha University

2014

Thesis contents

Chapter 1. Background

1.1 Introduction

Carbon fiber reinforced plastic composite (CFRP) consists of two parts, which are a matrix and a reinforcement. First, the reinforcement is carbon fiber (CF) with a high strength or stiffness to weight ratio and low coefficient of thermal expansion. It is considered as one of most excellent materials in the world. CF has a diameter of 5-10μm and composes mostly of carbon atoms. It is stacked parallel by sheets of carbon atom arranging in a regular hexagonal pattern [1]. The atomic configuration of carbon chains and their connections determined the mechanical properties of CF. Continuous fibers and discontinuous fibers are usually used as reinforcement where continuous fibers can provide maximum achievable mechanical properties but costly. Discontinuous fibers are short fibers obtained by chopping continuous fiber or recycled fibers or produced directly as short fibers. Continuous fibers usually perform as textile reinforcement to increase mechanical performance and reduce manufacturing cost. The textile structures used comprehensively are yarn, tow, strand for 1D textile, woven fabrics like plain, twill and satin weave, and 3D textiles. The matrix also plays an important role in the structure of CFRP. It binds the reinforcement together to form desired shape of composites. It also transfers the load between constituents and shares the load such as transverse stress and shear stress at interfaces. Thermosetting resins such as epoxy, polyester or vinylester and thermoplastic resin such as nylon, polyether ether ketone (PEEK) or polyphenylene sulfide (PPS) are used as matrix commonly for CFRP. Thermosetting resins have low viscosity, which provide excellent impregnation of the reinforcement and easy/fast fabrication processing speeds. But the heat resistance due to low T_g and volumetric shrinkage during curing is still challenge. Thermoplastic resins process the high heat resistance property and high fracture toughness of thermoplastic resin which allows high damage tolerance of composites. Also the damage occurred under loading can be repaired by heating for several times. However, the high viscosity at processing temperate causes the fabrication process more difficult and some damage on reinforcement.

CFRPs perform unsurpassed high strength-weight and modulus-weight ratios (specific gravity is 1/4 of iron, specific strength is 10 times stronger than iron, modulus

of elasticity is 7 times than iron), good corrosion resistance (does not rust), good electrical conductivity, excellent radiolucency and flexible shape of final product. They have been widely used in the aerospace, sports, automobiles, marine and chemical industries. The Airbus A350 XWB has used 53% CFRP as primary/secondary structure including wing, fuselage and other structural components. And the Boeing 787 also is built of 50% CFRP. In the aerospace field, micro air vehicles, body of rocket, primary structure of satellites, the frame of solar panel also use CFRP positively. In the environment and energy-related industries, CFRP has already used as wind power blade, tube trailer tank, batter-charging flywheel, fuel cell, tidal power blade, electric cable core and so on. In the automobile field, CFRP has been tried to use as hood, roof, compressed natural gas tank, body, and propeller shaft for the vehicles. Lexus LFA, Toray concept EV "TEEWAVE" AR1, BMW i3 are examples. For the industrial use, CFRP can be used as robot hand for liquid crystal panel, body for high-speed train, X-ray top panel, PC housing, bridge pier reinforcement and so on. Moreover, CFRP has been used as fishing rod, bicycle frame, hockey stick, badminton racket, golf shaft, soft ball bar, boats in sports field. And more and more applications are under developing.

Since excellent properties of carbon fiber was recognized from 1990s, CFRP industry grew fast. According to marketing report of carbon fiber and CFRP [2-3], in 2012, global demand for carbon fiber was ～38,500 tonnes and ～43,500 tonnes in 2013. The theoretical total manufacture capacities of carbon fiber in the world have reached to ～107,700 tonnes. The demand of CFRP was ～65,000 tonnes in 2012, and ～74,000 tonnes in 2013. Due to increased demand in aerospace because of the successful application of CFRP on airplane (A350, B787), steady growth in sports field, significant increasing demand in industries contributed by applications related to environment and energy, the global demand of carbon fiber is possible to increase to ～68,000 tonnes in 2015 and ～130,000 tonnes by 2020 [Fig.1-1]. At the same time, the total manufacture capacities of carbon fiber is estimated to grow accordingly to ～123,300 tonnes by 2015. The companies such as Toray are expanding their capacities positively. In 2012, the volume segment of carbon fiber used in each application field was approximately 23% for wind turbines, 18% for aerospace and defence, 17% for sports/leisure, 12% for molding & compound, 6% for civil engineering, 5% for pressure vessel and 5% for automotive and other. In 2020, analysts estimates that the carbon fiber consumption in

wind turbines will rise to about 36,000 tonnes, 23,000 tonnes for aircraft, 12,000 tonnes for sports, and 23,000 tonnes for automotive. For the CFRP, the global demand is possible to expand to ～108,000 tonnes in 2015 and ～208,000 tonnes by 2020. Global sales of CFRPs forecast to reach $28.2 billion by 2015 and $48.7 billion by 2020. The development of CFRP market shows a large potential growth.

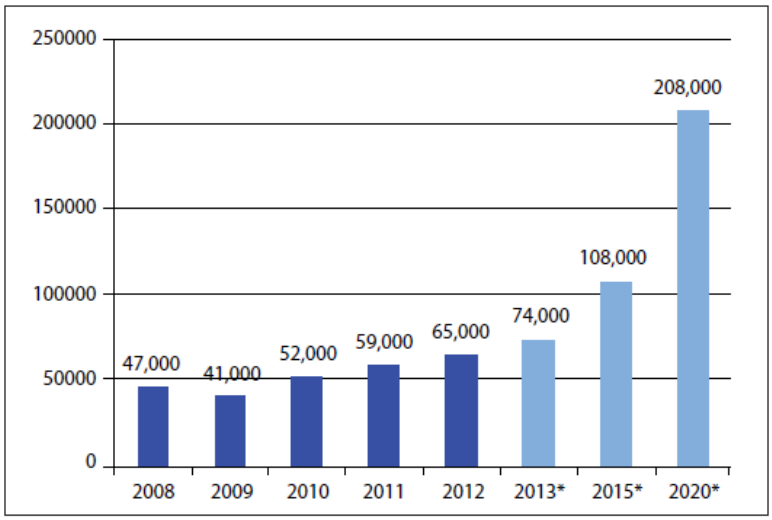

Fig.1-1. Global demand for CFRP in tonnes 2008-2020 (*estimated) [2].

CFRP performs excellent mechanical properties and has a prospective future. However, some limitations still exist. The major limitation is the cost due to high price of carbon fiber and fabrication process for application and so on. Although it can be balanced by the payoff achieved by weight saving especially in aerospace or automotive application, it is still difficult to show an economic advantage. The project such as the use of cheaper resin transfer molding (RTM) method to replace prepreg lay-up method (54% of total product in 2012), development of mass production to reduce the cost of carbon fiber, development of cheaper matrix resin is in progress. Another shortage is low impact resistance due to high rigidity and low toughness of carbon fiber, and low heat resistance due to low T_g of matrix. As increasing application of CFRP, the disposal of spent CFRP become urgent problems due to their difficulty to dispose. The recycling of carbon fiber from wasted or spent CFRP has attracted more and more attention. Reuse the recycled carbon fiber is also a new challenge. Some industrial applications that do not need 100% performance of carbon fiber or full length of carbon fiber are possible to use recycled carbon fibers.

1.2 Effect of matrix properties on the mechanical properties of CFRP (Chemical

modification)

According to rule of mixture (ROM) formula and the huge difference of the mechanical properties of reinforcement/matrix, the mechanical properties mainly depend on the mechanical properties of carbon fiber. Especially, the static modulus of CFRP can be predicted very well based on the modulus and volume fraction of carbon fiber. The mechanical properties of CFRP improve when using CF with high mechanical properties but not linearly due to other influence factors. However, the strength of CFRP reinforced by short fiber also largely relates to aspect ratio of carbon fiber [4]. The reinforcement form also shows the different effect. Long CF exhibits a better effect on reinforcing polymer than short CF. Fabric CFRP shows more sensitive to other factors such as matrix or interface than unidirectional CFRP due to existence of cross-over points. The mechanical properties of CFRP improve drastically with increasing the volume fraction of CF regardless of reinforcement form. Also the fiber orientation angle affects the mechanical properties significantly that decreases with increasing the angle (Fig.1-2). When it comes to 90° namely transverse direction, the mechanical properties especially the strength is influenced by interfacial shear stress and matrix stress significantly.

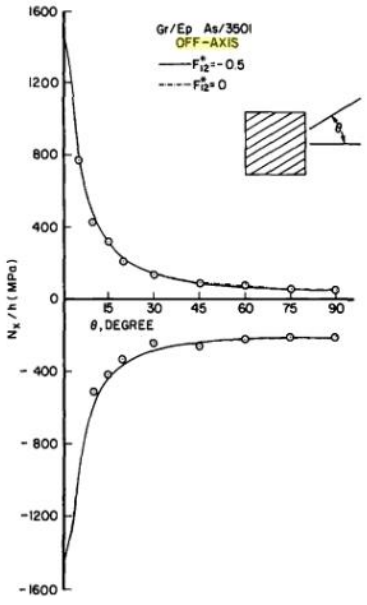

Fig.1−2.Tensile and compressive strengths of off-axis laminates as function of fiber orientation [5].

Matrixes not only carry some of load such as transverse stress, but also help transfer the load through the interface to carbon fibers. The strength or stiffness of matrix

contributes some to corresponding strength or stiffness of CFRP but not so significantly. But they dominate some mechanical properties especially transverse stiffness and strength of CFRP. The toughness of matrix can be considered the key influence factor to mechanical properties of CFRP such as fatigue, interlaminar fracture toughness or impact resistance properties. High toughness can provide high ability to resist the initiation and propagation of matrix crack, and reduce the stress concentration at defects, interface or carbon fiber breakage areas. The mechanisms are considered to be matrix deformation, increase of the plastic deformation zone size and nano void nucleation accompanying with nano crazing ahead of the crack tips. The high toughness of thermoplastic polymers can provide an excellent damage tolerance characteristic to CFRP resulting in high impact resistance and high fatigue strength [6-7]. Moreover, higher interlaminar fracture toughness of CFRP can be achieved by using toughened matrix to delay the initiation and growth of crack [8]. However, the effect of matrix toughness on the static strength of CFRP is not so significant because the matrix deformation is limited due to fiber-constrained space and reduced plastic deformation zone at crack tips. In order to achieve high toughness of matrix, many methods have been focused, such as chemical modification by polymer including rubber or thermoplastic monomer, physical incorporation with rubber or thermoplastic polymer, physical modification by micro/nano materials [9-10].

Another factor influencing the mechanical properties significantly is the fiber/matrix interface properties, especially the fiber/matrix adhesion. It relates to the load transferring ability from matrix to reinforcement. Weak or cracked interfaces probably cause fast debonding at interface and less load to transfer from matrix to CF, and finally resulting in fast failure of composite. The transverse strength increases with increasing fiber/matrix adhesion regarding to off-axis properties. The fiber/matrix adhesion has a significant influence on the fabric composites such as the static strength, interlaminar fracture toughness or fatigue strength [11-15]. For example, the improved fiber/matrix interaction can contribute to high crack propagation resistance to extend the fatigue life of CFRP. Several methods can used to improve the interfacial adhesion, such as chemical treatment of carbon fibers to increase the functional group on their surface to enhance the compatibility with matrix, coating the CF by sizing agent or polymer, treatment by coupling agent, or chemical modification of matrix to increase the

compatibility with CF or grafting CNT on the surface of CF [16-20]. A strong fiber/matrix adhesion is required to increase the efficiency of load transferring, but extremely stronger interface adhesion might cause the brittle behavior around interface, notch-sensitive behavior, an increase of carbon fibers interaction and decrease the toughness [21-23].

1.3 Effect of nano materials addition on the mechanical properties of CFRP (physical modification)

Many works have been focused on improvement of the mechanical properties of polymer matrix composite (PMC) by incorporation with nano structured materials into matrix physically. Namely the matrix is modified just by mixing with nano fillers without changing the chemical structure of polymer. Nano structured materials include particles such as SiO_2, TiO_2 and AlO_3, fibers such as carbon nanotube (CNT), cellulose fiber, carbon nano fiber (CNF), and platelet such as clay. They also have different size, stiffness or interfacial characteristics with matrix resulting in different effect on mechanical properties of PMCs. Increasing the amount of soft fillers such as rubber, it improves the toughness, impact toughness and fatigue properties, but reduces the modulus of PMCs and even the T_g. However, when incorporating with rigid filler such as SiO_2, Al_2O_3 or $CaCO_3$, both of impact toughness and modulus can be enhanced as well as heat resistance [24-27]. Special structured particle with a soft rubber core and a glassy shell named core shell rubber (CSR) nano particles shows more efficiency on improvement of impact toughness than nano clay [28]. Nano fibers with high stiffness such as CNT, CNF and cellulose fiber exhibit obvious effect on improvement of mechanical properties of PMCs. While polyvinyl alcohol (PVA) and Polyethylene terephthalate (PET) fiber whose stiffness is low also perform the same positive effect [29]. Nano fillers with particle shape such as silica particle, TiO_2, Al_2O_3, $CaCO_3$, platelet shape such as nano clay, have been proved that they can improve the fracture toughness, interlaminar fracture toughness, impact resistance, and fatigue properties of PMCs. Moreover, the fiber or tube shape nano fillers such as CNT improve the mechanical properties of PMCs more significantly than other shaped nano filler due to their high aspect ratio [30]. The large size of fillers can increase the viscosity of matrix and subsequently increase the difficulty of processing. Also for the CFRP, fillers with large size are difficult to be dispersed into bundles due to constrained space between

carbon fibers. The aspect of nano filler is the crucial factor to estimate the reinforced efficiency especially for toughness and fatigue properties. It significantly depends on diameter of particle or fiber, and thickness of nano platelet. With decreasing the size of nano filler, the surface/volume ratio increases linearly. A small volume content of nano filler can provide huge surface areas which can enhance the nucleation of polymer crystals in thermoplastic polymer [31] or the cross-linking density in thermosetting polymer, or provide more energy absorption methods, and finally improve the mechanical properties of PMCs. The nano filler/matrix interfaces also are very important. As discussed at above section, increase of interfacial adhesion can help to enhance the efficiency of load transfer between matrix phase and fillers. Especially for fatigue properties, it extends with improvement of interfacial adhesion. The interface adhesion influences the fracture feature and energy absorption mechanism largely. However, impact energy absorption prefers to the inferior adhesion at the interface due to different dominant fracture mode [32].

Many energy absorption mechanisms for addition of nano fillers have been discussed including crack pinning, crack deflection, pull-out or debonding of fillers, formation of interphase or immobilized layer between matrix and fillers, matrix deformation, plastic void growth, bridging, micro cracks and shear banding, but they are still not been clearly understood. Different nano fillers with different size, shape or stiffness exhibit different energy absorption mechanisms as shown in Table 1.1. For the rigid silica particles, the main reinforcing mechanisms are crack deflection, particle debonding and plastic void growth. Rubber cavitation, void growth and matrix plastic deformation are considered as reinforcing mechanism for nano rubber fillers. Similarly, fiber bridging, crack blunting, crack deflection effect are provided by addition of nano fibers [26-28, 33-34].

1.4 Non-destructive evaluation method

Thermoelastic stress analysis (TSA) is based on the temperature change distribution measured by Infared (IR) camera. The temperature of CFRP specimen changes due to deformation under loading according to thermoelastic effect. For the CFRP, since the transverse thermoelastic materials coefficient (K_T) is far higher than longitudinal thermo-elastic materials coefficient (K_L) (about 100 times), the thermo-elastically measured temperature change ΔT can be described as Eq.1 [35].

$$\Delta T = -K_T T \Delta\sigma_T \quad (1)$$

Where T is the ambient temperature (K) and $\Delta\sigma_T$ is corresponding stress change. From the temperature change distribution at surface of CFRP specimens, the stress change distribution can be obtained. The stress reduction happens when damage occurs. Therefore, the distribution of temperature change roughly reflects damage distribution. However, the microscopic heterogeneity of CFRP causes the thermoelastic output signal to be noisy. In order to remove the inhomogeneity noise such as construction pattern, the following image processing technique was applied, namely thermoelastic damage analysis (TDA).

$$[\Delta T(N)] = [T(0)] - [T(N)] \quad (2)$$

Where $[\Delta T(N)]$ represents the thermo-elastic information incremental between 0 and N cycle. $[T(0)]$ is the thermoelastic stress information before test and $[T(N)]$ is the thermoelastic stress information at N cycle [36]. TDA images reflect two-dimensional thermoelastic information related to only damage initiation and growth. The degree of temperature change roughly reflects the damage level in CFRP especially the fabric composite. TSA and TDA have been used to investigate the damage in laminated composites including woven fabric composites [37-38]. Fatigue damage progression of fabric composites under effect of toughened matrix resin has been investigated by the TSA method [36].

Table 1-1. Comparison of toughness mechanisms of micro-and nano reinforced polymer matrix composites [34].

Toughness mechanism	**Particle**			**Fiber or tube**		**Platelet**	
	Micro (rigid)	Micro (rubber)	Nano (powder)	Micro (fiber)	Nano tube or fiber	Micro platelet	Nano clay
Crack pinning	Yes	Yes	Yes	Yes	Yes		
Crack deflection	Yes	Yes	Yes	Yes	Yes	Yes	Yes
Debonding or pull-out	Yes	Yes	Yes	Yes	Yes		
deformation	Yes	Yes		Yes	Yes	Yes	
Fracture or filler		Yes		Yes	Yes		
Bridging	Yes	Yes		Yes	Yes		Yes
Microcracks	Yes	Yes	Yes	Yes	Yes		Yes
Shear banding		Yes					

Acoustic emission (AE) technique also has been used to investigate the damage occurred in composites increasingly. The basic principle of AE technique is to convert the acoustic wave in solids generated as a result of occurrence of a crack or plastic

deformation into the electrical signals, and to analyze it in terms of the energy, counting, amplitude and so on. AE can monitor the damage onset and accumulation in real time to investigate the fracture mechanisms and fracture processes in composites. Facture modes such as fiber/matrix debonding, matrix cracking, matrix plastic deformation, fiber pull-out, delamination, and fiber breakage can be characterized by a variety of AE parameters, such as amplitude distribution, frequency and wave forms. For example, Suh et al. concluded matrix cracking and fiber debonding to correspond to 60-80Hz and fiber failure to 1900Hz and pull-out to 400Hz [39]. The amplitudes of matrix cracking are roughly lower than 60dB, and fiber breakage is approximately 80-100dB. Currently, AE method has been comprehensively used to characterize the facture damage occurring at matrix, reinforcement or interfaces during tensile, flexural, DCB, impact and fatigue test [40-44].

Digital image correlation (DIC) method is another widely used non-destructive evaluation method to investigate the full field deformation of composite during mechanical test. A speckle pattern forms on the surface of CFRP specimen made by white and black paint. Displacement of speckle spots happens and is recorded by a CCD camera when the load is applying on the specimen. The correlation software such as V_{IC}-2D or 3D tracks blocks of pixels to measure surface displacement and build up full field strain maps. Based on this full field strain maps, inhomogeneity of strain distributions can be obtained which reflecting the influence of the whole components of composites. The damage distribution, damage feature, damage level, damage progression, and the in-plane elastic properties of CFRP can be investigated furthermore (Fig.1-3) [45-48].

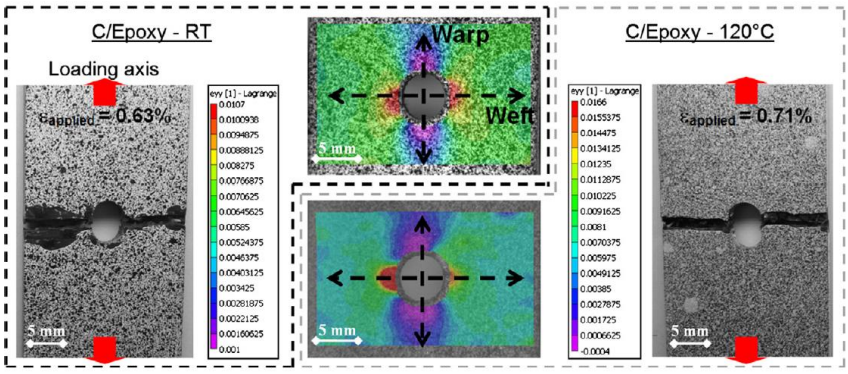

Fig.1-3.Quasi-isotropic C/Epoxy laminates at RT and 120 °C. Comparison of failed specimens (transverse failure in weft direction) and corresponding strain fields obtained

by DIC [45]

1.5 Objective of study

The study is aimed to investigate the effect of different matrix properties altered according to the chemical modification or physical modification by different nano fillers on the mechanical properties of CFRP. A numerical model has tried to be used to characterize the relationship between the matrix properties and fatigue life of CFRP, and supply some important information on how to design the matrix resin to achieve the expected mechanical properties of CFRP based on the consideration of cost. The thesis is divided into five chapters as follows:

The first chapter provides a background description of composite materials together with the main reasons for the study.

Chapter 2 describes the chemical modification of vinylester resins to alter their mechanical properties such as the toughness and CF/VE adhesive strength. Subsequently the influence of these mechanical properties of resin on the mechanical properties such as static and fatigue properties of CF/VE composites has been characterized. Thermoelastic stress analysis, CT-scan and SEM has been used to investigate the effect of different toughness and CF/VE adhesion of matrix on the initiation and propagation of fatigue damage of CFRP. The coupling effect of the above matrix properties on mechanical properties such as tensile or fatigue performance of composites has been discussed. Finally, a model was used to describe this relationship.

Chapter 3 describes the physical modification of matrix resin by different nano fiber with different size and the mechanical properties (such as nano PVA and MFC (micro fibrillated cellulose)) to change their mechanical properties including fracture toughness and CF/matrix adhesion. Then the effect of these different nano fibers on the mechanical properties of CFRP such as static and fatigue properties was investigated. The damage progression especially the fatigue damage under incorporation of nano fiber was discussed. Furthermore, the reinforcing mechanism of nano filler at micro scale was discussed. In addition, the effect of nano filler content on the fatigue performance of FR-PMC is also studied.

Chapter 4 gives a description of the effect of different matrix on mechanical properties of carbon fiber reinforced polymer composite pressure vessels. The carbon fiber reinforced modified vinylester and epoxy composite pressure vessels with simple

structure (90/15°) have been prepared. Then the burst pressure of each kind of composite vessel was tested. The DIC method has been used for the measurement of the strain distribution during burst pressure test. The initiation of crack and crack accumulation inside each kind of composite vessels under effect of different matrix resin has been discussed based on the strain distribution maps, together with CT-scan and optical microscopy.

Chapter 5 gives the conclusions of the thesis.

References

1. Stephen R. Swanson. Introduction to Design and Analysis with Advanced Composite Materials. 1997.pp.1-249.
2. The carbon fiber industry worldwide 2011-2020, by Tony Roberts, ISBN 1 871677 64 5.
3. Mark Holmes. Carbon fibre reinforced plastics market continues growth path, Reinforced Plastics. 2013;57(6): 24-29.
4. Mallick PK. Fiber-Reinforced Composites. P.130.
5. Kim RY. On the off-axis strength test of anisotropic materials, Test method and design allowables for fibrous composites, ASTM STP 734, C.C.Chamis, Ed., American Society for Testing and Materials, 1981. pp.91-108.
6. Hartwig G, Hübner R, Knaak S, Pannkoke C. Fatigue behaviour of composites. Cryogenics 1998;38(1):75-78.
7. Kawai M, Morishita M, Fuzi K, Sakurai T, Kemmochi K. Effects of matrix ductility and progressive damage on fatigue strengths of unnotched and notched carbon fibre plain woven roving fabric laminates Compos Part A: Appl Sci Manuf 1996;27(6):493-502.
8. Walter L. BRADLEY. “Relationship of Matrix Toughness to Interlaminar Fracture Toughness” in Application of Fracture Mechanics to Composite Materials. Composite Materials Series 1989, 6:159-187.
9. Jyongsik Jang, Hojung Yang. Toughness improvement of carbon-fibre/polybenzoxazine composites by rubber modification. Compos Sci Technol 2000; 60:457-463.
10. Sue HJ, Jones RE, Garcia-Meitin EI. Fracture behaviour of model toughened composites under mode I and mode II delaminations. Journal of materials science,

28.1993:6381-6391.

11. Oya N, Hamada H. Mechanical properties and failure mechanisms of carbon fibre reinforced thermoplastic laminates. Compos Part A: Appl Sci Manuf 1997; 28:823-832.
12. Albertsen H, Ivenqh J, Peters P, Wevers M, Verpoest I. Interlaminar fracture toughness of CFRP influenced byfiber surface treatment: Part 1: experimental results. Compos Sci Technol 1995; 54:133-145.
13. Ozkan T, Chen Q, Chasiotis I. Interfacial strength and fracture energy of individual carbon nanofibers in epoxy matrix as a function of surface conditions. Compos Sci Technol 2012; 72:965-975.
14. Botelho EC, Figiel L, Rezende MC, Lauke B. Mechanical behavior of carbon fiber reinforced polyamide composites. Compos Sci Technol 2003;63 (13):1843-1855.
15. Gamstedt EK, Skrifvars M, Jacobsen TK, Pyrz R. Synthesis of unsaturated polyesters for improved interfacial strength in carbon fibre composites. Compos Part A 2002; 33:1239-1252.
16. Montes-Morán MA, van Hattum FWJ, Nunes JP, Martínez-Alonso A, Tascón JMD,. Bernardo CA. A study of the effect of plasma treatment on the interfacial properties of carbon fibre-thermoplastic composites. Carbon, 2005;43(8):1795-1799.
17. Abdullah Kafi, Mickey Huson, Claudia Creighton, Jiyi Khoo, Luca Mazzola, Thomas Gengenbach, Frank Jones, Bronwyn Fox. Effect of surface functionality of PAN-based carbon fibres on the mechanical performance of carbon/epoxy composites. Compos Sci Technol 2014, 94 (9): 89-95.
18. Varelidis PC, McCullough RL, Papaspyrides CD. The effect on the mechanical properties of carbon/epoxy composites of polyamide coatings on the fibers. Compos Sci Technol, 1999; 59(12):1813-1823.
19. Robertson MAF, Bump MB, Verghese KE, Mccartney SR, Leko JJ, Rifle JS, Kim IC, Yoon TH, Designed interphase regions in carbon fiber reinforced vinyl ester matrix composites, J. Adhesion, 1999;71:395-416.
20. Sunny S. Wicks, Wennie Wang, Marcel R. Williams, Brian L. Wardle. Multi-scale interlaminar fracture mechanisms in woven composite laminates reinforced with aligned carbon nanotubes. Compos Sci Technol 2014; 100:128-135.
21. Goda K. The role of interfacial debonding in increasing the strength and reliability

of unidirectional fibrous composites. Compos Sci Technol 1999; 59:1871-1879.

22. Zhao FM, Takeda N. Effect of interfacial adhesion and statistical fiber strength on tensile strength of unidirectional glass fiber/epoxy composites. Part I: experiment results. Composites: Part A 2000; 31:1203-1214.
23. Drzal LT, Madhukar M, Fibre-matrix adhesion and its relationship to composite mechanical properties, J. Mater. Sci.1993; 28:569-610.
24. Viana JC. Polymeric materials for impact and energy dissipation. Plast Rubber Compos 2006; 35(6-7):260-267.
25. Bartczak Z, Argon AS, Cohen RE, Weinberg M. Toughness mechanism in semicrystalline polymer blends: II high-density polyethylene toughened with calcium carbonate filler particles. Polymer 1999; 40(9):23472365.
26. Liu ZH, Kwok KW, Li RKY, Choy CL. Effect of coupling agent and morphology on the impact strength of high density polyethylene/$CaCO_3$ composites. Polymer 2002; 43(8):2501-2506.
27. Wetzel BD, Haupert F, Zhang M. Epoxy nanocomposites with high mechanical and tribological performance. Compos Sci Technol 2003; 63(14):2055-2067.
28. Subramaniyan AK, Sun CT. Toughening polymeric composites using nanoclay: crack tip scale effects on fracture toughness. Compos Part A Appl Sci Manuf 2007; 38(1):34-43.
29. Phong NT, Gabr MH, Okubo K, Chuong B, Fujii T. Improvement in the mechanical performances of carbon fiber/epoxy composite with addition of nano (Polyvinyl alcohol) fibers. Compos Struct 2013; 99: 380-387.
30. Cooper CA, Ravich D, Lips D, Mayer J, Wagner HD. Distribution and alignment of carbon nanotubes and nanofibrils in a polymer matrix. Compos Sci Technol 2002; 62(7-8):1105-1112.
31. Ehrenstein GW. Polymeric materials. Munich: Hanser Publisher; 2001.
32. Miyagawa H, Drzal LT. The effect of chemical modification on the fracture toughness of montmorillonite clay/epoxy nanocomposites. J Adhesion Sci Technol 2004; 18(13):1571-1588.
33. Subramaniyan AK, Sun CT. Interlaminar fracture behavior of nanoclay reinforced glass fiber composites. J Compos Mater 2008; 42(20):2111-2122.
34. Sun LY, Gibson RF, Gordaninejad F, Suhr J. Energy absorption capability of

nanocomposites: A review. Compos Sci Technol 2009;69:2392-2409.

35. Potter RT, Greaves LJ. The Application of Thermoelastic Stress Analysis Techniques to Fibre Composites. 1987, Proc. SPIE 0817, Optomechanical Systems Engineering, pp.134-146.
36. Uenoya T, Fujii T. Influence of Matrix Toughness on Damage Initiation and Growth in Carbon Fiber Fabric Composites. J Reinf Plast Compos 2000; 19(1) :83-94.
37. Emery TR, Dulieu-Barton JM. Thermoelastic Stress Analysis of damage mechanisms in composite materials. Compos Part A: Appl Sci Manuf 2010; 41(12):1729-1742.
38. Toubal L, Karama M, Lorrain B. Damage evolution and infrared thermography in woven composite laminates under fatigue loading. Int J Fatigue 2006; 28 (12):1867 -1872.
39. Suh, KS, Lee, CR, Park KH, Park, JW. In-situ monitoring of failure and fracture mechanisms in carbon fiber/epoxy composite by an optical fiber sensor. Polymer (Korea), 1991; 16:15-21.
40. Ni Qing-Qing, Jinen Eiichi. Acoustic emission and fracture of Carbon Fiber Reinforced Thermosoftening Plastic (CFRTP) materials under monotonous tensile loading. Engineering Fracture Mechanics, 1993; 45(5):611-625.
41. Park JM, Kong JW, Kim JW, Yoon DJ. Interfacial evaluation of electrodeposited single carbon fiber/epoxy composites by fiber fracture source location using fragmentation test and acoustic emission. Compos Sci Technol, 2004; 64(7-8):983-999.
42. Bourchak M, Farrow IR, Bond IP, Rowland CW, Menan F. Acoustic emission energy as a fatigue damage parameter for CFRP composites. International Journal of Fatigue, 2007; 29(3):457-470.
43. Sause MGR, Muller T, Horoschenkoff A, Horn S. Quantification of failure mechanisms in mode-I loading of fiber reinforced plastics utilizing acoustic emission analysis. Compos Sci Technol 2012; 72:167-174.
44. Boominathan R, Arumugam V, Santulli C, Adhithya Plato Sidharth A., Anand Sankar R, Sridhar BTN. Acoustic emission characterization of the temperature effect on falling weight impact damage in carbon/epoxy laminates. Compos Part B: Engineering, 2014; 56:591-598.

45. Vieille B, Taleb L. About the influence of temperature and matrix ductility on the behavior of carbon woven-ply PPS or epoxy laminates: Notched and unnotched laminates. Compos Sci Technol 2011; 71:998-1007.
46. Behrad Koohbor, Silas Mallon, Addis Kidane, Michael A. Sutton. A DIC-based study of in-plane mechanical response and fracture of orthotropic carbon fiber reinforced composite. Compos Part B 2014; 66:388-399.
47. Tomasz Brynk, Rafal M. Molak, Miroslawa Janiszewska, Zbigniew Pakiela. Digital Image Correlation measurements as a tool of composites deformation description. Computational Materials Science 2012; 64:157-161.
48. Andrew Makeev. Interlaminar shear fatigue behavior of glass/epoxy and carbon/epoxy composites. Compos Sci Technol, 2013; 80(17):93-100.

Chapter II

Chemical modification of matrix, and effect of matrix properties on the mechanical performance of carbon fabric vinylester composites

2.1 Introduction

Due to the r**e**inforced effect at both the warp and weft direction, woven fabric fiber reinforced composites perform more balanced properties than unidirectional fiber reinforced composites. Moreover, woven fabric composites exhibit excellent drapability, reduced manufacturing cost, and increased resistance to impact damage, which lead to increased application in automotive, wind turbine blades, marine, aircrafts and sports industries [1]. As matrix materials of composites, thermosetting resins have been widely used due to their good impregnation of the reinforcement and easy/fast fabrication processing speeds. Among several types of matrix resins, fiber reinforced vinyl ester (VE) composites have attracted much attention due to relatively low cost, easy processing because of lower viscosity of VE than epoxy, the competitive mechanical properties compared to polyester because of containing epoxy molecules within the backbone, and good corrosion resistance[2-4].

The mechanical properties like static tensile, flexural, impact, and fatigue properties of CFRP are sensitive to damage accumulated inside. Here the fatigue properties was taken as the example, fatigue performance of CFRP (carbon fiber reinforced polymer composites) depends on the fatigue damage such as matrix cracking, transverse cracking, interfacial debonding, delamination or fiber breakage [5-7]. The early occurrence of matrix crack and transverse crack can degrade the stiffness of CFRP drastically, and also can lead to an early delamination, subsequently related to the final failure of composites. Delamination occurs early at the cross-over points between warp and weft yarns in woven fabric composites due to stress concentration, and causes the unequal stress distribution among CF layers. The former different damage occurred at the matrix or interfaces are closely related to the matrix and reinforcement properties. Therefore, it should be very effective to fabricate the CFRP with excellent mechanical properties by using constituents with high mechanical performance. However, it does not always

work expectably due to significant dependence on fatigue damage. Even when carbon fibers with higher modulus were used to reinforce the same epoxy, only a slight improvement in fatigue properties of unidirectional composites was obtained. And increase of toughness of matrix has led to improvement in the static properties but the poorer fatigue performance of composites [8]. Brittle matrix based CFRP yielded a higher fatigue limit than a ductile thermoplastic matrix based composites [9]. Therefore, it is necessary to study the fatigue damage mechanism clearly by the effect of matrix properties.

Some works has been focused on the influence of matrix properties like toughness or interfacial properties like fiber/matrix bonding on fatigue behavior of CFRP. In general, when the improvement of the CF/matrix adhesion is achieved, the fatigue performance of a broad range of composites could be enhanced if keep the other parameters (like loading) constant due to improved load transfer efficiency. The CF/matrix adhesion can affect the shear and transverse properties and corresponding damage development significantly under fatigue loading. The remarkable improvement in fatigue life of CF/epoxy composites has been provided by a strong fiber/matrix adhesion at high applied stresses. While the effect of fiber/matrix adhesion on the fatigue properties was less significant at low applied fatigue stress [10]. The improved fiber/matrix interaction contributed to high crack propagation resistance [11]. However, the interaction between the fiber strength distribution and debond propagation affected by interfacial adhesion led to further fiber breakage related to final failure of composites [12]. Furthermore, an increase in fiber/matrix adhesion resulted in more fiber-fiber interactions [13]. On the other hand, matrix toughness also played an important role in fatigue damage progression. Sjogren et al. [14] found that the onset of transverse crack delayed and density of transverse cracks decreased as the toughness of matrix increased in GFRP. Gassan et al. [15] demonstrated the brittle composites showed greater damage which became more significant under high loads and an extensive region of final damage propagation was found. Kawai et al. [16] have investigated the influence of matrix resin systems with different ductility on the fatigue strength and fatigue damage mechanisms of woven fabric composites. They also found that the tougher matrix resin improved the fatigue performance. Uenoya [17] revealed that the toughened resin system could improve the tension fatigue properties by inhibition of fatigue damage development in

early fatigue process.

However, a high CF/matrix interfacial bond tends to cause the brittle behavior of matrix and stress concentrations around the fiber breaks. But it can be released by increasing the matrix toughness. Similarly, the stiffness or strength of composites probably decreases when toughness increases significantly, while it can be improved by increasing the interfacial adhesion in some degree [18-20]. In general the trade-off between stiffness and toughness of matrix also exist. In order to achieve the expected mechanical properties of CFRP based on the consideration of cost, more studies and analytical models are needed to well understand the coupling effect of two or more parameters of matrix properties on the fatigue damage initiation and growth in composites, such as toughness, strength, and interfacial adhesion.

The effect of the matrix and interface properties on the fatigue damage initiation and growth in the CFRP mainly exhibits at the fatigue initial and middle stage in the form of fatigue stiffness loss. The fatigue stiffness degradation occurs mainly at these two stages. The fatigue damage at the fatigue final stage was dominated by CF breakage. The final failure of specimens also was close related to the degree of stiffness loss. In this study, the investigation of the CF breakage at fatigue final stage has not been conducted although it determines the final failure of CFRP. However, based on the fatigue damage evolution investigation, the effect of matrix properties on the initiation of occurrence of comprehensive breakage of CF was discussed. In this study, the mechanical properties especially fatigue properties of CF/VE composites based on different vinylester resins with different toughness and CF/matrix adhesion have been characterized. The coupling effect of the above matrix properties on mechanical properties such as tensile or fatigue damage initiation and growth in composites has been investigated.

2.2 Experimental methods

2.2.1 Materials and preparation of CF/VE composites

The plain woven carbon fiber cloth (Mitsubishi Rayon TR3110MS) was used as reinforcement. Five types of vinylester resins, A and AX series (AC, AD, AE, AF) supplied by DH Materials Inc. were used as matrix resin. VE resin A is a bisphenol A epoxy based vinyl ester conventional resin as control resin with low toughness and low interfacial shear strength (IFSS) between CF and resin. AX series VE resins are

chemical modified based on control resin A. VE resin AX display different mechanical properties such as the tensile strength, toughness and the adhesive strength to CF. AC exhibits high IFSS, AD exhibits high toughness, AE exhibits medium high toughness and IFSS and AF exhibits high toughness and IFSS. 328E (Kayaku akzo corporation) was used as curing agent for AX (AC, AD, AE, and AF) resin, and acetyl acetone peroxide (Nof corporation) was used for control resin. 8%CoOCt was used as a promoter.

VE resin was first mixed with promoter and curing agent with a ratio of 100/0.3/1 for resin AX, 100/0.2/1 for resin A, then degassed in a vacuum oven for 15 minutes to remove voids. The mixture was then hand lay-upped with plain woven carbon fiber clothes with a CF volume fraction of ～50%. Eight CF fabrics taken from the same roll were used for each specimen. They were carefully aligned with no angles between each other. The layup of testing specimens is shown in Fig.2-1. The CFRP plate was obtain after curing at room temperature for 24 h and post curing at 60 ℃ for 3 h. Parallel sided specimens were prepared to make their wrap yarns direction coincident to the loading direction. Namely, both static tensile and fatigue cyclic loads were applied along the wrap direction.

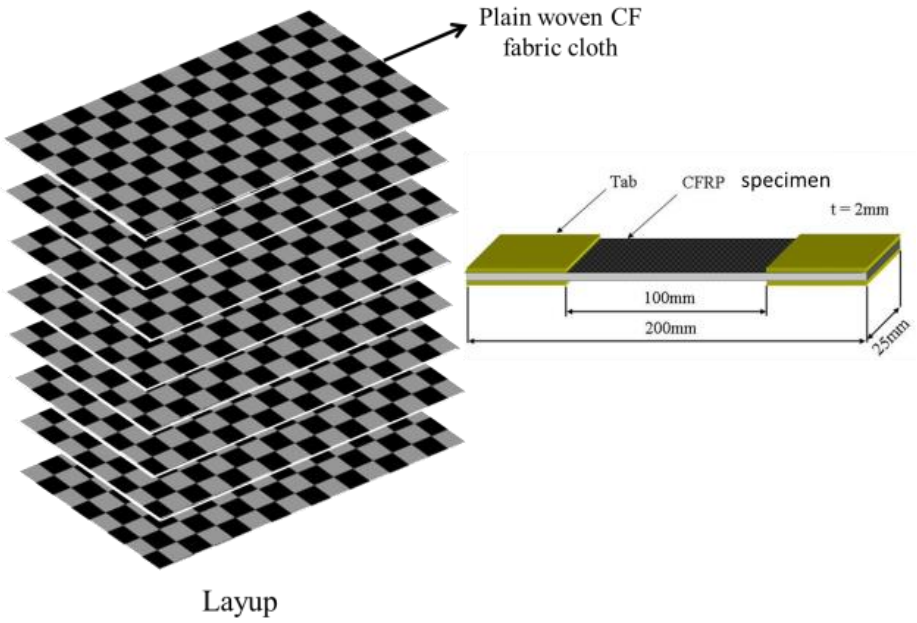

Fig.2-1. Layup of carbon fabric composites.

2.2.2 Mechanical testing

The interfacial shear strength between CF and resin was obtained by microdroplet test. The droplets of liquid VE resin were first dropped on the single fiber, then cured at room temperature for 24 h and post cured at 60 ℃ for 3h. The embedded lengths of the droplets with a range from 70μm to 130μm were measured by an optical microscope. The test was carried out by a microdroplet instrument (Model HM410). The IFSS between the single fiber and VE resin was calculated by the Eq.1.

$$\tau_d = \frac{F_d}{\pi D_f L} \quad (1)$$

Here, τ_d is the interfacial shear strength, F_d is the maximum load, D_f is the fiber diameter and L is the embedded length.

The fracture toughness tests of neat VE resin were conducted using a cross-head speed of 10 mm/min according to ASTM D5045-99 at room temperature. All neat resin were cured at room temperature for 24 h and post cured at 60 ℃ for 3h. The single edge notch bend (SENB) specimens with the pre-crack made by tapping on a fresh razor blade placed in the notch were used to test the fracture toughness (K_{IC}).

The tensile properties were investigated by using a Shimadzu autograph universal testing machine according to ASTM D3039-08. The testing speed was set to 1 mm/min. The specimen dimension was about 200 x 25 x 2 mm with a gage length of 100mm. The average thickness of CF/A, CF/AC, CF/AD, CF/AE and CF/AF was 1.97, 1.97, 2.02, 1.98 and 1.99 mm respectively.

The 3 points bending tests were performed under an autograph universal testing machine at a cross-head speed of 5 mm/min according to JIS K7074. The span was set to 80mm. Dimensions of the specimen was 15x100x2 mm.

The fracture toughness was characterized by double cantilever beam (DCB) test using a universal mechanical testing machine according to ASTM D5528-01. The DCB specimens are prepared as Fig.2-2 with a dimension of 20x150x2 mm. The corrections for the end-block, DCB arm bending and root rotation were considered. The testing speed was set to 2 mm/min. The mode-I interlaminar fracture toughness for initiation (G_{IC}) and propagation (G_{IP}) of composites was calculated by the modified compliance calibration (MCC) method. The MCC methods were listed as Eq.2 and Eq.3.

$$G_{IC} = \frac{3m}{2(2h)}\left(\frac{P_c}{B}\right)^2\left(\frac{BC}{N}\right)^{2/3} F \qquad (2) \qquad G_{IP} = \frac{3m}{2(2h)}\left(\frac{P_p}{B}\right)^2\left(\frac{BC}{N}\right)^{2/3} F \qquad (3)$$

Where G_{IC} is the fracture toughness at initial crack stage, G_{IP} is the fracture toughness at propagation stage, P_p is the applied load, δ_p is the displacement, C is the compliance corresponding to each crack length, a is the crack length, P_c is the initial maximum load, B is the specimen width, $2h$ is the thickness in equation, N is the end-block correction factor, F is the large displacement correction factor, m is the slope of a plot of $(BC/N)^{1/3}$ versus $(a/2h)$.

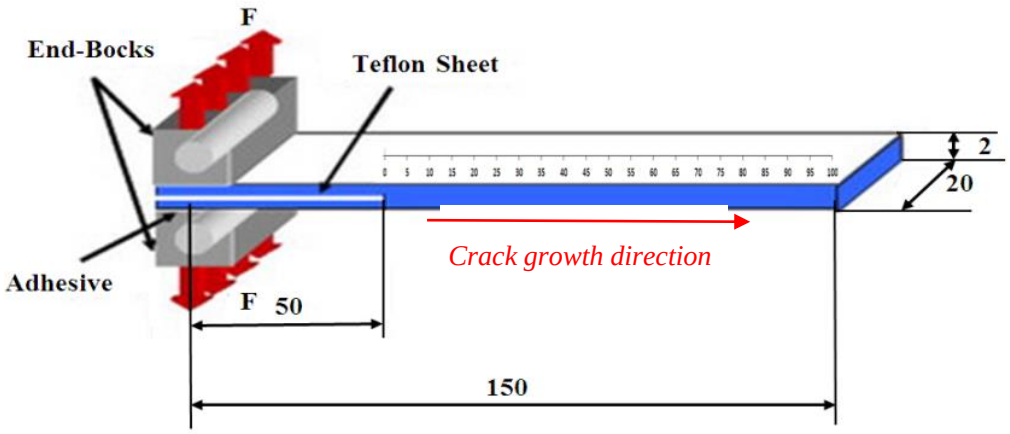

Fig. 2-2. Dimension and geometry of DCB specimens.

Tension-tension fatigue test was conducted at stress-ratio $R = +0.1$ and frequency $f = 5Hz$ according to ASTM D3479 on the ServoPulser 50KN equipment at room temperature. Each fatigue test was run to 1 million cycles unless final failure happened before this limit. The specimen dimension for fatigue life test was 200 x 25 x 2 mm with a gauge length of 100mm. In order to investigate the damage propagation in CF/VE composites, 3-dumbbell type of sample with 3 narrow sections prepared by a diamond grindstone were used to test, as shown in Fig.2-3. The test was conducted at same condition with former tension fatigue test. When came to expected cycles, fatigue machine was stopped and one narrow section was cut down, then tabs were glued to pursue test. The cut narrow section was taken to observe by CT-scan (Skyscan1172Micro-CT), and cross-section was observed by scanning electron microscopy (SEM) by JSM-7001FD equipment.

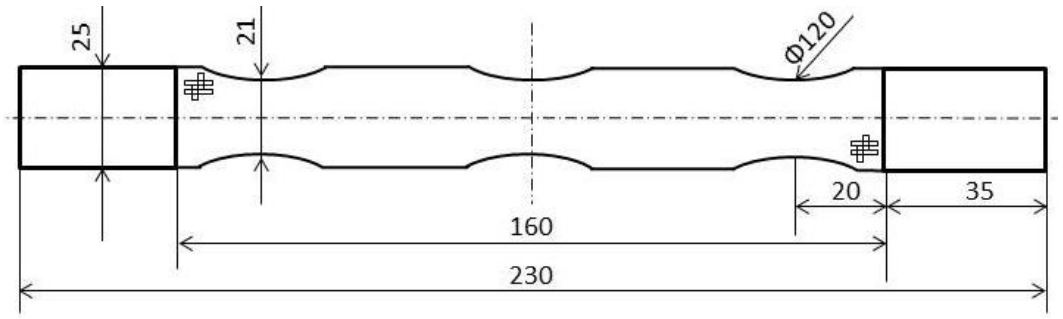

Fig. 2-3. Dimension of 3-dumbbell shape specimens

The temperature change information was taken by a thermo-camera with 0.14 mm spatial resolution at a certain cycle during fatigue test under the same testing condition with former tension fatigue test. Then the TSA images were obtained by using a commercial thermoelastic stress analyzer system (JEOL, model JTG-8010).

The puncture impact was conducted by Hydroshot (Shimadzu HTM) with a hardened steel hemispherical impactor of diameter 12.7 mm. The loading speed when impactor hitting specimens was set to 6.3 m/s. Dimensions of the specimen was ～50x50x2 mm. The cross section at failure area was cut and observed by optical microscopy. The punch was driven vertically downward through the specimens who were tightly clamped to prevent slippage. At least 5 specimens were tested. E_m was the absorbed energy when the loading force was the maximum. And E_p was the absorbed energy when the loading force was half of the maximum loading force.

2.3 Results and discussion

2.3.1 Matrix properties

More than 5 specimens of each type of VE resin were tested. The results are shown in Fig.2-4, which confirms that the expected fracture toughness of resin A and AX series are correct. According to microdroplet test, the IFSS between each VE resin and CF are shown in Table.2-1. AX series resins performed higher IFSS than control resin A. The results confirm that resin A with low toughness and low IFSS, AC with high IFSS, AD with high toughness, AE with medium high toughness and IFSS, AF with high toughness and IFSS have been successfully prepared.

2.3.2 Static tensile properties

CF/conventional VE (CF/A) composite performed a low tensile strength of 611 MPa with a slight scatter because of the different batches. The static tensile strength of all

CF/VE composites is shown in Table.2-2. Tensile strength of CF/AX series composites increased by a range from 13.4 to 37.3% compared to CF/A composite. Here CF/AF composite performed highest tensile strength as 839 MPa. A good relation between CF/matrix adhesion and tensile strength of CFRP was found. Typical stress-strain curves for each type of composites are shown in Fig.2-5. The curves are almost linear with a slight increase of modulus as increase of strain, which might due to inherent stiffening of CF and improvement of a local fibers orientation under increasing tensile load [21, 22]. The stiffness of each type of composites was almost same due to the dominant effect of CF (Fig.2-5), which were for CF/A, CF/AC, CF/AD, CF/AE and CF/AF respectively. The improvement of tensile strength of CF/AX series composites was contributed by an increased the strain at failure.

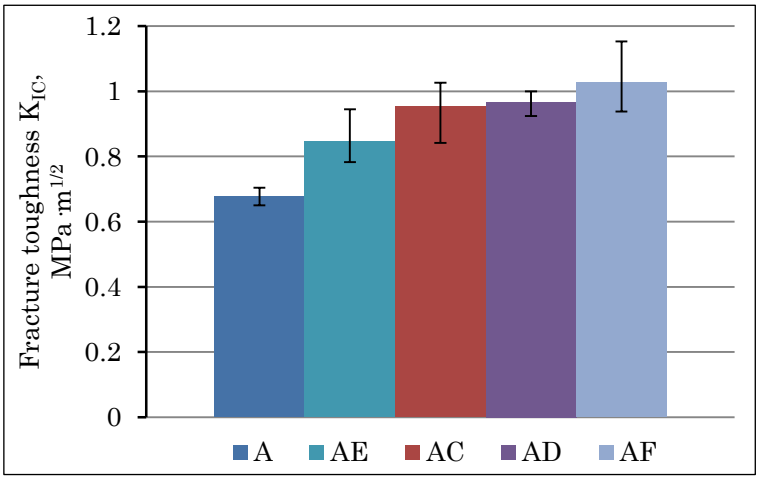

Fig.2-4. Fracture toughness of VE resins

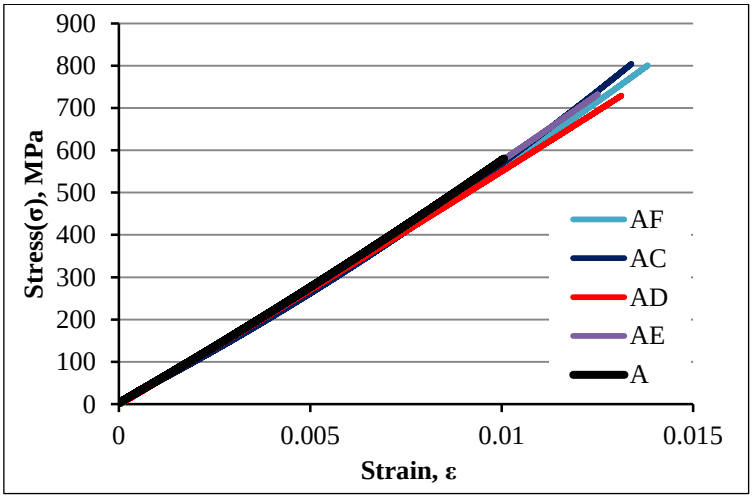

Fig.2-5. Typical stress-strain curves of CF/VE composites.

Table.2-1. Interfacial shear strength (IFSS) between VE resins and CF

	IFSS (MPa)	Std. dev.
A	24.6	± 1.2
AC	36.1	± 3.1
AD	30.4	± 4.7
AE	30.0	± 2.5
AF	35.8	± 2.6

Table.2-2. Tensile strength of CF/VE composites

	Average tensile strength, MPa	Std. dev.
CF/A	611	± 43.0
CF/AC	810	± 39.9
CF/AD	728	± 36.0
CF/AE	693	± 31.2
CF/AF	839	± 49.9

The tensile specimens of CF/VE composites showed the different macroscopic failure behavior (Fig.2-6, top). CF/A composite displayed a relative straight failure mode with CF warp bundles being pulled out. And a slight interlaminar delamination was found in CF/AD composite while severe interlaminar delamination occurred in CF/AE composite. The fracture mode of CF/AC and CF/AF composites was a straight failure mode which was a typical failure mode of CFRP with high interfacial bonding. The macroscopic failure mode of CF/VE composites indicates the composite showing higher strain at failure failed with lower degree with respect to internal damage. Further, micro fracture models after tensile test of all specimens were carefully observed by SEM (Fig.4, bottom). The fracture surface of CF/A composite (Fig.2-6-A-2) showed that most of carbon fibers split individually, severe CF debonding and interlaminar delamination occurred. Fewer carbon fibers in CF/AD and CF/AE were pulled out (Fig.2-6-AD-2, AE-2) and slight interlaminar delamination happened. The warp CF bundle was pulled out as well might due to delamination happened before failure. Almost no carbon fiber was pulled out from resin in CF/AC and CF/AF composites, and delamination was negligible (Fig.2-6-AC-2, AF-2). It was known that it becomes harder to pull CF out from matrix and delaminate CF layers with increasing the interfacial bonding. It confirmed that the CF/matrix adhesive bonding provided a dominant effect on the

improvement of tensile strength of composites. The higher CF/matrix adhesion were able to increase the load transfer capability and delay the initiation and growth of damage during tensile loading to slow down the failure of CF and finally improved the strain at failure of CFRP. In addition, the main difference of fracture surfaces between CF/AD and CF/AE, CF/AC and CF/AF was the matrix deformation, which was much more obvious in CF/AD or CF/AF due to higher fracture toughness of matrix. The higher toughness of matrix also brought a positive effect on reducing damage in composite and finally extended the strain at failure to improve tensile performance. It was further confirmed by AE investigation that lower accumulated velocity and lower degree of damage in CF/AX composites was found (Fig.2-7).

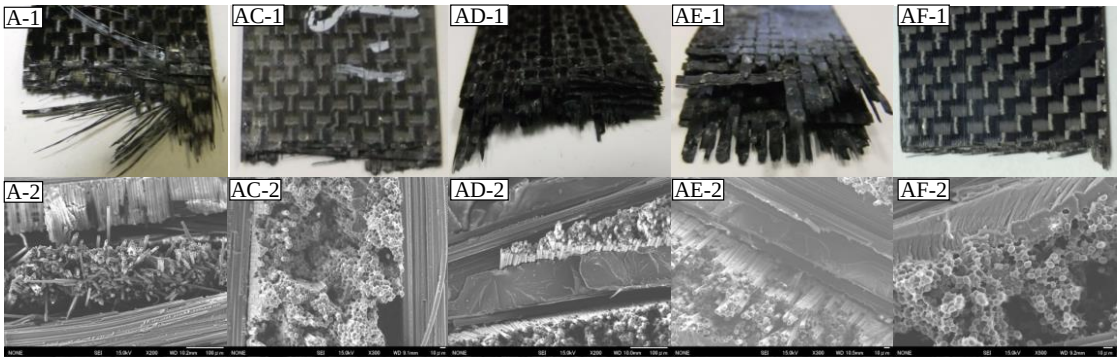

Fig.2-6. Macro failure mode (top) and SEM images of the fracture surface (bottom) of CF/VE composites after tensile test.

2.3.3 Flexural properties of CF/VE composites

The flexural properties of CF/VE composites are shown in Fig.2-8. CF/A composite shows a lowest flexural strength which is just 630 MPa. The flexural strength of CF/AX composites increases by a range from 25.7% to 37.1%. The flexural modulus of CF/AX composites display unchangely compared to CF/A composite which probably due to dominant effect of CF on stiffness of CFRP. The major contribution is the improved strain at failure due to lower degree of accumulated damage. CF/A composite shows different fracture mode with that of CF/AX composites. CF/VE composite specimens fail mainly at bending side indicating a low bulking capability. On the contrary, CF/AX composite specimens fail at both of bending side and tension side accompanying with a large scale of delamination or CF breakage. An increase of CF/VE adhesion and matrix

toughness improves the bulking capability and energy absorption ability. Moreover, a good relationship is also found between flexural strength and CF/VE adhesion, namely, the flexural strength increases with increasing CF/VE adhesion.

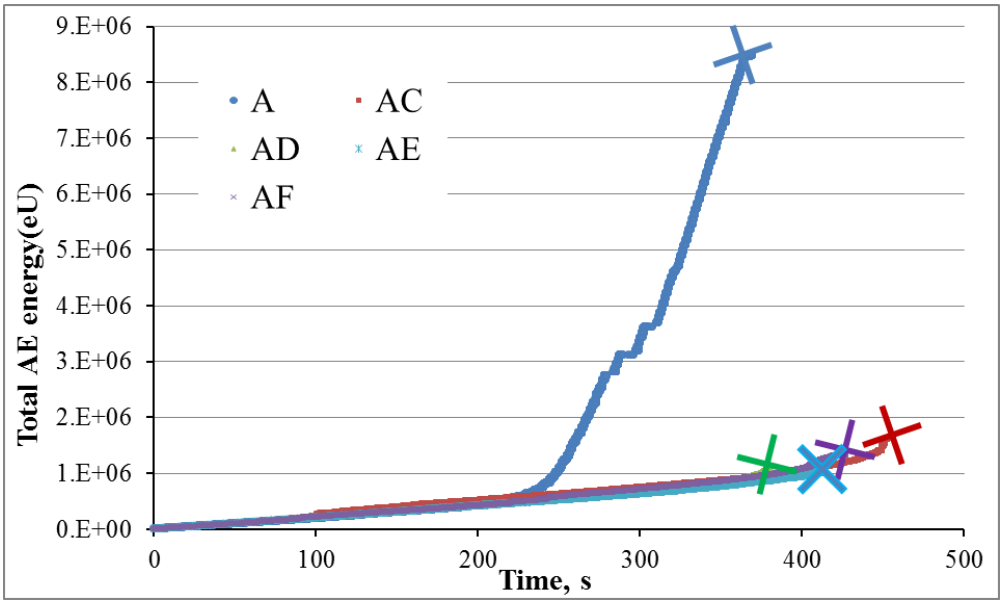

Fig.2-7. Energy-time curves according to AE investigation of CF/VE composites.

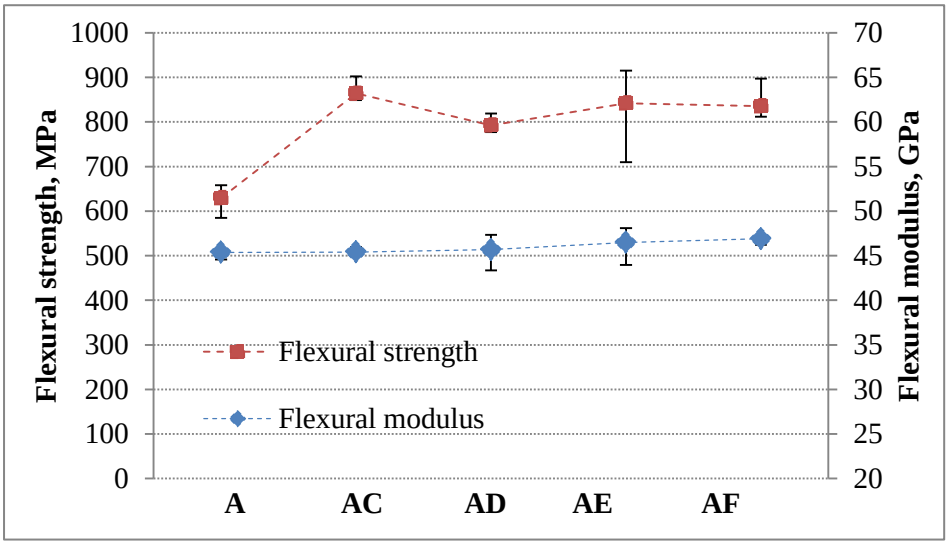

Fig.2-8. Flexural properties of CF/VE composites.

2.3.4 Mode I interlaminar fracture toughness of CF/VE composites

Fig.2-9. shows the mode-I interlaminar fracture toughness for initiation (G_{IC}) and propagation (G_{IP}), determined by double cantilever beam (DCB) test. The G_{IC} and G_{IP} values of CF/A composite are highest with a value of 369 and 410 J/m^2 respectively.

The G_{IC} values of CF/AC, CF/AD, CF/AE, and CF/AF composites decrease by a range from 13.7 % to 64 %, and G_{IP} values decrease by a range from 4.4% to 52.2% respectively. It was worth noting that almost an inverse correlation was found between the interlaminar fracture toughness and the static strength of composites as well as the adhesion between CF and VE resin (compared to Tabe.2-2 and Fig.2-8).

The fracture surfaces of CF/VE composites were investigated by SEM, as shown in Fig.2-10. The low magnification images in Fig.2-10-A-1 and AC-1 show that the fracture surface of conventional VE is dominated by the interfacial debonding while the fracture surfaces of CF/AX composites consisting of interfacial debonding failure and matrix cohesive failure. Matrix cohesive failure has been considered to be an evidence of a strong interfacial adhesion between CF and matrix resin. Herein, a stronger interfacial adhesion in AX composites than conventional VE composite is confirmed.

According to Hine et al's theory [23], the total G_{IC} consist of some individual energy contribution described as Eq. 5,

$$G_{TOT} = G_M + G_{BK} + G_P + G_{DEB} \quad (5)$$

Where the total fracture toughness (G_{TOT}) consists of energy involved matrix deformation (G_M), fiber breakages (G_{BK}), fiber pull-out (G_P) and interfacial debonding (G_{DEB}). Fracture surfaces of CF/A composite are shown in Fig.2-10-a (the inserted is observed at high magnification). The CFs with smooth surface debond and are pulled out from matrix accompanying with some CFs fracture. In addition, bulk matrix fracture is also found. The higher G_{IC} or G_{IP} of CF/A composite might be expected to be mainly contributed by G_{BK}, G_P and G_{DEB} as a consequence of interfacial debonding failure where carbon fiber debonding, pull-out and fiber breakage are considered as the major energy contribution to the interlaminar fracture toughness of composites [24]. On the other hand, due to comprehensive matrix failure, carbon fiber debonding, pull-out and fiber breakage are not so significant resulting in relatively lower G_{IC} and G_{IP} of CF/AX composites.

For the CF/AX composites, delamination mainly propagates along matrix where the energy contribution to total G_{IP} is dominated by matrix toughness. The interfacial failure area was observed further, as shown in Fig.2-10-AC-2 to AF-1. The inserted figures are high magnification SEM images observed at the cohesive failure area. It is found that

hackle pattern and cohesive matrix failure are obvious features at interfacial fracture surfaces indicating that matrix deforms during crack propagation. Matrix deformation (G_M) has been identified as an important energy contribution to the G_{IC} and G_{IP} of composites. The main contributions to G_{TOT} for CF/AX composites might be the deformation of matrix (G_M). The hackle pattern of CF/AF and CF/AD composite is more obvious in the form of larger tiny deformed matrix flakes and the tougher cohesive fracture surface is found than CF/AC or CF/AF. It indicates that a larger scale of matrix deformation occurs, which contributed to higher G_M. Therefore, the G_{IC} and G_{IP} value of CF/AX composites are close related to the toughness of matrix.

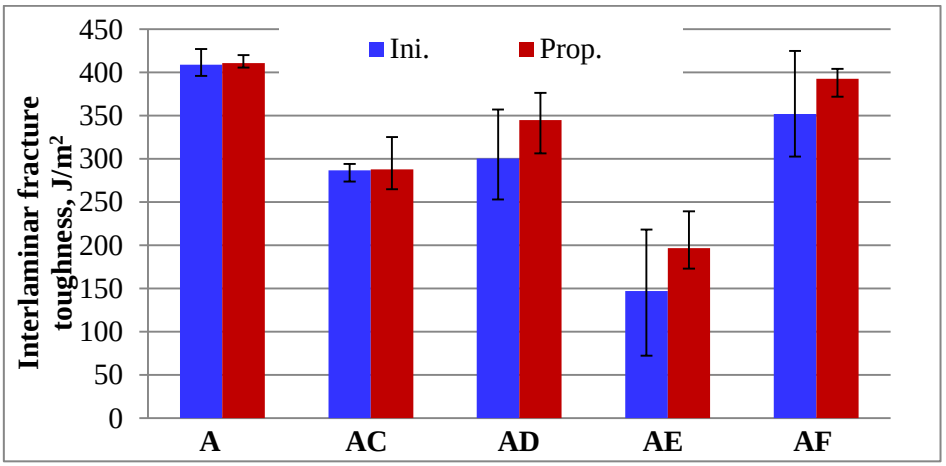

Fig.2-9. Initiation and propagation fracture toughness of CF/ VE composites.

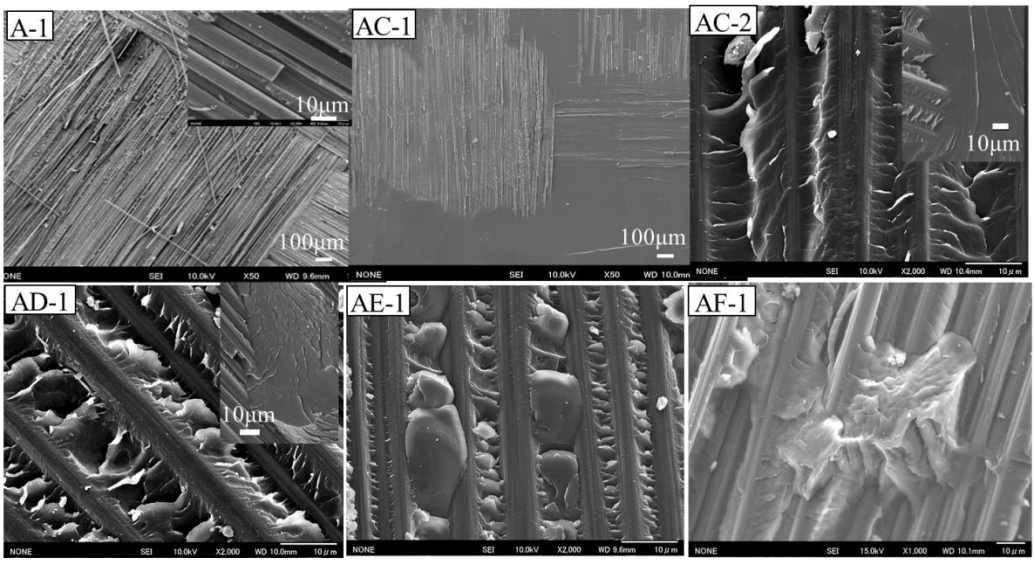

Fig.2-10. SEM images of fracture surfaces of CF/VE composites at the crack propagation area: A-1: Low magnification image of A; AC-1: Low magnification image of AC; the rest: high magnification of AC, AD, AE,AF.

2.3.5 Tension-tension fatigue properties

The fatigue life of CF/VE composites versus different maximum cyclic stress (S-N curve) are plotted in Fig.2-11. Tension-tension fatigue test results at the maximum applied cyclic stress of 567 MPa which is 70% of the static tensile strength of CF/AC composite are shown in Fig.2-12. Due to slight batch to batch variations the fatigue life of CF/A and CF/AD composite showed a large scatter. Herein, the average fatigue life of CF/A and CF/AD was taken to discuss. CF/A and CF/AD composites, especial CF/A composite whose fatigue life were low failed without a large scale of delamination can be considered as sudden death. It might be explained by random suddenly breakage of warp bundles due to defect of CF or stress concentration, and subsequently resulted in comprehensive breakage of CFs caused by stress redistribution. While a comprehensive interlaminar delamination happened in the specimens with higher fatigue life after failure. The specimen of CF/A and CF/AD whose fatigue life was long and who failed with comprehensive delamination was taken to investigate the fatigue damage initiation and propagation latter. The fatigue life of CF/AE composite was several times longer than CF/A composite where both of the matrix toughness and CF/matrix adhesion increased slightly. With improvement of toughness of matrix increasing continuously, fatigue life extended correspondingly that CF/AD composite performed a slight longer fatigue life than CF/AE composite. Similarly, fatigue life increased significantly when the CF/matrix adhesion was improved in CF/AC composite compared to CF/AD composite. Further, CF/AF composite performed better fatigue properties than CF/AC composites just when matrix was further toughened. The fatigue life of CF/AC and CF/AF composite has been improved significantly by several ten times than CF/A composite. Therefore, it can be described that with increasing both of fracture toughness of matrix and CF/VE adhesion, the fatigue life of CF/VE composites increased. In the other word, both of matrix toughness and CF/VE adhesion contributed to the improvement of fatigue performance of CF/VE composites positively.

Fatigue properties of CF/AX composites at other maximum applied stress exhibit similar behavior as their performance at maximum applied stress of 567MPa. Namely, fatigue life of CF/VE composites increase with increasing of matrix toughness and CF/VE adhesion. It is clearly observed when the maximum applied stress is high. At low maximum applied stress (527 MPa), they still perform similar trend due to fatigue

test stopped at 1 million cycles, but it needs further confirmation.

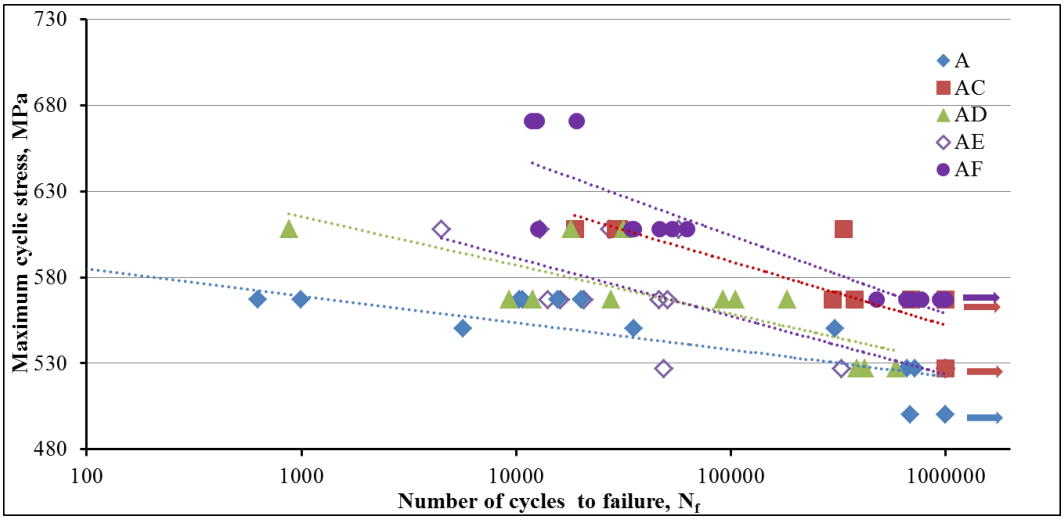

Fig.2-11. S-N curves of CF/VE composites

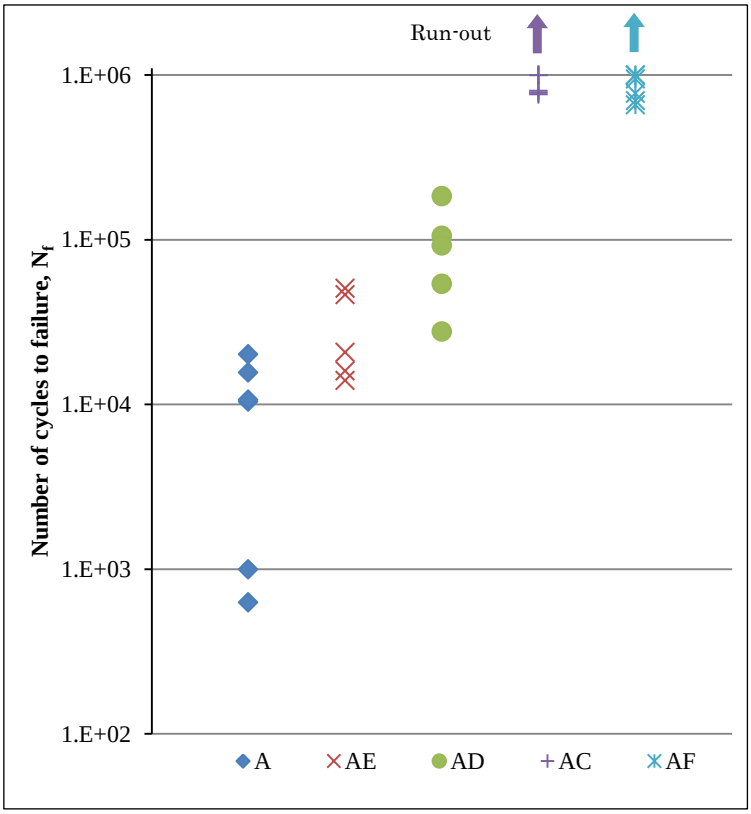

Fig.2-12. Fatigue life of CF/VE composites at maximum cyclic stress of 567MPa

With an increase of loading cycles, internal damage must be accumulated in the specimen such as fiber debonding, transverse cracks, delamination at the cross-over points between warp and weft yarns. Significant fiber breakage might occur at the final

stage of fatigue as well as interlaminar delamination. Due to those damages accumulation, observed Young's modulus are decreasing for all specimens with an increase of loading cycles. Therefore, damage D_{stiff} was estimated by Young's modulus decrease that measured in situ by extensometer and expected to represent the fatigue damage degree of composite materials [25]. However, due to a limited gage length of the extensometer (25mm), the stress-strain curve measured by the extensometer does not reflect the damage progression occurring outside the gage length. Occurrence of final failure of specimens does not always occur within the gage length. On the other hand, stroke between two specimen grips reflects the all internal damage in the specimen. Therefore, another parameter D_{slope} based on slope of stroke displacement-stress curves is induced. However, it is also influenced by the chucks deformation as well as slip between the specimen and the grip. In addition, the accuracy of stroke measurement is not accurate as high as that of the extensometer. Theoretically, no differences exist between two parameters as long as both measurements are perfect. Herein, two parameters were displayer for readers' convenience. D_{stiff} and D_{slope} are shown as Eq.6.

$$D_{stiff}=1-E(n)/E_0$$

$$D_{slope}=1-S(n)/S_0 \qquad (6)$$

E(n) and S(n) is the dynamic modulus and dynamic slope of displacement-stress curve at cycle number n respecitively. E_0 and S_0 is the initial modulus and initial slope of displacement-stress curve at the first cycle of fatigue test respecitively. Damage D_{stiff} estimated from σ-ε curves is more straightly reflecting the internal damage accumulation, such as matrix cracks much affecting the stiffness of the composite. Damage D_{slope} shows the averaged damage, in other words, the sum of all damage in the specimen.

Typical damage evolution of each type of CF/VE composite during fatigue test based on D_{stiff} and D_{slope} are displayed in Fig.2-13. The damage evolution of composites can be described as three stages that are initial stage, middle stage and final stage. CF/A composite showed a most rapid damage growth at initial stage (Fig.2-13-inserted). Similarly, CF/AC and CF/AE composites also displayed a fast development of damage at fatigue initial stage. Damage in CF/AD composite grew slowly compared to CF/A,

CF/AC and CF/AE composites. Damage in CF/AF composite displayed a most slow linear growth until ~5x10^5 cycles. A good relation between damage degree of composites at initial stage and matrix toughness was observed. Namely, damage initiated lately and grew slowly with increasing the fracture toughness of matrix resin. At fatigue middle stage, the damage in CF/A composite accumulated fastest. CF/AE and CF/AD also developed damage faster than CF/AC and CF/AF composites. CF/AC and CF/AF showed a no apparent increase of damage before final fatigue stage. This damage growth speed is consistent with the interfacial bonding between CF and each resin. At final stage, fiber breakage is dominant damage mode which cause specimens to fail rapidly. CF/A, CF/AD and CF/AE didn't show an apprent final stage might ascribe to fiber breakage happened in the specimens throughout middle stage. CF/AC composite showed a rapid stiffness degradation at final stage due to severe fiber breakage, which occurred eralier than CF/AF composite. In comparison with D_{stiff} curve of CF/AF composite, D_{slope} curve shows a gradual growth at middle and final stage (shaded region in Fig.2-13) due to occurrence of damage beyond the measure area of extensometer. CF/AD and CF/AC composite also showed the similar behavior. It indicated that D_{slope} certainly reflected the overall damage evolution of specimens especially at fatigue middle and final stage.

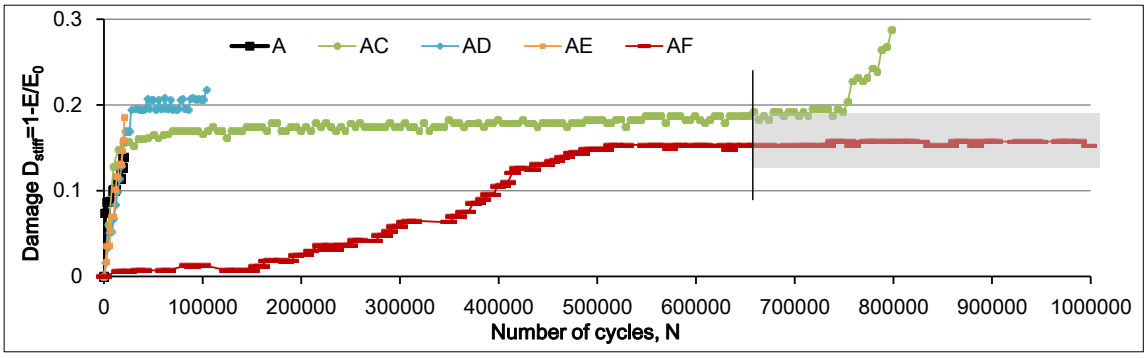

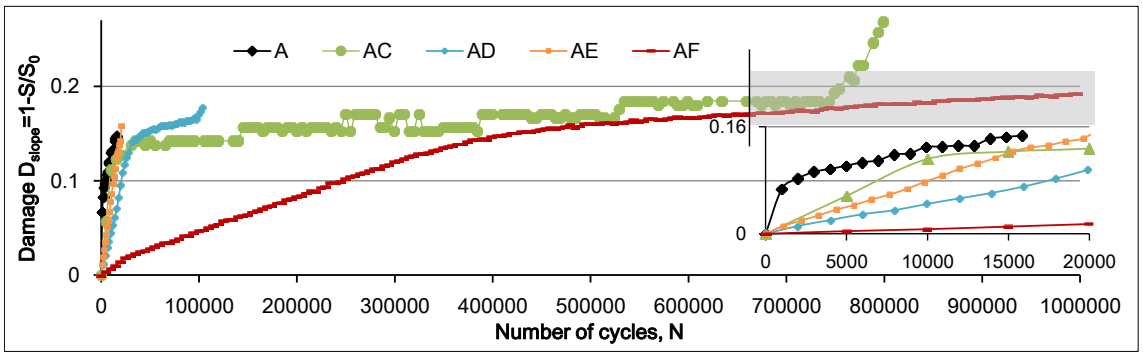

Fig.2-13. Damage evolution based on parameter D_{stiff} and D_{slope} (inserted: enlarged figure at fatigue initial stage)

2.3.6 Thermoelastic stress analysis and damage analysis

The detailed description of TSA and thermoelastic damage analysis (TDA) was demonstrated as Ref [17]. The TSA images were taken under a cyclic load of 5kN with a stress-ratio of 0.1. Before loading the maximum applied stress of 567 MPa, first TSA image was taken as the original statement without any damage in each specimen, as shown in Fig.2-14 (bottom left) in which the palette represents the temperature change during cyclic loading. The green disk regions represent the longitudinal (warp) bundle cells with a lower temperature change due to lower longitudinal thermoelastic materials coefficient while blue areas represent the weft bundle cells (Fig.2-14-top left). From TSA images at 1000 cycles of CF/VE composites (Fig.2-14, top), the green band shape regions circled by white cycle between two green disk regions represent the matrix cracks according to the decreased temperature change. The stress reduction happened at damage area can cause temperature to decrease. CF/A composite displayed a most severe damage mainly including transverse crack due to low toughness of resin and CF/A adhesion. On the other hand, damage in CF/AX composites initiated separately and showed a lower density than CF/A composite. More matrix cracks appeared in CF/AD, CF/AE as well as CF/AC than CF/AF composite because of lower toughness of matrixes than AF resin. It was confirmed by SEM observation (Fig.2-17) that transverse cracks with highest density in CF/A composite, high density in CF/AC and CF/AE, low density in CF/AD and almost no damage in CF/AF composite were found at ~1000 cycles (A, AC, AD, AE, AF-1k). No serious voids in the specimens were found according to SEM images and CT-scan images in next section. It indicated that the influence of defect in composites could be considered insignificant due to low void content. Therefore it showed that the fracture toughness of resin played a dominant role on the resistance to fatigue damage initiation in CF/VE composites. In addition, the damage degree of surface caused by matrix cracks performed similarly with that inside layers of specimen, which already had been demonstrated by other authors before [26]. The red cycle shape damage appeared at the boundary of bundles (Fig.2-14-A-1k) reflected the influence of inside local delamination occurring at cross-over points between warp and weft, as shown in Fig.2-15-A-1k observed at 1st CF layer by CT-can.

When the number of loading cycles increased, all the CF/VE composites showed an increase of damage in the form of increase of crack density and local delamination as confirmed by Fig.2-18. There was almost no significant damage growth in CF/A composite from ~5000 cycles to ~10^4 cycles because of the saturated transverse crack density namely the characteristic damage state (CDS) [27]. From ~5000 cycles of CF/A, ~10^3, ~$5x10^4$, ~$2x10^4$ and ~$4x10^5$ cycles of CF/AC, CF/AD, CF/AE and CF/AF respectively, the green disk regions represent matrix cracks occurred at weft bundles according to the lower temperature change caused by damage. Moreover, the red cycle regions appeared at the boundary of bundles represented local delamination that occurred serious inside of specimens as same behavior with CF/A composite (Fig.2-14-A-10k). It indicated that the transverse crack at weft bundles was almost saturated. When the weft bundles delaminate completely, the occurrence of new transverse crack becomes hard. CF/AC and CF/AE came to CDS of transverse crack faster than CF/AD. Before CDS of transverse crack, damage in CF/AC and CF/AE grew faster than CF/AD which was consistent with the result of stiffness degradation (Fig.2-13, inserted). Furthermore, the growth of damage in CF/AF was most slow and came to CDS of transverse crack even after $4x10^5$ cycles indicating that a higher ability of resistance to initiation and propagation of transverse cracks existed. It further confirmed by SEM observation, after ~1000 cycles of CF/A composite (Fig.2-18-A-1k), several ten thousand cycles of CF/AC and CF/AE (Fig.2-18-AC-5k, AE-10k), ~$4.5x10^4$ cycles of CF/AD (Fig.2-18-AD-45k), ~$5x10^5$ cycles of CF/AF composite (Fig.2-18-A-500k), almost constant density of transverse crack was found. Therefore, it can say that damage developed slowly and transverse crack saturated lately with increasing the fracture toughness of matrix resin while the CF/matrix adhesive strength didn't exhibit any obvious effect on damage initial and growth at the initial stage of fatigue test.

Furthermore, the TDA was applied to investigate the damage degree at low fatigue cycles. As explained by Fujii et al. [17], TDA images present two-dimensional thermoelastic information related to only damage initiation and growth by removing the inhomogeneity noise such as construction pattern. The degree of temperature change roughly reflects the damage level in a woven fabric composite. TDA images of all CF/VE composites are shown in Fig.2-16, where the palette represents the damage

degree. It revealed that the damage initiated earlier and grew faster until CDS of transverse crack with the decrease of fracture toughness of matrix resins.

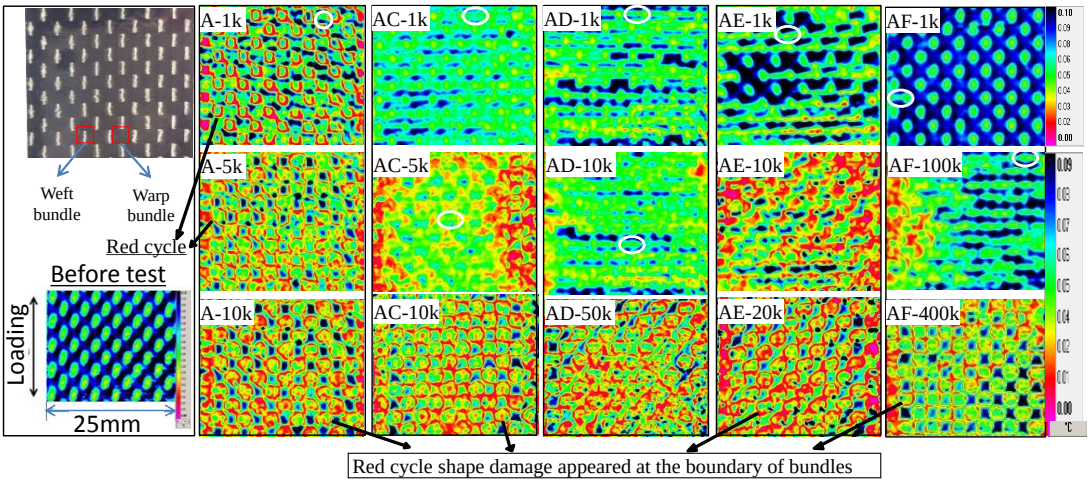

Fig.2-14. TSA images of CF/VE composites (A, AC, AD, AE, AF) before fatigue test (bottom left) and at expected cycles, the symbol k represents 1000.

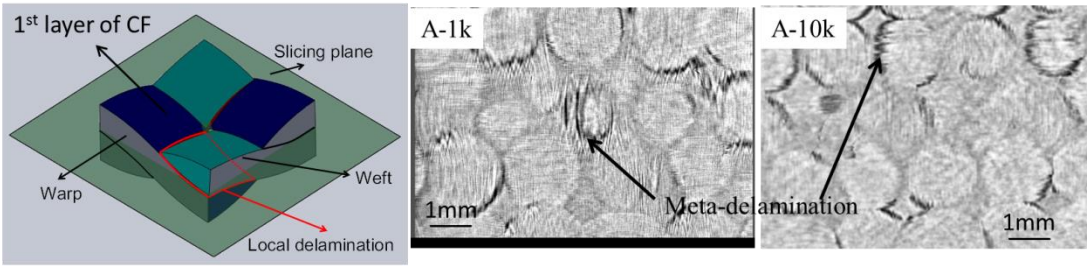

Fig.2-15. The local delamination occurring at cross-over points between warp and weft in the 1st CF layer (in other words, outermost layer closed to the surface) of CF/A composite observed by CT-scan at 10^3 cycles (A-1k) and 10^4 cycles (A-10k) respectively.

The damage in CF/VE composites was further observed by SEM after certain fatigue cycles, as shown in Fig.2-17 and 2-18. From Fig.2-18, matrix cracks first initiated at CF/VE interface in CF/A composite separately and subsequently linked to form a transverse crack rapidly due to low toughness of matrix and weak CF/A adhesion. On the other hand, matrix cracks in CF/AX composites (here AC with highest IFSS and AE with lowest IFSS were chosen as examples) occurred at matrix closed to CF/matrix interface. The formation mechanism of transverse crack provided a good evidence to confirm that AX resins performed stronger CF/matrix adhesion than control resin. In

addition, the similar formation behavior of transverse cracks with CF/A was also found in CF/AX composites. The above results confirmed that the CF/matrix adhesive bonding had less effect on the resistance to the initiation and propagation of transverse crack in CF/AX composites based on results obtained by TSA method because cracks initiated at matrix and propagated along matrix. With increasing matrix toughness, the initiation and propagation of matrix was delayed to reduce the degradation of stiffness of CFRP at fatigue initial stage. Moreover, the stress concentration around CF/matrix interface probably increased when CF/matrix adhesion increased and subsequently caused the matrix cracks more likely to initiate around interface (CF/AC composite).

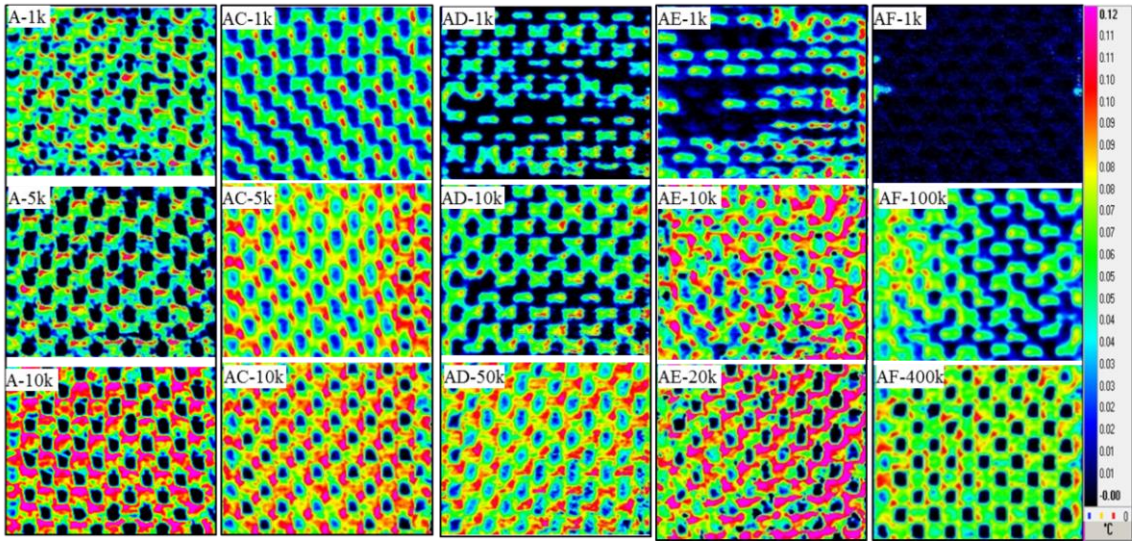

Fig.2-16. TDA images of CF/VE composites (A , AC, AD, AE, AF) at expected cycles.

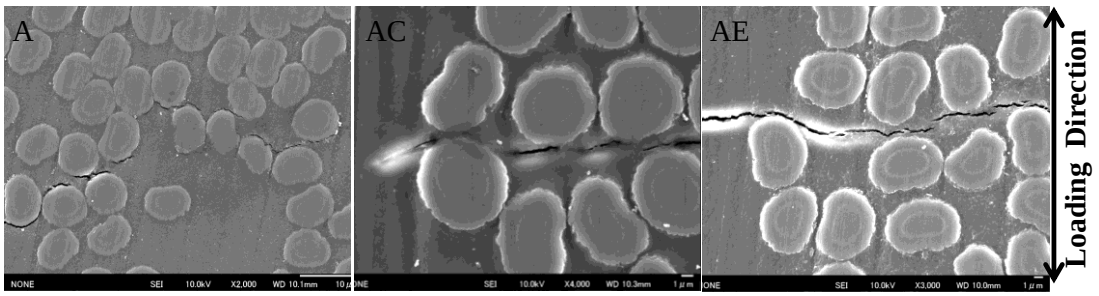

Fig.2-17. SEM images of transverse crack in CF/A, CF/AC and CF/AE at 1000 cycles.

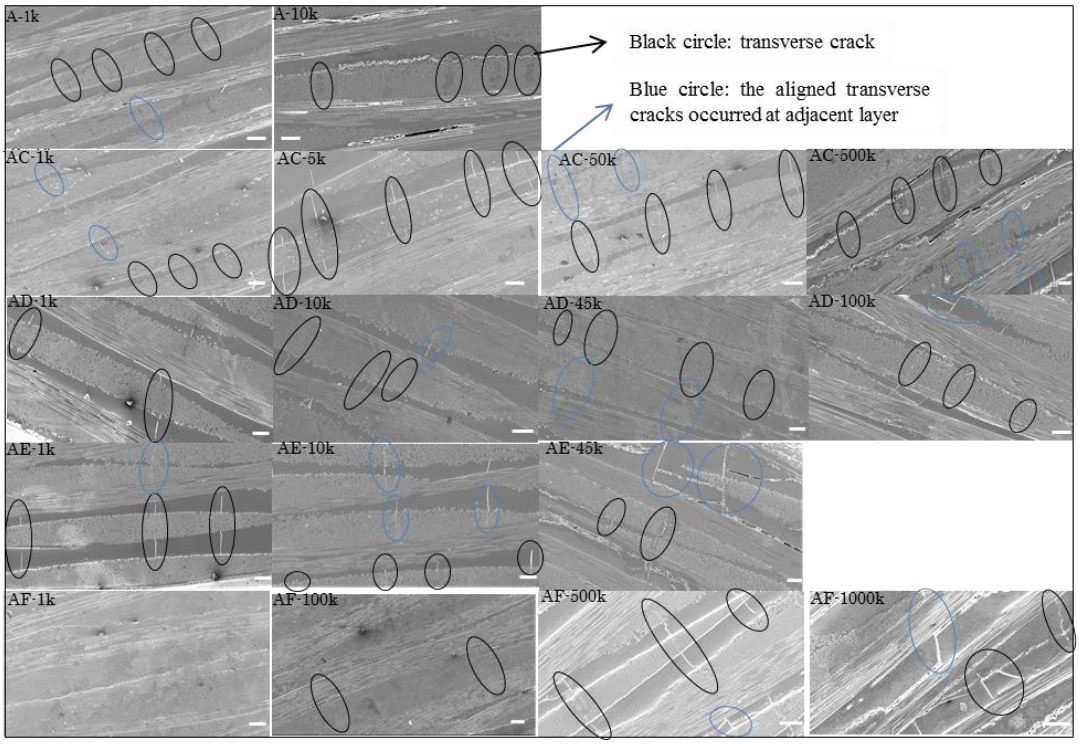

Fig.2-18. SEM images of damage in CF/VE composites (A, AC, AD, AE, AF) at expected cycles (The scale bar is 100 μm).

2.3.7 Fatigue damage growth

The damage at fatigue middle stage mainly including local delamination and interlaminar delamination between CF layers was further investigated by CT-scan after expected fatigue cycles, as shown in Fig.2-19 and 2-20. The symbols L and T represent longitudinal and transverse cross section of specimens respectively. The loading direction is longitudinal direction. The delamination of all CF/VE composites initiated from edge of specimens and grew faster at edges, caused by edge effect and stress concentration at edge of narrow section. Here, the center area of specimens was chosen to observe by CT-scan. Local delamination has already occurred in CF/A composite at ~1000 cycles due to earlier initiation of transverse cracks (Fig.2-19-A-1k-T and L). The length of local delamination is almost 2mm that equalizes the width of weft or warp bundle. The local delamination was localized at CF bundle cells at both transverse and longitudinal direction. As fatigue cycles increasing, the density of local delamination increased (Fig.2-19-A-10k). The adjacent local delamination linked together through matrix crack at gap between CF layers or transverse cracks to form long interlaminar delamination at both transverse and longitudinal direction. The interlaminar

delamination propagated along interface between weft and matrix resin also occurred and progressed as confirmed by Fig.2-18-A-10k. The delamination in CF/A composite at ~10^4 cycles was severe that almost every interface between CF layers was delaminated, which resulted in CF broke sporadically and related to finial failure. Local delamination almost didn't happen before ~$4.5x10^4$ cycles in CF/AD composite. At ~$4.5x10^4$ cycles (Fig.2-19-AD-45k), a few of local delamination occurred separately and was localized at bundle cells as same behavior with CF/A composite. When came to ~10^5 cycles ((Fig.2-19-AD-100k), severe interlaminar delamination occurred accompanying with matrix cracks happened increasingly (Fig.2-18-AD-100k). In CF/AE composite, local delamination occurred earlier than CF/AD composite due to fast growth of transverse cracks at fatigue initial stage. At ~10^4 cycles (Fig.2-19-AE-10k), a small amount of local delamination happened at both transverse and longitudinal direction. The density of local delamination of CF/AE composite was lower than CF/A composite at same fatigue cycles but higher than CF/AD composite where the CF/matrix adhesion decreased. At ~$4.5x10^4$ cycles (Fig.2-19-AE-45k), as same behavior with CF/A and CF/AD, local delamination grew longer and linked to form interlaminar delamination drastically which was faster than CF/AD composite.

Local delamination in CF/AC composite as well as CF/AE composite occurred earlier than CF/AD composite before ~$5x10^4$ cycles due to earlier initiation of transverse crack. At ~$5x10^4$ cycles (Fig.2-20-AC-50k), many transverse bundles delaminated along warp/weft bundles interface. The density and length of delamination in CF/AC composite lower and shorter than CF/AE composite which might be ascribed to both higher fracture toughness and IFSS of matrix resins than AE. At ~$5x10^5$ cycles (Fig.2-20-AC-500k), density and length of delamination increased, but propagated slowly than CF/AD composite. At ~$7x10^5$ cycles (Fig.2-20-AC-700k), severe interlaminar delamination was found, which caused each CF laminate isolated and increase of stress concentration to accelerate the breakage of CFs resulting in final failure of composites. For the CF/AF composite, even at ~10^5 cycles (Fig.2-20-AF-100k), only a small amount of local delamination occurred with a short length at both transverse and longitudinal direction. With increasing fatigue cycles (Fig.2-20-AF-500k), increased local delamination appeared but was separated and localized. Even when it came to ~10^6 cycles (Fig.2-20-AF-1000k), the delamination

weren't as serious as CF/AC composite at ~7x10^5 cycles that contributed to longer fatigue life. The damage in CF/AF composite initiated later and grew more slowly than other composites due to both of higher matrix toughness and CF/AF adhesion. Base on above observation, a conclusion can be made that the initiation of delamination depended on toughness of matrix significantly while the growth of delamination close related to CF/matrix adhesion.

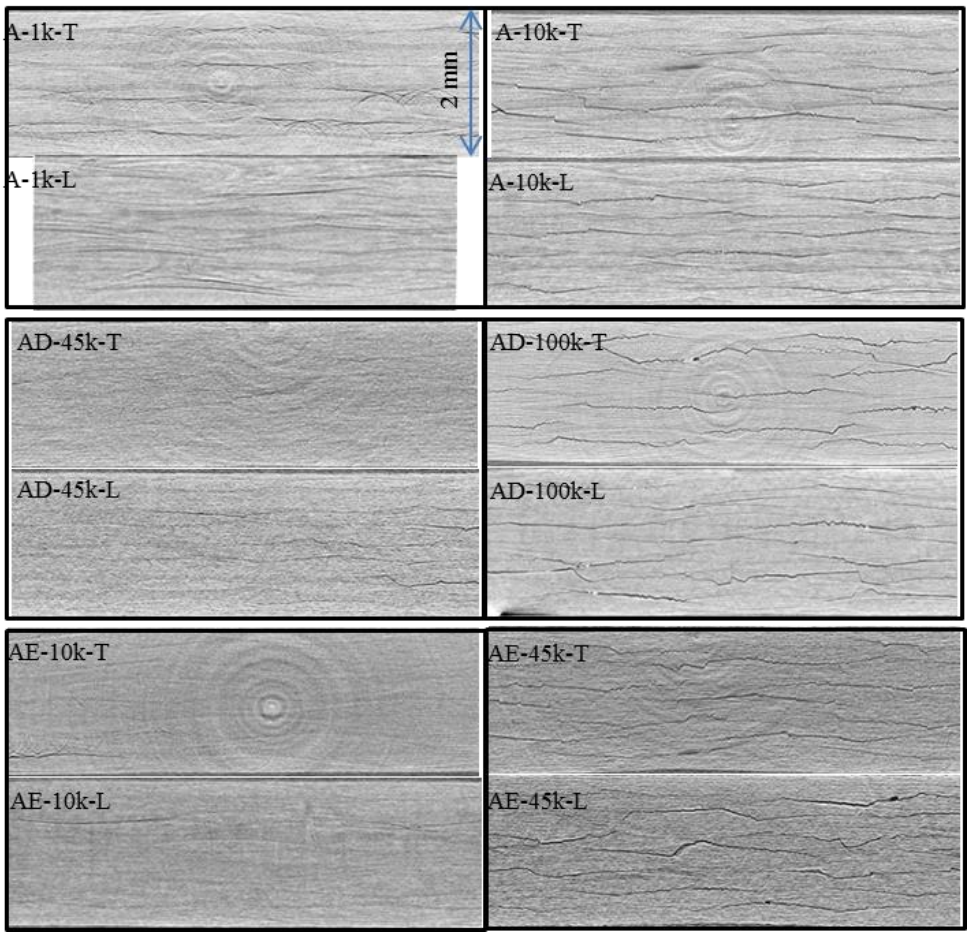

Fig.2-19. CF-scan images of CF/VE composites (A, AD and AE) with short fatigue life.

It was observed that the fracture mode of fatigue delamination of all the specimens mainly was interfacial debonding failure that why the interfacial bonding played so important role at fatigue middle and even final stage. As shown in Fig.2-21, interface deboning with smooth CF surfaces and low degree of matrix deformation was found in CF/A composite. Interfacial debonding accompanying with a slight degree of cohesive matrix failure was found in CF/AX composite indicating that the fatigue cracks were deflected during their propagation. The hackle pattern caused by shear failure of matix

was found among CFs in CF/AX composites. The failure feature of matrix at interface and cohesive failure area is close related to fracture toughness of AX matrix, where tougher behavior (inserted) indicating a larger scale of matrix deformation of CF/AD and CF/AF composites was observed.

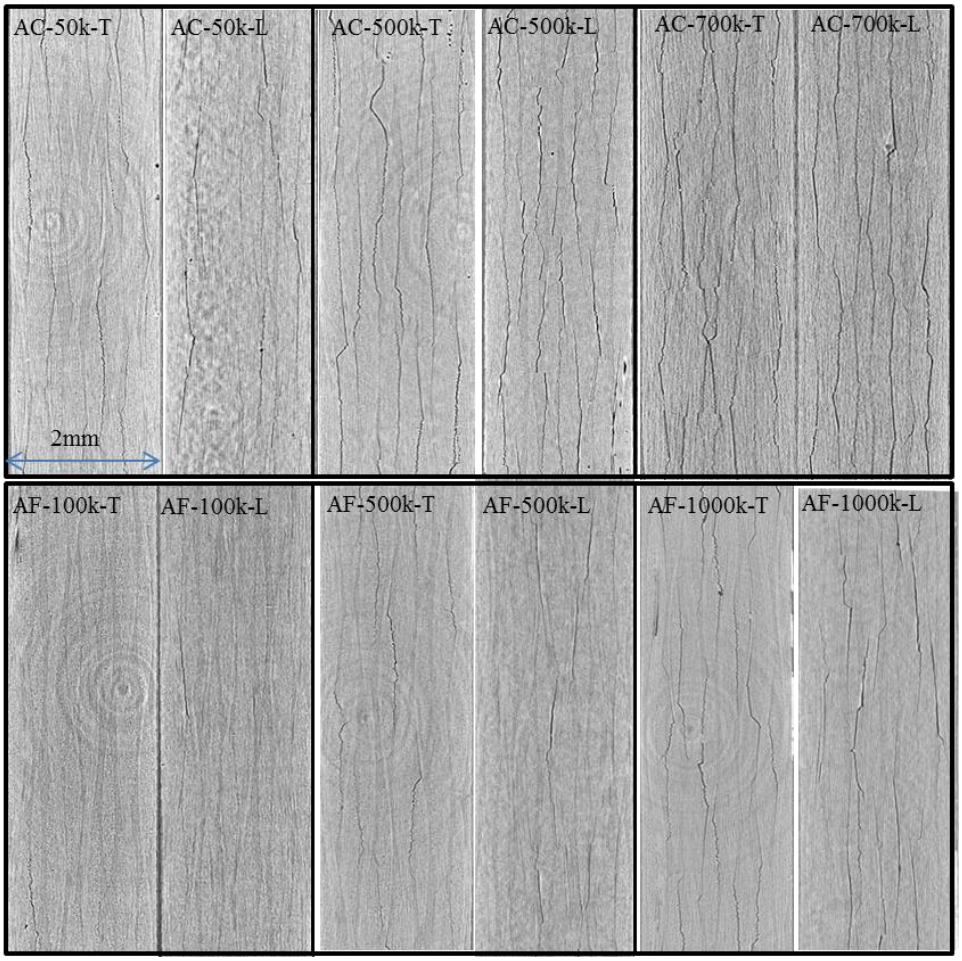

Fig.2-20. CF-scan images of CF/VE composites (AC and AF) with long fatigue life.

2.3.8 Model of relationship between matrix properties and fatigue life of CFRP

Based on above experiment data, the relationship between matrix properties (fracture toughness of matrix and CF/VE adhesion) and fatigue life of CF/VE composites was plotted in Fig.2-22. x axis represents the increment ratio of fracture toughness (K_{IC}) of AX resins compared to control resin A. y axis represents the increment ratio of CF/AX adhesive strength (IFSS) compared to CF/control resin A. z axis represents the increment ratio of fatigue life of CF/AX composites compared to CF/A composite. The 3D graph was plotted to reflect how the matrix properties influence the fatigue life of

CF/VE composites. Correspondingly, it is possible to use following equation (Eq.7) to fit the mode and describe the relationship.

$$N_f = a \cdot e^{bx+cy} \quad (7)$$

Where a, b and c are depended on materials, loading conditions and so on. Here, a=7.75E-5, b=6.94, c=2.61 by fitting the experiment data. The multiple correlation coefficient between the resin properties and the number of cycles to failure of CF/VE composites was 0.995 indicating a strong positive fit. Fatigue life of CF/VE composites increases exponentially with the increase of toughness or IFSS. Especially, the positive coupling effect was clearly observed. However, the optimum toughness and IFSS must exist as discussed in the introduction because of brittle behavior of matrix at interface when the fiber/matrix adhesion is extreme high as well as the stiffness or strength of composites drop when toughness increases. The further experiment is in progress. It was found that b>c indicating that IFSS contributes to the fatigue properties more than the toughness of matrix. The IFSS dominated the tensile strength of CFRP resulting in the higher capability to resist the breakage of CF bundles at warp. The high IFSS can provide higher resistance to propagation of delamination resulting in delaying the failure of CFs at warp. When CF/VE adhesion or toughness is low, the coupling effect of matrix toughness and CF/VE adhesion on the fatigue properties is unobvious. With the increase of K_{IC} or IFSS, the coupling effect becomes more significant, but further confirmation is necessary.

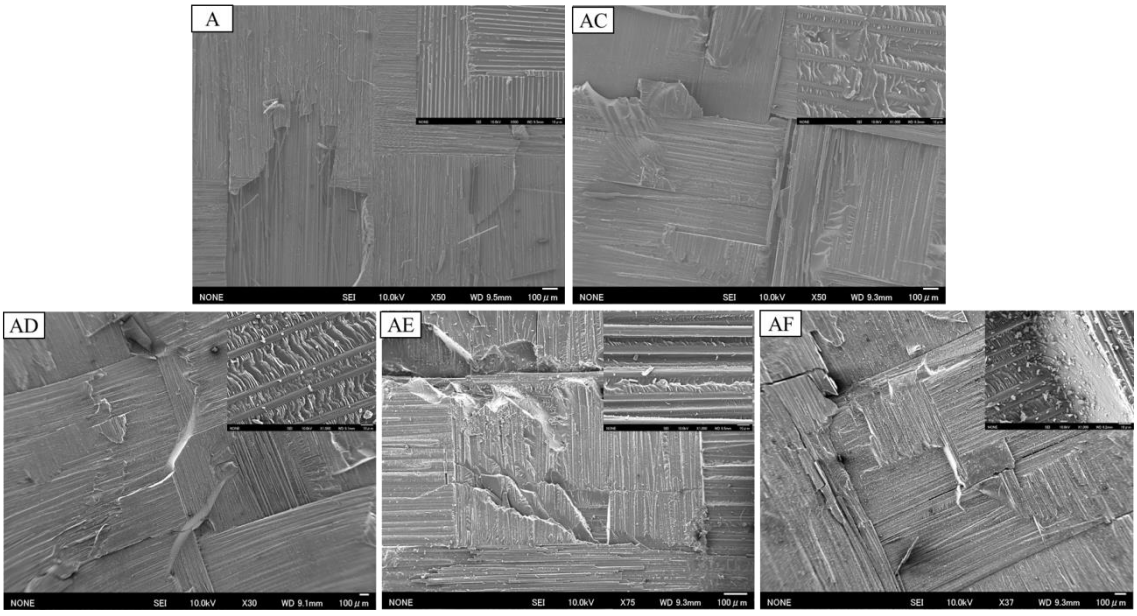

Fig.2-21. SEM of delaminated area of CF/V composites after fatigue failure (inserted figures are magnified images).

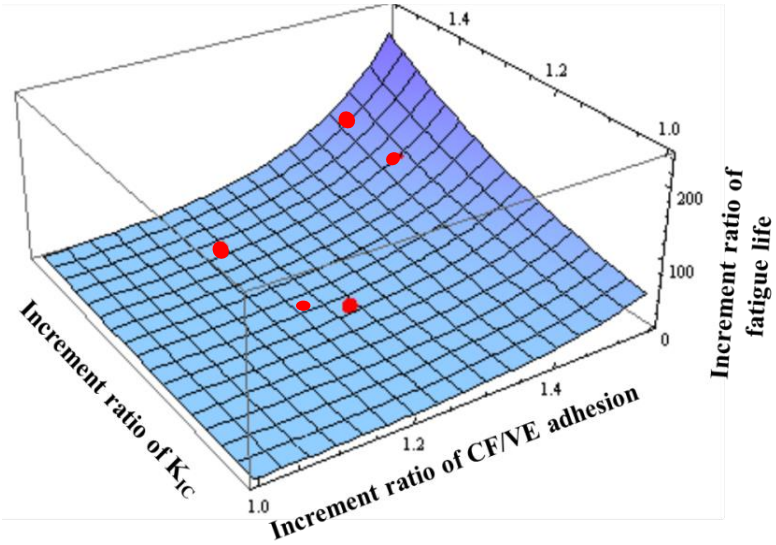

Fig.2-22. Relationship between the matrix properties (K_{IC} and CF/VE adhesion) and fatigue life of CF/VE composites

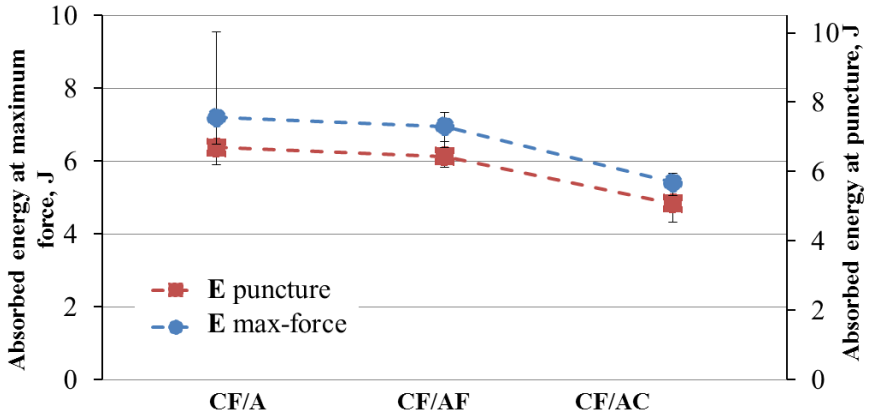

Fig.2-23. Puncture impact properties of CF/VE composites

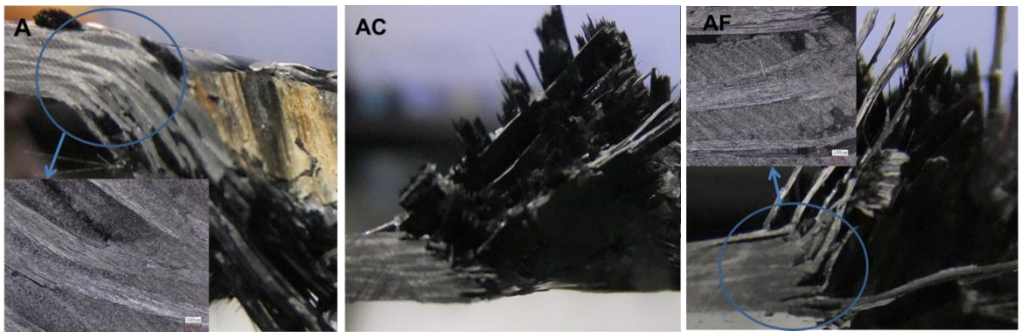

Fig.2-24. Cross section photos of CF/VE composites after impact.

2.3.9 Impact properties

The impact resistance behavior of woven fabric CF/VE composite was investigated by low speed puncture impact test. The impact properties of CF/VE composites under low speed puncture impact are shown in Fig.2-23. Herein, E_m and E_p are used to characterize the impact energy absorbed at maximum impact force and puncture energy absorbed when impact force decrease to half of maximum impact force. It is found that both of E_m and E_p of CF/AX composites are lower than CF/A composite. E_m and E_p of CF/AF composite show a slight decrease by 3.9% and 3.4% respectively. While E_m and E_p of CF/AC composite decrease by 24.1% and 24.8% respectively. Furthermore, the cross-section was observed by optical microscopy and SEM (Fig.2-24). It was found that they behaved different fracture mechanism. The fracture mechanism of CF/A composite is bending failure accompanying with matrix cracking and delamination occurrence might due to low CF/A adhesion. On the other hand, CF/AC composite displays a shear failure feature that carbon fibers break easily without absorbing much energy. The higher CF/AC adhesion results in more brittle behavior of resin at CF/VE interface or interlaminar area namely notch-sensitive behavior. For the CF/AF composite, the failure mode is the combination of bending and shear failure feature. The bending failure and damage occurs in matrix or interface result in consuming more energy during impact test. It might be contributed by the improved matrix toughness of AX than AC. The impact strength of CFRP increased with the increase of G_{IC} of CFRP because of the more energy absorption during deformation.

2.4 Conclusion

The static tensile and flexural strength of CF/VE composites were much affected by the matrix properties: fracture toughness of matrix and CF/VE adhesive strength. An improvement by up to 37.3% of tensile strength and up to 37.1% of flexural strength was achieved via modulating the parameters of the mechanical properties of VE resins. The influence of two matrix properties on the static properties of CF/VE composites has been investigated. CF/VE composites performed different failure mode and strain at failure due to the effect of matrix properties under the static tensile or flexural loading. On the contrary, the interlanmiar fracture toughness of CF/VE as well as impact resistance capability decreased compared to CF/A composite. The different fracture

mode dominated the energy absorption during fracture of specimens. Tension fatigue life of CF/VE composites was improved by several ten times via modulating the parameters of the mechanical properties of VE resins. Based on TSA method and further SEM observation, the fracture toughness of resin affected the initiation and growth of matrix cracks especially transverse cracks dominantly because cracks tended to initiate at matrix and propagate along matrix due to high IFSS. At middle stage of fatigue test, delamination tended to initiate early in composites made by matrix resin with lower fracture toughness due to earlier initiation of transverse crack. High CF/VE adhesive strength performed a positive effect on the resistance to delamination growth to extend fatigue life of composites finally. At fatigue final stage, serious delamination caused fast failure of specimens. A simple model has been used to characterize the relationship between matrix properties and fatigue life of CF/VE composites. The positive hybrid effect of fracture toughness of matrix and CF/VE adhesion on the static tensile strength and fatigue life of CF/VE composites was found.

References

1. Mouritz AP, Bannister MK, Falzon PJ, Leong KH. Review of applications for advanced three-dimensional fibre textile composites. Compos Part A: Appl Sci Manuf 1999; 30(12):1445-1461.
2. Daniels WE. Vinyl Ester Polymers. In Encyclopedia of Polymer Science and Engineering, 2nd ed.; Mark, H. F., Ed. Wiley: New York, 1985;17: 393.
3. Kootsookos A, Burchill PJ. The effect of the degree of cure on the corrosion resistance of vinyl ester/glass fibre composites. Compos Part A: Appl Sci Manuf 2004; 35(4):501-508.
4. Zhu J, Imam A, Crane R, Lozano K, Khabashesku V, Barrera E. Processing a glass fiber reinforced vinyl ester composite with nanotube enhancement of interlaminar shear strength. Compos Sci Technol 2007; 67(7-8):1509-1517.
5. Fujii T, Amijima S. Okubo K. Microscopic fatigue processes in a plain-weave glass-fibre composite. Compos Sci Technol 1993; 49 (4):327-333.
6. Gao F, Boniface L, Ogin SL, Smith PA, Greaves RP. Damage accumulation in woven-fabric CFRP laminates under tensile loading: Part 1. Observations of damage accumulation. Compos Sci Technol 1999;59 (1):123-136.
7. Yoshioka K, Seferis JC. Modeling of tensile fatigue damage in resin transfer molded woven carbon fabric composites. Compos Part A: Appl Sci Manuf 2002; 33(11):1593-1601.
8. Curtis PT. The fatigue behaviour of fibrous composite materials, Journal of Strain Analysis for Engineering Design. 1989; 24(4):235-244.
9. Hartwig G, Hubner R, Knaak S, Pannkoke C. Fatigue behaviour of composites. Cryogenics. 1998; 38(1):75-78.
10. Deng S, Ye L. Influence of fiber-matrix adhesion on mechanical properties of graphite/epoxy composites: I. Tensile, flexure, and fatigue properties. J. Reinf Plast Comp 1999; 18(11):1021-1040.
11. Burau MN, Perrin F, Denault J, Dickson JI. Interlaminar fatigue crack propagation in continuous glass fiber/polypropylene composites, Int J Fat 2002; 24(2-4): 99-108.
12. Gamstedt EK, Effect of debonding and fiber strength distribution on fatigue-damage propagation in carbon fiber-reinforced epoxy. J Appl Polym Sci 2000;

76(4):457-474.

13. Goutianos S, Peijs T. Fatigue damage mechanisms in carbon-epoxy multi-fibre model composites. Adv Comp Lett 2001; 10(1), 21-32.
14. Sjögren BA, Berglund LA. The effects of matrix and interface on damage in GRP cross-ply laminates, Compos Sci Technol 2000; 60(1):9-21.
15. Gassan J, Dietz T. Fatigue behavior of cross-ply glass-fiber composites based on epoxy resins of different toughnesses. Compos Sci Technol 2001; 61(1): 157-163.
16. Kawai M, Morishita M, Fuzi K, Sakurai T, Kemmochi K. Effects of matrix ductility and progressive damage on fatigue strengths of unnotched and notched carbon fibre plain woven roving fabric laminates. Compos Part A: Appl Sci Manuf 1996; 27(6): 493-502.
17. Uenoya T, Fujii T. Influence of Matrix Toughness on Damage Initiation and Growth in Carbon Fiber Fabric Composites. J Reinf Plast Compos 2000; 19(1) :83-94.
18. Zhao FM, Takeda N. Effect of interfacial adhesion and statistical fiber strength on tensile strength of unidirectional glass fiber/epoxy composites. Part I: experiment results. Compos Part A: Appl Sci Manuf 2000; 31 (11):1203-1214.
19. Goda K. The role of interfacial debonding in increasing the strength and reliability of unidirectional fibrous composites. Compos Sci Technol 1999; 59(12):1871-1879.
20. Oya N, Hamada H. Mechanical properties and failure mechanisms of carbon fibre reinforced thermoplastic laminates. Compos Part A: Appl Sci Manuf 1997; 28(9-10):823-832.
21. Curtis GJ, Milne JM, Reynolds WN. Non-Hookean behaviour of strong carbon fibres. Nature 1968; 220: 1024-1025.
22. Shioya M, Hayakawa E and Takaku A. Non-hookean stress-strain response and changes in crystallite orientation of carbon fibres. J Mater Sci 1996; 31(17): 4521-4532.
23. Gagel A, Fiedler B, Schulte K. On modelling the mechanical degradation of fatigue loaded glass-fibre non-crimp fabric reinforced epoxy laminates. Compos Sci Technol 2006; 66(5):657-664.
24. Hine PJ, Brew RA, Duckett RA, Ward IM. Compos Sci Technol 1992;43: 37
25. Rikards R, Buchhoiz FG, Bledzki AK, Wacker G, Korjakin A. Compos Sci Technol 1996; 32:439.

26. Nishikawa Y, Okubo K, Fujii T, Uenoya T. Fatigue Damage Evaluation of Plain-Woven Carbon/Epoxy Composites Using Thermo-Elastic Technique. J Soc Mat Sci 2005; 54(5):494-499 (In Japanese).
27. Reifsnider KL, Talug A. Analysis of fatigue damage in composite laminates. Int J Fatigue 1980; 2(1):3-11.
28. Rahmanian S, Thean KS, Suraya AR, Shazed MA, Mohd Salleh MA, Yusoff HM. Carbon and glass hierarchical fibers: Influence of carbon nanotubes on tensile, flexural and impact properties of short fiber reinforced composites. Materials and Design 2013; 43:10-16.
29. Manikandan V, Winowlin Jappes JT, Suresh Kumar SM, Amuthakkannan P. Investigation of the effect of surface modifications on the mechanical properties of basalt fibre reinforced polymer composites. Compos Part B 2012; 43: 812-818.

Chapter III

Physical modification of matrix by nano fiber, and its effect on the mechanical performance of carbon fabric polymer composites

3.1 Introduction

Recently, fiber reinforced polymer matrix composites (FR-PMC) have been widely applied in aerospace, automotive, wind turbine blades, marine, aircrafts, sports fields because of unsurpassed strength-to-weight ratio. The mechanical properties of FR-PMC depend on damage development significantly under loading. The damage modes in FR-PMC under loading usually include matrix cracking, transverse cracking, interfacial debonding, delamination and fiber failure [1]. Many studies were conducted to significantly improve the mechanical properties of FR-PMC by arresting/trapping/delaying the growth of those damages due to an addition of nano materials to the matrix, such as nano silica [2], nano rubber particle [3], nano clay [4], nano fiber including CNT [5], nano polyvinyl alcohol (PVA) fiber [6], carbon nano fiber [7] and so on. Incorporation of nano materials with polymer matrix can act an effect on delay the initiation and propagation of matrix cracks and subsequent delamination under cyclic loading, which must resultantly extend the fatigue life of FR-PMC.

The energy absorption mechanisms in micro scale when incorporating nano fillers have been widely discussed. For the rigid silica particles, the main reinforcing mechanisms are crack deflection, particle debonding and plastic void growth. Rubber cavitation, void growth and matrix plastic deformation are considered as reinforcing mechanism for nano rubber fillers. Similarly, fiber bridging, crack blunting, crack deflection effect are provided by addition of nano fibers. With incorporation of nano fillers, toughness of matrix can be improved greatly according to former reinforcing mechanism, subsequently delay the initiation and propagation of matrix crack to delay the failure of composite specimens. On the other hand, the fiber/matrix adhesion performs stronger with addition of nano fillers resulting in improvement of load transfer efficiency to slow down the fiber breakage. However, few works have been focused on the investigation of the effect of nano fillers on matrix or interfacial properties to find

out the optimum volume of nano fillers to achieve excellent fatigue performance of FRP. As it has been mentioned before [8-9], optimum interfacial adhesion exists for achieving optimum tensile properties of FRP.

When surface-treated nano rubber particles (5-10 wt%) are dispersed into epoxy (EP) matrix, the interlaminar fracture toughness and fatigue performance can be significantly improved [10]. However, the observed Young's modulus and heat resistance of the composites probably degrade. Nano fibers having high strength, high Young's modulus and high T_g (glass transition temperature) are considered more effective reinforcement than nano particles for PMC due to their high aspect ratio. CNT has superior mechanical properties, considered as one of excellent nano fillers to improve the durability of PMC [11-13]. Unfortunately, the cost and carcinogenicity limit its application. Furthermore, the issues are still challenging such as surface treatment for better adhesion of CNT to polymer matrix and the dispersion of CNT into the matrix system.

PVA is a cheap, nontoxic, odorless and environmentally friendly thermoplastic polymer. Cellulose nano fiber such as MFC (micro fibrillated cellulose) extracted from plant pulp possess high strength and high stiffness combined with lower density than 1.5g/cm^3, biodegradability, renewability and good compatibility with resin [14-15]. The incorporation volume of nano PVA or MFC fiber can be reduce by reducing the diameter of fiber and subsequently reduced the effect on the viscosity of matrix after modification. In our previous works, cellulose fibers having the web-like network structure have already been used to improve the interfacial adhesion in a bamboo polymer composite [16] and interlaminar fracture toughness. The great possibility of fatigue life extension for CF/EP composites was also shown [17-18]. However, few works have been focused on the effect of nano fiber addition on the fatigue performance of FR-PMC.

In this study, the effect of the different nano fiber (such as nano PVA and MFC) with different size and stiffness on mechanical properties of resin including matrix toughness and CF/matrix adhesion was investigated. Furthermore its effect on the mechanical properties, especially fatigue performance of FR-PMC is investigated. The damage onset and propagation behavior of FR-PMC with addition of nano fiber was discussed. In addition, the effect of nano PVA or MFC content on the fatigue performance of FR-PMC is also studied.

3.2 Experimental methods

3.2.1 Materials

The plain woven carbon fiber cloth (Mitsubishi Rayon TR3110M) was used as reinforcement. A bisphenol A epoxy based vinyl ester conventional resin as control resin supplied by DH Materials Inc. was used as matrix resin for CF/VE composites. Acetyl acetone peroxide (Nof Corporation) was used as curing agent. 8%CoOCt was used as a promoter. Poly(vinyl alcohol) powder (Mw = 22.000 g/mol, degree of saponification = 86.5–89 mol%, pH = 5–7.5) supplied by Nacalai tesque (Kyoto, Japan) was used to prepare the nano PVA fiber. In addition, micro-fibrillated cellulose (Celish KY110G, water slurry containing 10 wt% fibers was used as filler to modify epoxy (E-828). The TEM image of MFC with a net structure is shown in Fig.3-1-b. The diameter was 50-200nm and mechanical properties are found elsewhere [19]. Modified aliphatic polyamine (JER cure-113) supplied by Japan Epoxy Resins company was used as curing agent for epoxy.

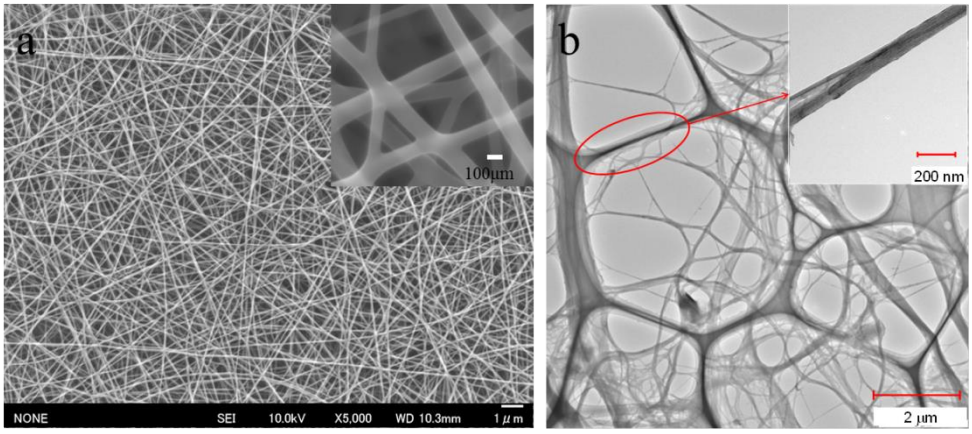

Fig.3-1. SEM image of nano PVA fiber (a) and TEM image of MFC (b).

3.2.2 Preparation of nano fibers modified CFRP

PVA powder (20 wt%) was added into distilled water to form solution. The detail fabrication process by electro-spinning was well demonstrated by the previous work in our laboratory [6]. The prepared nano PVA fibers were then put into oven at 100 ℃ for 72 hours to remove water completely. Nano PVA was directly mixed into the vinyl-ester resin with different contents (0, 0.03, 0.05 and 0.1 wt%) for 40 min by a process

homogenizer at a rotating speed of 15.000 rpm. Then promoter and curing agent was added into former mixture by a ratio of 100/0.2/1, then degassed in a vacuum oven for 10 minutes to remove voids. The mixture was then hand lay-upped with plain woven carbon fiber clothes with a CF volume fraction of ～50%, then cured at room temperature for 24 h and post cured at 60 ℃ for 3 h. In addition, CF/EP/MFC composites were prepared according to the previous works in our laboratory [15] with addition of 0.3 wt% and 0.8wt% MFC.

3.2.3 Mechanical testing

Single fiber test (SFT) was conducted to investigate the Weibull distribution of strength of CF (Mitsubishi Rayon TR50S) according to ASTM D 3379-75. The gauge length was 25 mm. About 60 fibers were tested under an EZ-test machine with a cross-speed of 1mm/min at room temperature. The Weibull scale and shape parameters were determined by obtained data.

The single fiber fragmentation test was used to investigate the CF/resin interfacial shear strength (IFSS) and CF fracture behavior with different nano fiber content. Single CF was embedded into pure resin or nano fiber modified resin and cured. The test was conducted under a polarization microscope. The average fragment length l at satuated state was in situ measured and the fracture behavior of fiber or matrix was observed. Then IFSS (τ) was calculated by Eq.1.

$$\tau = \frac{\sigma_{f(l_c)} d}{2 l_c} \qquad (1)$$

where σ_f is the CF strength at the critical length as evaluated based on above SFT, d is the CF diameter and l_c is the critical fragment length of CF. Where the critical fragment length is calculated from the average fragment length l by l_c=4l/3.

The fracture toughness tests of bulk VE resin were conducted according to ASTM D5045-99 at room temperature. All neat resin with addition of nano PVA fiber were cured at room temperature for 24 h and post cured at 60 ℃ for 3h. The single edge notch bend (SENB) specimens were used to test the fracture toughness (K_{IC}) under 3 points bending load. The pre-crack with several ten or hundred micro meters at tip of the notch was made by tapping the specimens on a fresh razor blade placed in the notch. The cross-head speed was set to 10 mm/min. More than 5 specimens of each kind of

VE/PVA sample were tested.

The tensile properties of CFRP were investigated by using a Shimadzu autograph universal testing machine according to ASTM D3039-08. The testing speed was set to 1 mm/min. The specimen dimension was 200 x 25 x 2 mm with a gage length of 100mm.

The mode-I interlaminar fracture toughness of CFRP was characterized by double cantilever beam (DCB) test using a universal mechanical testing machine according to ASTM D5528-01. Dimension of DCB specimens are 20x150x2 mm. The corrections for the end-block, DCB arm bending and root rotation were considered. The testing speed was set to 2 mm/min. The interlaminar fracture toughness for initiation (G_{IC}) and propagation (G_{IP}) of composites was calculated by the modified compliance calibration (MCC) method as described at chapter II. In order to investigate the delamination propagation rate under the different energy release rate range (da/dN-ΔG), the mode-I fatigue DCB test was conducted by an electromagnetic fatigue testing machine (MMT-101NB-10) under displacement-ratio $R = \delta_{max}/\delta_{min} = 0.1$ and frequency $f = 3Hz$ at room temperature.

Tension-tension fatigue test was conducted at stress-ratio $R = +0.1$ and frequency $f =$ 5Hz according to ASTM D3479 on the ServoPulser 50KN equipment at room temperature. Each fatigue test was run to 1 million cycles unless final failure happened before this limit. The specimen dimension for fatigue life test was 200 x 25 x 2 mm with a gauge length of 100mm. In order to investigate the damage propagation in CF/VE composites, when came to expected cycles fatigue test was stopped and specimens was cut into 20x20 mmm, and then taken to observe by CT-scan (Skyscan1172Micro-CT). Longitudinal-section was also carefully grinded and observed by scanning electron microscopy (SEM) by JSM-7001FD equipment.

The TSA images were obtained by using a commercial thermoelastic stress analyzer system (JEOL, model JTG-8010) through a thermo-camera with 0.14mm in spatial resolution. The TSA images were obtained at a certain cycle during fatigue test under the same testing condition with former tension fatigue test.

The puncture impact was conducted by Hydroshot (Shimadzu HTM) with a hardened steel hemispherical impactor of diameter 12.7 mm. The loading speed when impactor hitting specimens was set to 6.3 m/s. Dimensions of the specimen was ～50x50x2 mm.

The punch was driven vertically downward through the specimens who were tightly clamped to prevent slippage.

3.3 Results and discussion

3.3.1 Matrix properties

3.3.1.1 Fracture toughness

The prepared nano PVA fibers in this study have a diameter of about 80～100 nm. The modulus Young's modulus of nano PVA fibers have a broad range of 2-400 GPa which strongly depends on diameter of nano fibers. As reported by Fu et al.[20], Young's modulus of nano PVA fibers increased dramatically when the scales became very small (<80 nm). After incorporation of nano PVA fibers in to matrix, the fracture toughness of modified VE resins with different ratio of nano PVA fibers is shown in Fig.3-2. Fracture toughness of modified VE resin increases slightly by up to 14.3% compared to unmodified VE. The fracture toughness of VE containing nano PVA fibers increases with increasing nano fillers content. According to fracture surface of specimens at the initiation region, the pre-crack were well prepared with several ten or hundred micrometers. The fracture surface of unmodified VE is smooth without obvious matrix deformation or crack deflection. On the other hand, the fracture surface of modified VE resin shows rougher than that of unmodified VE (Fig.3-3, 0.1wt% nano PVA fiber modified VE as example), where deflected flow lines, river pattern and a few local agglomerations of nano PVA were observed (Fig.3-3 magnified). It revealed that the energy absorption mechanism like bridging effect of nano PVA fiber and defection of matrix cracks existed. The toughening mechanism of resin by nano fillers has been discussed by many works, including crack deflection, crack pining, crack blunting, bridging effect, void nucleation [21-24].

In our previous study, the critical energy release rate (G_{IC}) of epoxy also increased with incorporation of nano cellulose fiber. It is found G_{IC} value of EP/$MFC_{0.3}$ and EP/$MFC_{0.8}$ increases 48.4% and 87% compared to pure EP respectively. The tougher fracture surface in the form of deflected river pattern and patch pattern after failure was also observed. Furthermore, the same effect also was provided by other nano fillers such as CNT, nano clay and nano rubber particles [25-26]. The addition of rigid nano particles seems has a more obvious effect on improvement of matrix toughness or

modulus.

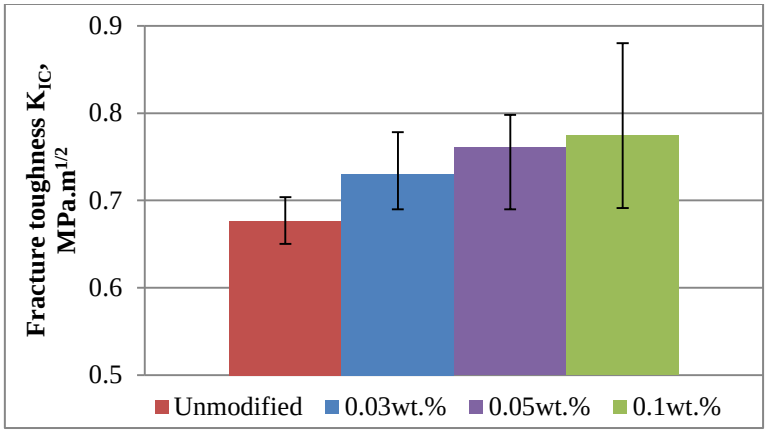

Fig.3-2**.** Fracture toughness of VE modified with different nano PVA ratio

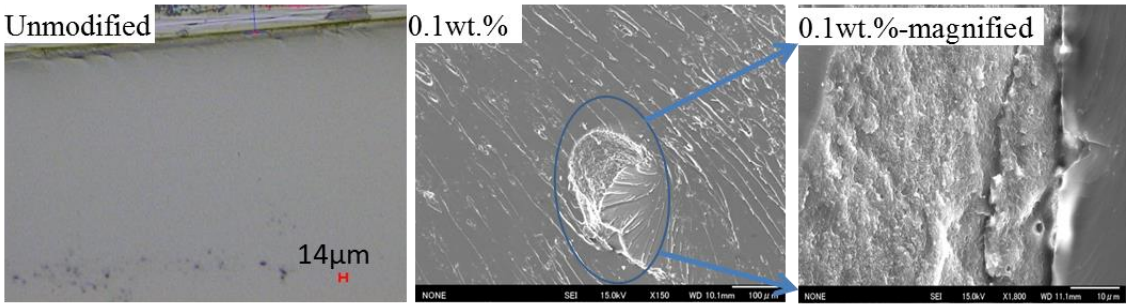

Fig.3-3. Fracture surface of unmodified VE and 0.1wt% nano PVA modified VE

3.3.1.2 CF/matrix adhesion

The strength of single CF always shows a large scatter due to the presence of flaws of CF. The average strength of CF usually displays a dependence on CF length. The two parameter Weibull distribution is commonly used to describe the statistical strength distribution of CF as Eq.2.

$$P(\sigma) = 1 - exp(-\frac{l}{l_0}\left[\frac{\sigma}{\beta}\right]^m) \qquad (2)$$

where m is the shape parameter, β is the scale parameter, l and l_0 presents CF length and a reference length (gauge length of tested specimens) respectively. The failure possibility (P) is estimated by P=(i-0.3)/(n+0.4). Where i is the i-th number in ascendingly ordered strength data and n is the total tested sample number. The average CF strength ($\sigma_0(l)$) depends on CF length can be simply calculated by Eq.3 according to Eq.2 at a same failure possibility.

$$\sigma_0(l) = \sigma_0(l_0)\left(\frac{l_0}{l}\right)^{1/m} \quad (3)$$

Fig.3-4 shows the Weibull strength distribution of single CF by fitting the experimental data. The shape parameter m is 5.7804, and the scale parameter β is 3573 MPa for CF used in this study.

Single fiber fragmentation test was used to investigate the interfacial adhesion between CF and matrix with incorporating by nano filler such as nano PVA. It was observed by a polarization microscope as shown in Fig.3-5. The birefringence patterns of different specimens using cross-polarized light are displayed at the saturation strain level. The magnification of three images is same. The CF breakage area was also observed by optical microscopy without polarized light as shown in the inserted figures. The CF breakage area is circled by blue cycles while interfacial debonding region is circled by red cycles. It can been seen that the dominated fracture mode is interfacial debonding occurring after broken of CF. A large scale of CF/VE debonding happens and no matrix crack is found at CF broken region indicating that the CF/VE adhesion is low. A little difference between specimens is the interfacial debonding degree and the length of CF fragment. The results show that the addition of nano PVA does not show an obvious effect on improvement of adhesion between CF and VE might due to low incorporation weight fraction and relative weak PVA fiber/VE adhesion.

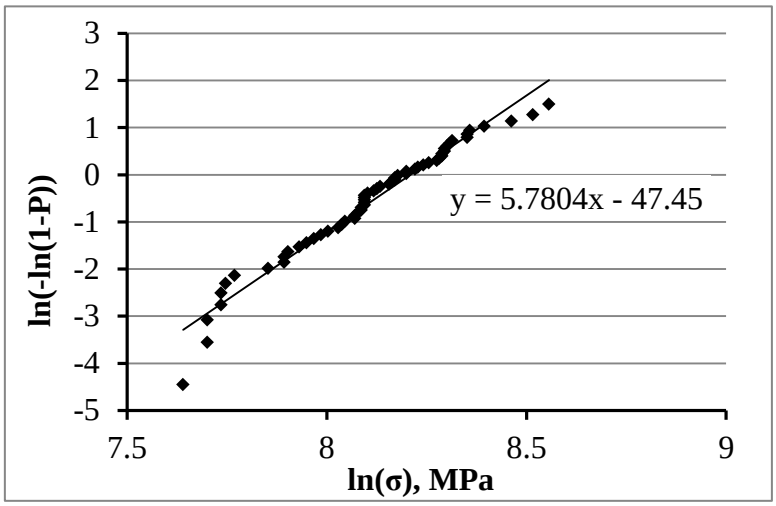

Fig.3-4. Weibull coordinates for 25 mm gauge length of Single CF tensile test. Solid line presents Weibull strength distribution by fitting experimental data.

However, when cellulose nano fiber was used to modify EP, the CF/EP adhesion

could be improved obviously. IFSS of CF/EP/$MFC_{0.3}$ and CF/EP/$MFC_{0.8}$ composite increases by 16.6% and 40% respectively compared to unmodified EP (Fig.3-5, top). The CF/EP adhesion gradually increases with increasing MFC weight fraction. Furthermore, the micro damage behavior was observed by optical microscopy (Fig.3-6, bottom). The dominant fracture mode is interfacial debonding (red circled region) occurred after broken of CF and the slight matrix crack also happens at CF broken region in all the specimens. The main difference between different specimens is interfacial debonding degree according to the birefringence patterns. The reduced interfacial debonding degree is found with increasing the content of MFC which confirms that the improved CF/EP adhesion is achieved. On the other hand, a slight interfacial debonding happens in CF/EP/$MFC_{0.8}$ specimens. It further confirms that much stronger adhesion between CF and matrix existed. In addition, it has been reported that other nano particles also have positive effect on improvement of fiber/matrix adhesion [27-28]. But the mechanism about improvement of interfacial adhesion by nano fibers is still unclear.

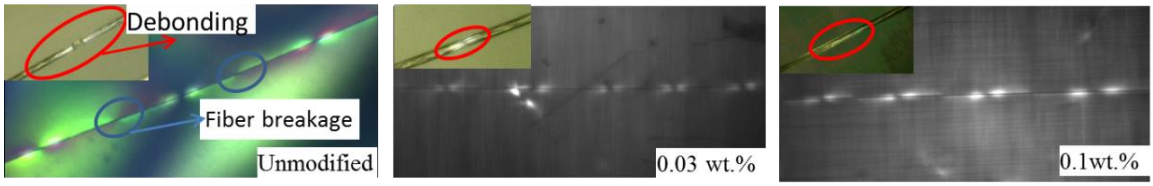

Fig.3-5. Single carbon fiber fragmentation test based on unmodified and modified VE

3.3.2 Static tensile properties o CFRP

The effect of addition of nano PVA fiber on the static tensile properties of CF/VE composites are shown in Fig.3-7. The tensile strength of CF/VE composite modified by nano PVA fiber increases slightly by up to 11% compared to unmodified composite. A slight increase of strain at failure is observed (Fig.3-7, right). With addition of nano PVA, energy dissipation is achieved resulting in lower degree of damage accumulated especially the delamination and fiber breakage during tensile loading. Young's modulus of nano PVA fibers modified CF/VE composites is almost unchanged because it is dominated by young's modulus of reinforcement. Similarly, it has been proved that only a slight effect on static tensile properties of CFRP can be provide when incorporating with cellulose nano fiber (such as MFC) (～5.8%) or polyethylene terephthalate (PET)

fiber (up to 10%) in our previous work [29], and also other nano fibers such as CNT [6,17] regardless of their stiffness or size, which might due to dominant effect of CFs phase properties on tensile properties. A slight improvement of tensile properties especially fabrics composites might due to the resistance to occurrence of transverse cracks in the weft bundles when incorporation with nano fibers, finally decrease the damage and increase the strain at failure.

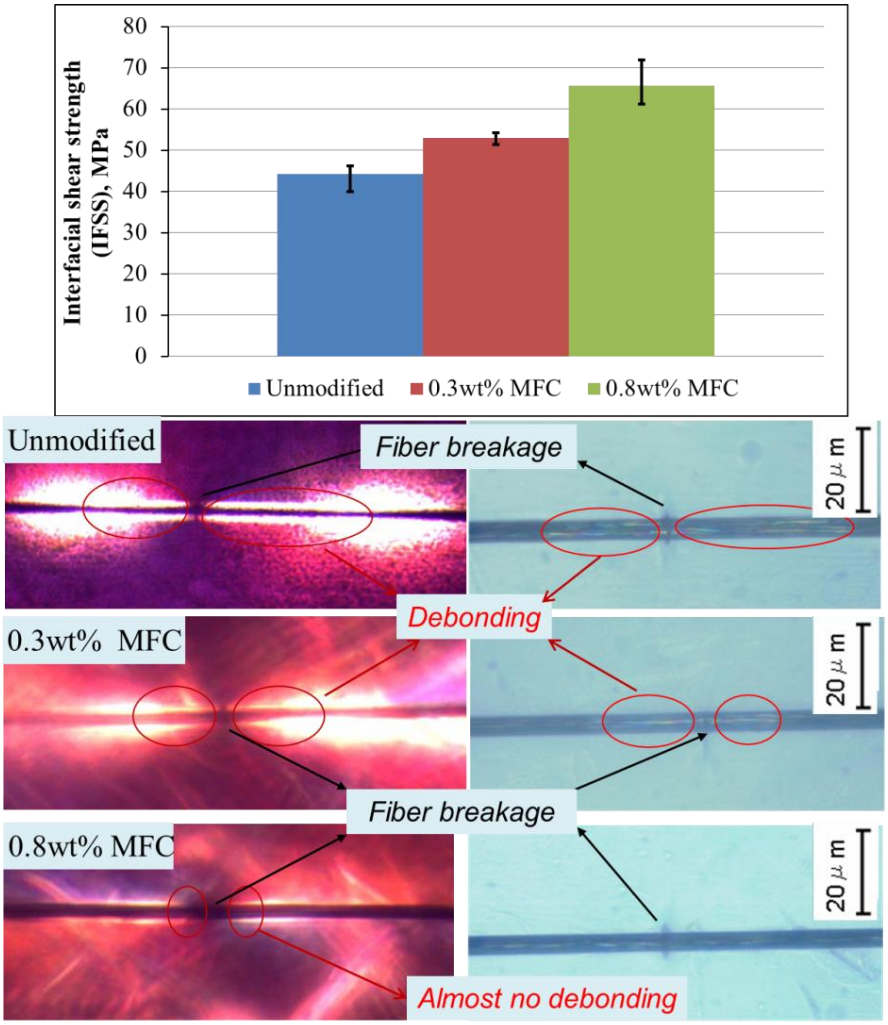

Fig.3-6. IFSS between CF and EP modified by different ratio of MFC (top) and typical micro damage modes (bottom) according to single fiber fragmetation test

The fracture surfaces of tensile specimens after failure are shown in Fig.3-8. The CFs failure behavior in modified composite is almost same as unmodified composite that many single CFs are pulled out from matrix and split indicating a low CF/VE adhesion. However, the different behavior at transverse bundles and resin rich regions especially

at gap between laminates is found. Tougher fracture surface especially at resin rich area is found in nano PVA fibers modified CF/VE composites. The poor nano PVA/matrix interface acts as a crack initiation hotspot and cracks tend to propagate along nano fiber/matrix interface to deflect and blunt crack, which contributes to more energy dissipation (Fig.3-8-magnified). The improved matrix toughness could inhibit the progression of cracks, subsequently, contributing to high strain at failure. Similarly, it has been revealed that extensive matrix deformation has been found in CF/EP composites containing MFC than unmodified CF/EP composite [30].

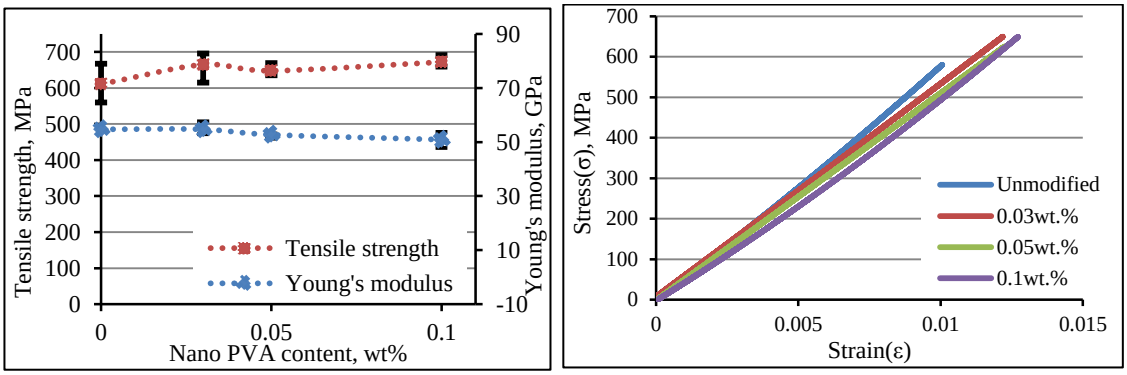

Fig.3-7. Tensile properties (left) and typical stress-strain curves (right) of nano PVA modified CF/VE composites

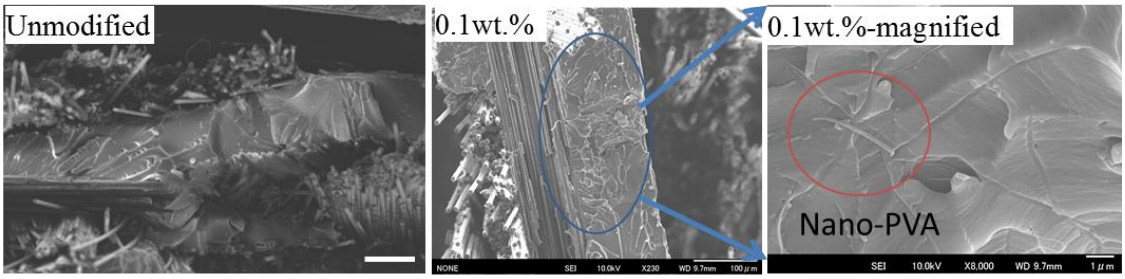

Fig.3-8. Fracture surface after tensile test of unmodified CF/VE and 0.1wt% nano PVA modified CF/VE

3.3.3 Mode-I interlaminar fracture toughness

The effect of addition of nano fibers on the mode-I interlaminar fracture toughness of CFRP was investigate by double cantilever beam (DCB) test. For the thin nano PVA fiber, the initiation (G_{IC}) and propagation (G_{IP}) value of CF/VE/PVA composites are shown in Fig.3-9-left. The G_{IC} and G_{IP} of CF/A composite has a value of 380 and 393 J/m^2 respectively. The G_{IC} value of CF/VE/PVA$_{0.03}$ composite increases by ～4.5%,

and G_{IP} value shows almost unchangely. For CF/VE/$PVA_{0.1}$ composite, G_{IC} and G_{IP} values increase by 14.7% and 11.7% respectively. For the stronger and network structured nano fibers like MFC, they displays more obvious effect on improvement of interlaminar fracture toughness of CFRP (Fig.3-9, right). The G_{IC} value of CF/VE/$MFC_{0.3}$ and CF/VE/$MFC_{0.8}$ composites increase 33.1% and 40.4% respectively. And for G_{IP} value, it increases 58.7% and 89.7% respectively. The better mechanical properties and higher incorporated weight fraction of MFC might be considered as reasons that achieve better effect. In addition, the interlaminar fracture toughness of CFRP can be improved by addition of other nano fibers such as CNT and halloysite fibers as well [31-32]. However, DWCNT and MWCNT sometimes bring about the negative effect or unobvious effect on interlaminar fracture properties of FR-PMCs due to aggregation or reduction of amount of carbon fiber breakage [33-34].

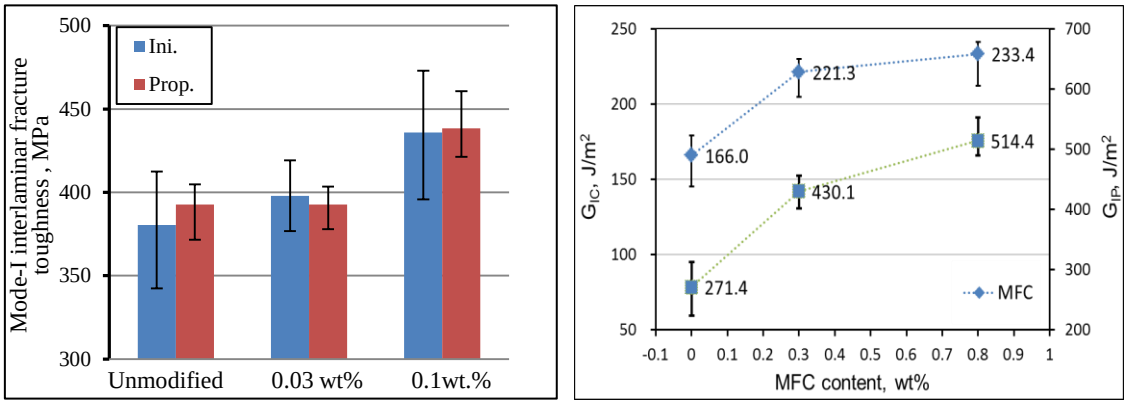

Fig.3-9. Mode-I interlaminar fracture toughness at initial (G_{IC}) and propagation (G_{IP}) stage of CF/VE/PVA (Left) and CF/EP/MFC (Right) composites.

The fracture surface at delaminated areas of CF/VE/PVA composites was further observed by SEM (Fig.3-10). The dominant fracture feature is the interfacial debonding accompanying with CF breakage as same behavior with unmodified composite (Fig.2-10-A-1). Higher degree of CF breakage and matrix breakage indicating cracks jump to another interface is found in modified composites. Matrix cohesive failure at interlaminar interface is also observed in modified composite as displayed in Fig.3-10-a. From magnified image at matrix cohesive failure area (Fig.3-10-b), tougher surface contributed by the addition of nano PVA is observed. It was found that nano PVA was dispersed well in the matrix while just a small amount of nano PVA was found on the

CF/VE interface. The broken nano PVA fibers, nano voids, debonded nano PVA fibers, tilted and deflected cracks are observed. It indicates that the nano PVA bridging effect, crack pinning, and crack deflection are considered as main energy absorption mechanism. Nano fiber/VE interface debonds easily due to weak adhesion. Subsequently cracks propagate along interface, and coalesce with other cracks. During this process, many micro matrix cracks are initiated around nano fiber and spread into matrix around nano fibers. They can stop by other nano fillers or coalesce with other micro cracks. Finally, tougher fracture surface is formed and it contributes to improved bulk toughness. In addition, the fracture surface of other nano fibers like MFC and CNT modified CFRP, they show a major cohesive fracture feature. Many matrix containing nano filler remain on fracture surface contributed by the improved interfacial adhesion. For the CNT modified CFRP, the CNT bridging and CFT pull-out are considered main energy absorption mechanisms to contribute enhanced G_{IC} or G_{IP}.

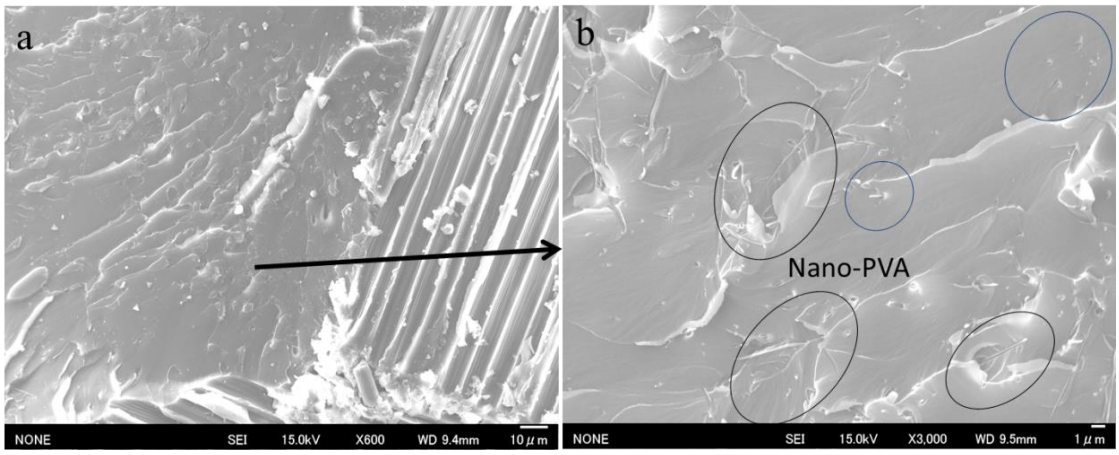

Fig.3-10. Fracture surface of CF/VE/PVA composites observed by SEM

3.3.4 Tension-tension fatigue properties

Although the effect of nano fibers on improvement of static tensile properties of CFRP is slight, they have a significant influence on the fatigue properties. The tension-tension fatigue properties of CF/VE composites modified by different nano PVA fibers content are shown in Fig.3-11. The fatigue life of modified CF/VE composites containing 0.03-0.1wt% nano PVA fibers extends by 3-50 times at a maximum cyclic stress of 567 MPa compared to unmodified composite. At the maximum cyclic stress of 527 MPa, the average fatigue life of unmodified composites is close to 800000 cycles.

The modified composites still perform similar trend with former behavior at the maximum cyclic stress of 567 MPa that extending significantly (fatigue test stopped at 1 million cycles). When incorporating too many nano PVA fibers into VE, the dispersion quality of nano fillers in matrix declines in form of some aggregation acting as stress concentration spots, which might be main reason that improvement of fatigue properties keeps constant with increasing nano filler content. In addition, nano PET fiber as thermoplastic fiber which is same as nano PVA fiber has performed the similar effect that improving fatigue life of CF/EP composites by several ten times at different maximum applied stress level [29]. Nano PVA and PET fibers exhibit inferior mechanical properties like stiffness or strength than CNT or MFC, but they still perform comparable positive effect. Instead of weak nano fillers, MFC possess better stiffness or strength than EP, and provide a significant effect on improvement of fatigue properties of CF/EP composites with a low weight fraction as well (Fig.3-12). The fatigue life of CF/EP/$MFC_{0.3}$ composite extended by 10-30 times at different maximum applied stress compared to unmodified composite. It is interesting to note that when content of MFC increases to 0.8wt%, the fatigue life is improved by several times at different maximum stress level, namely, effect on improvement of fatigue properties declines when incorporates 0.8wt% MFC. In addition, $\sigma_{applied}=a*\log(N_f)+b$ by linear best fitting S-N experimental data is possible to be used to predict the N_f at different maximum stress level. Constant a= -36.9, -33.2, -38.3, constant b= 704.9, 743.2, 738.5, and stability index R^2=0.80, 0.97, 0.82 for CF/EP composites with 0, 0.3, 0.8 wt% MFC respectively.

Other nano fillers like CNT, nano clay, nano silicate, and nano rubber, they also can provide a significant effect on improvement of fatigue properties of CFRP [5-7]. The reinforcing effect is independent on the shape of nano fillers and even their stiffness, but the efficiency depends on their shape and size significantly. Nano fibers are considered as more effective reinforcement than nano particles for FR-PMCs due to their higher aspect ratio. From above results, the needed weight fraction of PVA or MFC decreases significantly to achieve improvement of fatigue life by the same extent. It decreases with a decrease of size as well. Although the micro mechanism is still not so clearly understood, the fiber bridging effect, crack blunting, crack deflection and cavitation effect of nano particles have been discussed comprehensively [2-7].

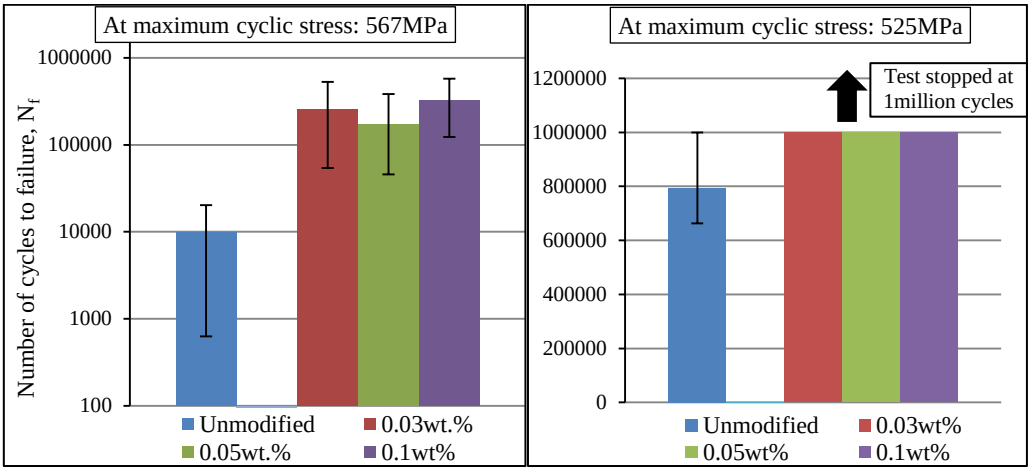

Fig.3-11. Fatigue proerties of nano PVA modified CF/VE composites

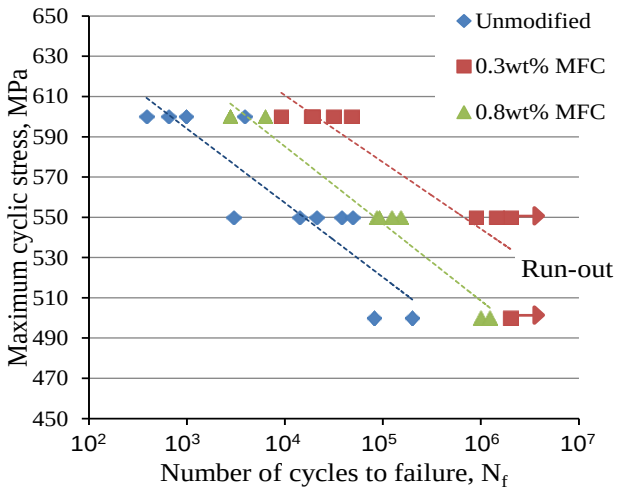

Fig.3-12. Tension-tension fatigue properties of CF/EP composite with different content of MFC.

3.3.5 Stiffness degradation during fatigue test

Internal damage accumulates in the fabric composite specimen such as fiber debonding, transverse cracks, meta-delamination at the cross-over points between warp and weft yarns, interlaminar delamination and final CF breakage with increasing loading cycles. As a result, observed Young's modulus decreases virtually for all specimens as fatigue cycles increase. Therefore, damage parameter D_{slope} estimated by evolution of slope of stroke displacement-stress curves and D_{stiff} estimated from fatigue moudulus loss are expected to represent the fatigue damage degree of composite materials. D_{slope} was obtained by outputting the displacement and stress information

directly from fatigue machine. Fatigue modulus was obtained from σ-ε curves by extensometer. Although fatigue stiffness is more straightly reflecting the internal damage accumulation, due to a limited gage length of the extensometer, the stress-strain curve measured by the extensometer does not reflect the damage progression occurring outside the gage length. Damage D_{slope} shows the average damage, in other words, the sum of all damage in the specimen. Especially at fatigue final stage, the stroke between two specimen grips reflects more precise damage information in the specimen. D_{slope} and D_{stiff} are shown as Eq.4.

$$D_{stiff}=1- E(n)/E_0$$

$$D_{slope}=1-S(n)/S_0 \quad (4)$$

E(n) and S(n) is the dynamic fatigue modulus and slope of displacement-stress curve at cycle number n respectively. E_0 and S_0 is the initial modulus and initial slope of displacement-stress curve at the first cycle of fatigue test.

For the thin nano PVA modified CF/VE composites, typical damage evolution based on D_{slope} of CF/VE/ PVA composites during fatigue test are displayed as Fig.3-13. At fatigue early stage, damage increases significantly due to occurrence of matrix cracks mainly including transverse cracks. Modified CF/VE composites shows a slower increase of damage as the number of fatigue cycles increases than unmodified CF/VE composites, indicating a slower drop of stiffness (Fig.3-13-inserted). CF/VE/$PVA_{0.03}$ shows a slight faster growth of damage than CF/VE/$PVA_{0.05\ or\ 0.1}$ composite. In the other word, a resistance to initiation and growth of matrix cracks at fatigue early stage is probably provided by addition of nano PVA fibers. Modified composites show a slower decrease of stiffness as the number of fatigue cycles increases than unmodified composite, indicating that less damage occurred and accumulated. Stiffness of unmodified composite drops slowly after ～3000 cycles. While stiffness loss speed change of modified composites starts after ～10000 cycles regradless of the ratio of nano PVA. The stiffness dagradation slows down indicating the satuation of transverse crack at weft named the characteristic damage state (CDS) [35]. Namely, unmodified CF/VE composite displays an earlier satuation state of transverse crack and beginning of delamination than modified composites. After ～10000 cycles, stiffness of modified

reduces gradually until final failure, and more slowly than that of unmodified composite. In a word, fatigue damage in unmodified composite initiate early and accumulate fastly, subsequently cause specimen to fail fast. At fatigue final stage, modified CF/VE composite shows a rapid stiffness degradation due to severe fiber breakage. The severe interlaminar delamination forms at this stage, stress concentration and redistribution accelerate failure of CFs at warp bundles.

In addition, for nano fiber with different size/stiffness/structure like MFC with a web-like network structure modified CF/EP composites, they also show similar behavior as CF/VE/nano PVA composites (Fig.3-14). It shows a slower decrease of stiffness as the number of fatigue cycles increases than unmodified CF/EP composite, and slows down after CDS of transverse crack. Unmodified CF/EP composite displays an earlier satuation state of transverse crack and beginning of delamination than modified composites. At last, fatigue damage in unmodified composite initiate early and accumulate fastly, subsequently cause specimen to fail fast at a stiffness decay ratio of ～18%. For the CF/EP/$MFC_{0.3}$ composite, occurrence and growth of damage is delayed, and specimen still fails at almost the same stiffness decay ratio as unmodified CF/EP. However, although fatigue damage accumulate a little more slowly in CF/EP/$MFC_{0.8}$ composite, earlier failure of specimens occurs at a stiffness decay ratio of ～15% indicating a low damage accumulation capability.

The fracture feature are close related to matrix and interface properties. CF/EP fatigue specimens with different MFC ratio exhibit different fracture modes (Fig.3-15). A comprehensive delamination is found in unmodified CF/EP composite caused by early occurrence and fast growth of delamination indicating a low interfacail adhesion. For CF/EP/$MFC_{0.3}$ composite, a lower degree of delamination compared to unmodified composite is found. On the other hand, CF/EP/$MFC_{0.8}$ composite shows almost a straight fracture mode that cracks propagate transversely rapidly accompanying with some CF bundles breakage. It behaves brittlely like a sudden failure that all the layers broke simultaneously without absorbing much energy. Moreover, almost no delamination is found around failure area. It indicates that interfacial adhesion is enhanced by addition of MFC resulting in increased resistance to propagation of interlaminar delamination.

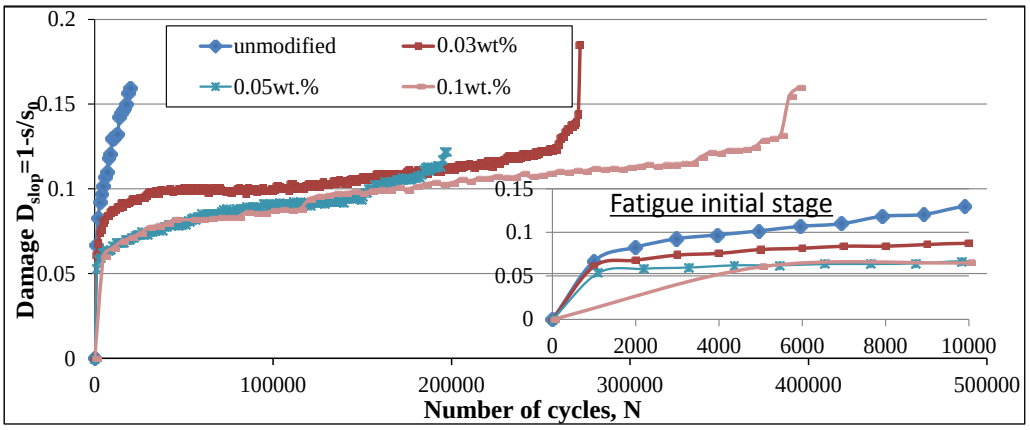

Fig.3-13. Damage evolution based on stiffness loss of CF/VE composites with addition of nano PVA

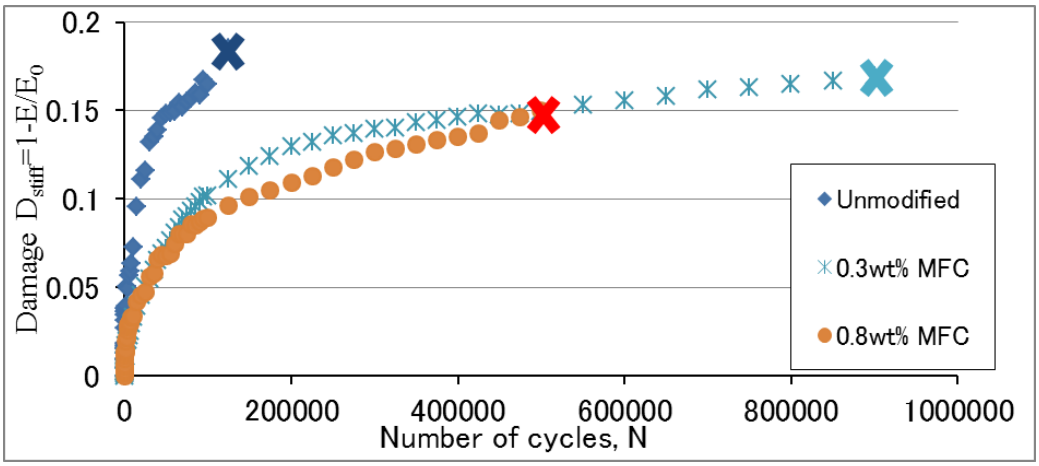

Fig.3-14 Typical stiffness degradation of CF/EP/MFC composites

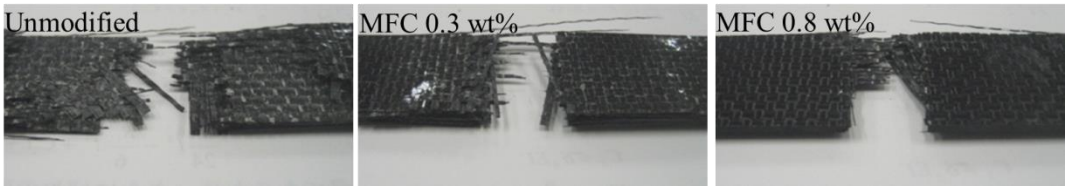

Fig.3-15. Fracture mode after fatigue failure of CF/EP/MFC composites

3.3.6 Fatigue damage resistance mechanism

3.3.6.1 Fatigue damage progression

The fatigue damage progression of carbon fiber fabric composite who failed at high fatigue cycles is shown in Fig.3-16 [3, 10]. At fatigue early stage (Stage ①), interfacial debonding between CF and matrix occurs early due to weak CF/matrix adhesion. Then

transverse cracks at weft yarn form by propagation of matrix cracks along CF/matrix interface due to stress concentration at cross-over point. Transverse cracks approached to the warp bundles and can be arrested by warp/weft interface, subsequently initiates the meta-delamination between weft and warp bundles (Stage ②) due to high stress concentration at the crack tips. The density of transverse crack increases as the number of fatigue cycles increases and finally reaches a saturated state (stage ③). The observed stiffness of composite reduces significantly until CDS of transverse crack, and then slows down due to the slight influence of delamination. Simultaneously meta-delamination grows continuously. The occurrence of transverse crack and meta-delamination causes the loss of capability of weft bundles to share the tensile load, and subsequently results in much load transferring to warp bundles. It might cause CF breakage in warp bundles sporadically. Further, interlaminar delamination occurs at final stage due to the inhomogeneous stress redistribution between CF layers and processes to cause final failure of specimens (Stage ④).

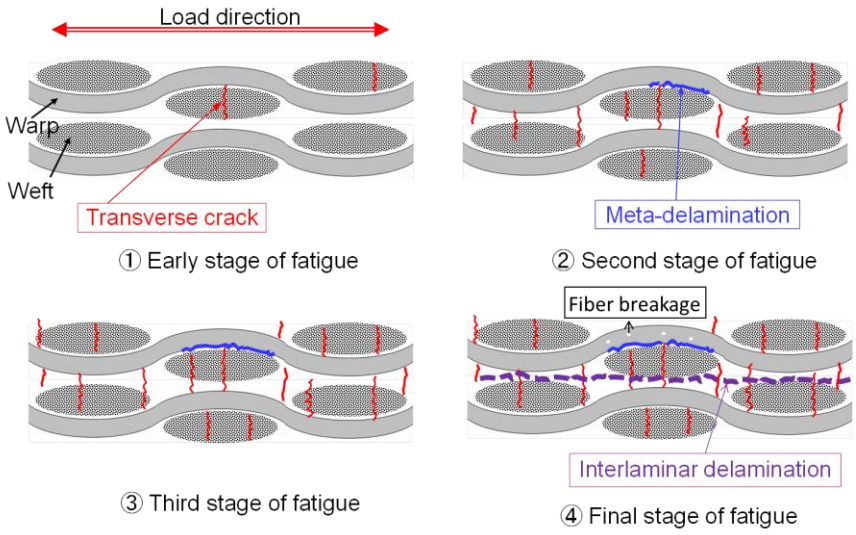

Fig.3-16 Fatigue damage progression of fabric composite

3.3.6.2 Damage resistance at fatigue early stage

3.3.6.2.1 Damage investigation by TDA at fatigue early stage

Internal fatigue damage occurs at CF/matrix interface and matrix first at fatigue early stage. TSA and TDA are very effective non-destructive evaluation methods to investigate the fatigue damage during test. Herein, fatigue damage at early stage of

CF/VE composite containing different ratio of nano PVA fibers during fatigue test has been investigated by TSA and TDA. As described at chapter 2, unmodified CF/VE composite (CF/A) displayed severe damage due to low toughness of resin. Less damage in 0.03 wt% nano PVA fiber modified CF/VE composite such as matrix crack than unmodified CF/VE composite is found (Fig.3-17). Furthermore, TDA is applied to characterize the damage degree during fatigue loading at fatigue early stage (Stage ①). As demonstrated by Fujii et al. [36], TDA images present two-dimensional thermo-elastic information relates to only damage initiation and growth by removing the inhomogeneity noise such as construction pattern. The degree of temperature change roughly reflects the damage level in woven fabric composites. TDA images of CF/VE composites with different nano PVA fiber content at certain cycles are shown in Fig.3-18, where the palette represents the damage degree. The damage almost occurs in weft bundles at fatigue initial stage in all the specimens due to stress concentration at cross-over point. Damage mainly including matrix crack occurs in unmodified CF/VE composite early and appears severe due to low toughness of resin at even 1000 cycles. Lower degree of damage in 0.03 wt% nano PVA fiber modified CF/VE composite than unmodified CF/VE composite is found at same cycles. CF/VE interfacial debonding occurs easily because of weak CF/VE adhesion, and subsequently propagates and coalesces with other matrix cracks to form transverse cracks. In the modified composite, increased toughness of matrix and energy dissipation caused by damage like nano fiber/VE debonding is helpful to delay the initiation and propagation of crack. The damage degree of surface caused by matrix cracks was almost same with that inside layers of specimen, which already had been demonstrated by other authors before [37]. Further, with increasing the number of loading cycles, all the CF/VE composites exhibit an increase of damage degree. Damage in unmodified CF/VE composite shows a faster growth.

Furthermore, damage value V_d was induced to quantify the damage degree occurred in CF/VE composites as Eq.5.

$$V_d = \Sigma D_i * A_i \qquad (5)$$

The increment [ΔT_d] of damage demonstrated by Fujii et al. [36] is divided by 0.01k (ten times of temperature resolution of thermo-camera) into several levels. Each level is

defined as D_i. A_i is damage area ratio, defined as the number of pixels at damage level D_i divided by the total pixels of measured TDA image. The damage evolution based on TDA during the fatigue initial stage was described as a V_d-N graph in Fig.3-18 (Right). It was found that damage grew rapidly before 10000 cycles, and then grew gradually with increasing the number of cycles. It is consistent with the result of stiffness degradation well. Furthermore, unmodified composite showed the faster damage growth than nano PVA fiber modified composite which confirmed the result discussed by TDA.

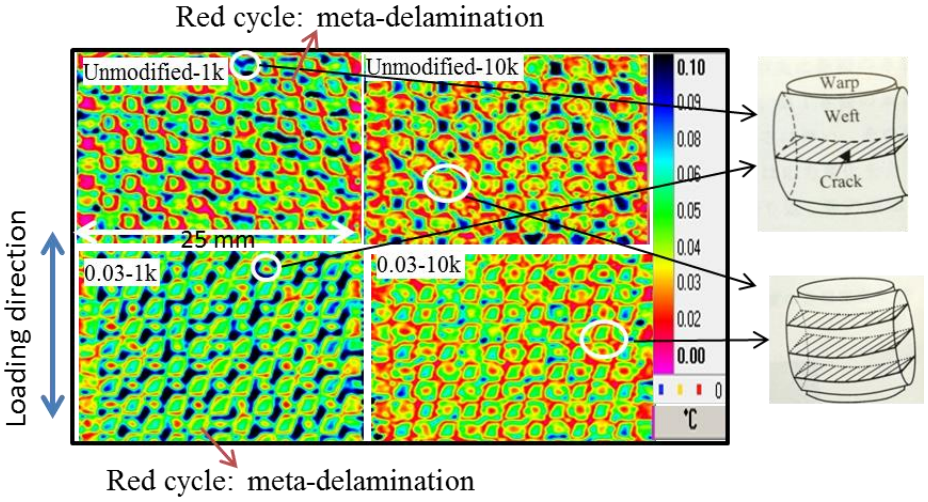

Fig.3-17. TSA image of nano PVA modified CF/VE composites at expected cycles

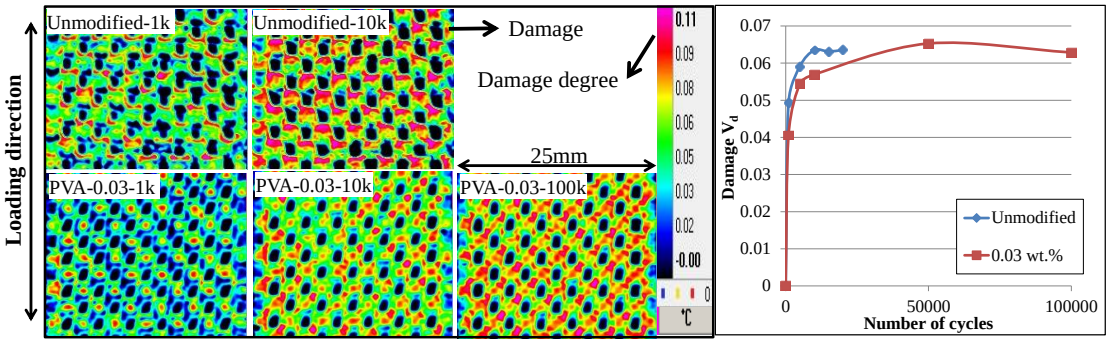

Fig.3-18. TDA images of nano PVA modified CF/VE composites at expected cycles, symbol k represents 1000.

In order to investigate the damage in CF/VE composites, the longitudinal section of fatigue specimens after certain cyclic loading cycles was further observed by SEM, as shown in Fig.3-19. The transverse cracks are circled by black circles while delamination is circled by red circles. Under the same number of fatigue cycles, lower density of transverse cracks was found in modified CF/VE composites. And the space between

neighboring transverse cracks was small. It provided good evidences to confirm the results discussed by TDA. A growth of meta-delamination and interlaminar delamination was observed in all specimens as well as matrix cracks at resin rich areas, which caused the gradual degradation of stiffness at fatigue middle and final stage. Moreover, lower degree of meta-delamination was found in modified composite than unmodified composite at same number of cycles. No serious voids in the specimens were found according to SEM images and CT-scan images in next section. It indicated that the influence of defect in composites could be considered insignificant due to low void content.

3.3.6.2.2 Resistance to transverse cracks at weft bundles

From the typical damage evolution based on fatigue stiffness loss (Fig.3-13,3-14), a lower degree of fatigue damage was accumulated at fatigue early stage (Stage ①) indicating an enhanced resistance to occurrence and growth of matrix crack including transverse crack. As discussed at section 3.3.1.1, fracture toughness of bulk resin can be enhanced by the addition of nano fibers. The rougher fracture surface of bulk EP specimens confirms that cracks are resisted and deflected associating with high energy dissipation by bridging or crack deflection effect of nano fillers. It revealed that resistance to initiation and propagation of matrix crack could be enhanced by addition of nano fillers. It has been noted that the capability to resist the initiation and propagation of matrix can be enhanced by incorporation of CNT, nano clay or nano rubber [25-26,31-32] due to particle debonding, plastic void growth, rubber cavitation, matrix deformation, fiber bridging.

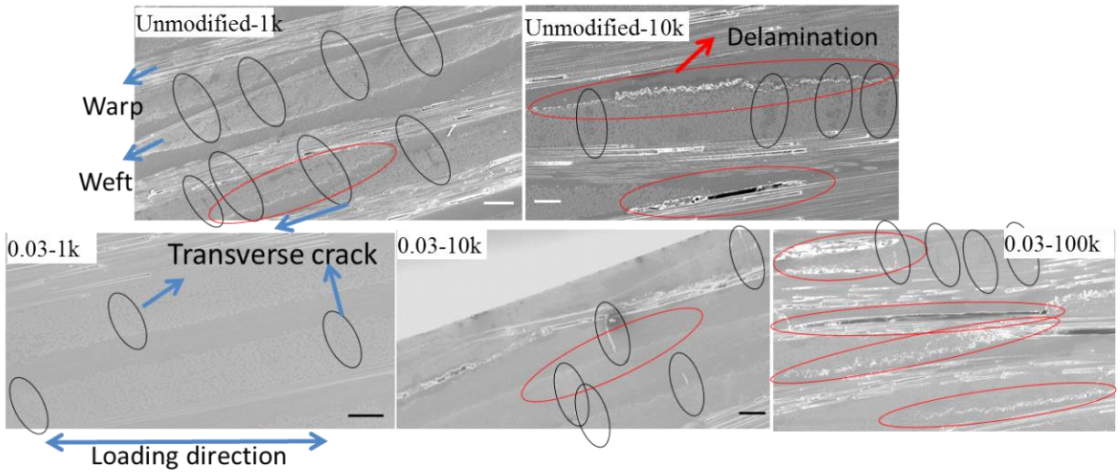

Fig.3-19. SEM images of damage in CF/VE composites (unmodified and 0.03wt% nano PVA modified) at expected cycles (The scale bar is 100 μm).

In addition, single notched UD CF/EP/MFC composites (90°) were conducted by the static and cyclic 3 points bending load to investigate the ability to resist the propagation of cracks in transverse bundles. Dimension of specimens is shown in Fig.3-20. The sum length of notch and pre-crack made by a fresh razor blade was ～1mm. The cyclic bending test was conducted at stress-ratio $R = +0.1$ and frequency $f = 7Hz$ to obtain the threshold value of energy release rate range (ΔG_{Ith}) of crack initiation. ΔG_{Ith} and propagation critical energy release rate (G_{IC}) value of CF/EP/$MFC_{0.3}$ increased by 156.7% and 42.9% respectively. After failure, the fracture surface was observed by SEM (Fig.3-20). It is found that the dominant fracture mode of unmodified composite is interfacial failure where the CF surface is smooth and the matrix deformation is unobvious. It is a lower energy dissipation mode when cracks initiate and propagate along the weak CF/EP interface. On the fracture surface of CF/EP/$MFC_{0.3}$ composite, the residual resin adhered on CF surface and residual CF fracture fragments are found. It consumes more energy during crack propagation because of crack deflection and CF breakage. It is evidence that CF/$EP_{0.3}$ performs stronger adhesion than CF/unmodified EP. More residual resin adhered on CF surface and more residual CF fracture fragments are observed on the fracture surface of CF/EP/$MFC_{0.8}$ composite indicating the existance of much stronger CF/EP adhesion. In a word, a positive effect on the resistance to propagation of cracks in transverse bundles to slow down the decay of fatigue modulus and delay the initiation of meta-delamination was provided by addition of MFC.

3.3.6.3 Resistance to meta-delamination

As discussed in section 3.3.6.1, meta-delamination occurs at fatigue stage ②. In the unmodified composite, transverse cracks occur at resin rich area and grow, then are stopped by warp bundles. But they still promote the occurrence of meta-delamination due to high stress concentration at crack tips. Meta-delamination propagates easier along warp/weft interface as the number of cyclic loading increases due to weak CF/matrix adhesion, subsequently causes fast accumulation of early fatigue damage. The occurrence and growth of meta-delamination reduces the capability of weft bundles

to share the tensile load resulting in the stiffness loss of composite gradually. With incorporation of nano fiber into CFRP, the propagation of meta-delamination can be delayed based on result from da/dN-ΔG (Fig.3-21) under even same ΔG (Section 3.3.6.4). At same fatigue cycles, weft bundles in modified composite can share more loads and resulting in less load transferring to warp bundles. The initiation of interlaminar delamination could be delayed as well. The slower stiffness degradation rate, lower density of meta-delamination inside (Fig.3-23) was found in modified composite than unmodified composite, which provided evidences to confirm a slower growth of meta-delamination in modified composites.

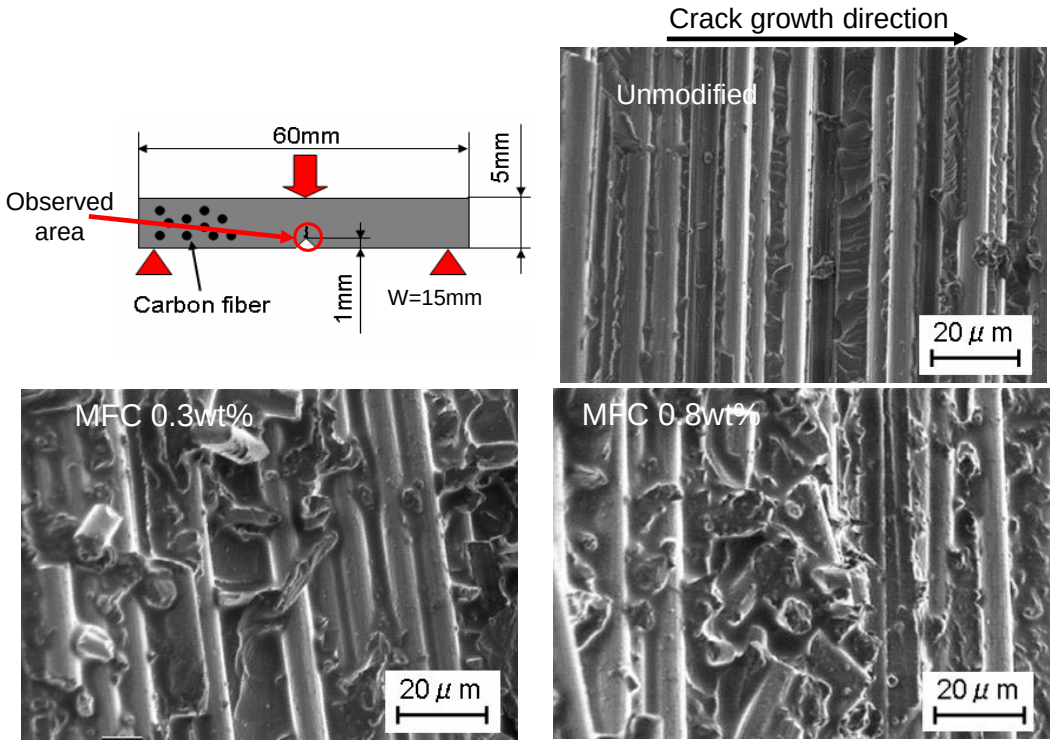

Fig.3-20. Fracture surface of the notched 3 points transverse bending specimens of UD CF/EP composites with various MFC content after test.

In CF/VE/PVA composites, based on TSA images, the red cycles appeared at the boundary of bundles (Fig.3-17) reflected the influence of meta-delamination inside of specimens which has been confirmed by CT-scan. At 1000 and 10000 cycles, it is clearly observed that more severe meta-delamination is found in CF/unmodified VE composite. It further confirms that propagation of meta-delamination could be delayed with addition of nano fillers.

In addition, the effect of PET fiber on resistance to delamination initiated by transverse crack in CF/EP composite has been investigated in the previous work in our laboratory [38-a]. PET fibers mainly were dispersed among the warp/weft interfaces or interlaminar interfaces due to their high diameter of ～700nm. However, they perform a good ability to inhibit the propagation of crack along warp bundles when 0.3wt and 0.5wt% was incorporated in to epoxy. The cohesive failure feature was observed where resin containing PET remained on the fracture surface. Similarly, glass fiber with a diameter of ～500 nm also performed an effect on resistance to propagation of crack along the surfaces of warp bundles [38-b]. It was considered that glass fibers acted as the obstacle to contribute more energy absorption in the form of crack deflection and interfacial debonding during crack propagation.

3.3.6.4 Delamination resistance at fatigue middle and final stage.

It has been noting that the final fatigue failure are close related to the growth rate of interlaminar delamination. It was found that propagation of interlaminar delamination under the cylic loading was prohibited by addition of MFC (Fig.3-15). In order to confirm it, fatigue mode-I DCB test was conducted. The mode-I delamination propagation rate versus the energy release rate range (da/dN-ΔG) is plotted in Fig.3-21. The length of delamination cracks was determined based on the compliance-crack length relationship found in the former static DCB test. G_{IC} is the value of interlaminar fracture toughness under static loading. ΔG_{th} represents the threshold value for crack propagation, namely, crack does not propagate when ΔG is lower than this value. It was found that da/dN of CF/EP composites decreased by a factor of ~one with incorporation of only a small amount of MFC under the same ΔG. It indicates that the capability of resistance to growth of delamination is enhanced significantly by the addition of MFC under cyclic loading. ΔG_{th} value of modified CF/EP composites increases by 1.6-1.7 times compared to that of unmodified composite. It provides as an evidence of resistance to initiation of delamination under effect of MFC. At middle linear region, Paris law can be used to fit the experiment data as $da/dN=c(\Delta G)^m$. The constant c is 1.0E-24, 1.0E-21 and 8.0E-25 for 0, 0.3 and 0.8 wt% MFC modified CF/EP composites respectively. The slope of da/dN-ΔG is almost same regardless of content of MFC. In addition, G_{IC} value of modified composite is 1.6-2 times higher than unmodified

composite which is confirmed by static DCB test.

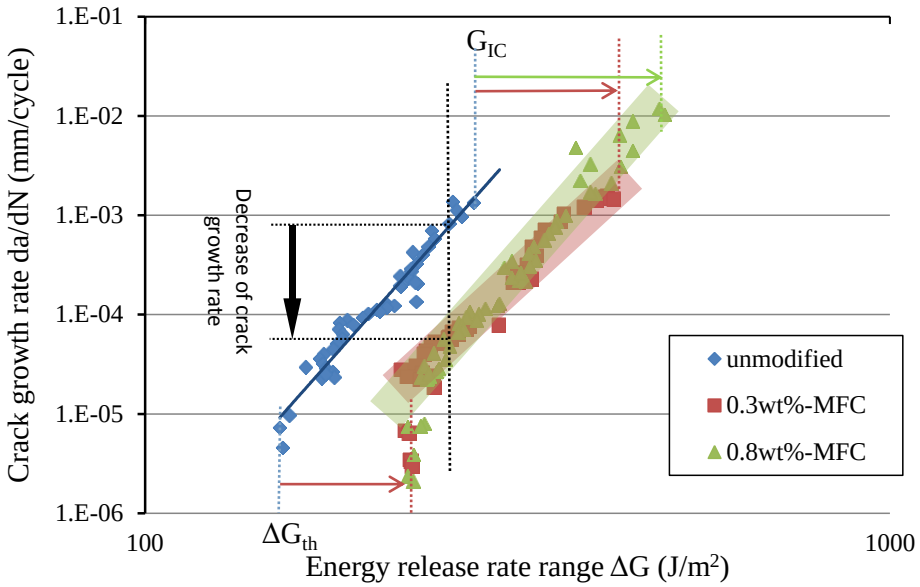

Fig.3-21. Crack growth rate of CF/EP composites modified with different ratio of MFC.

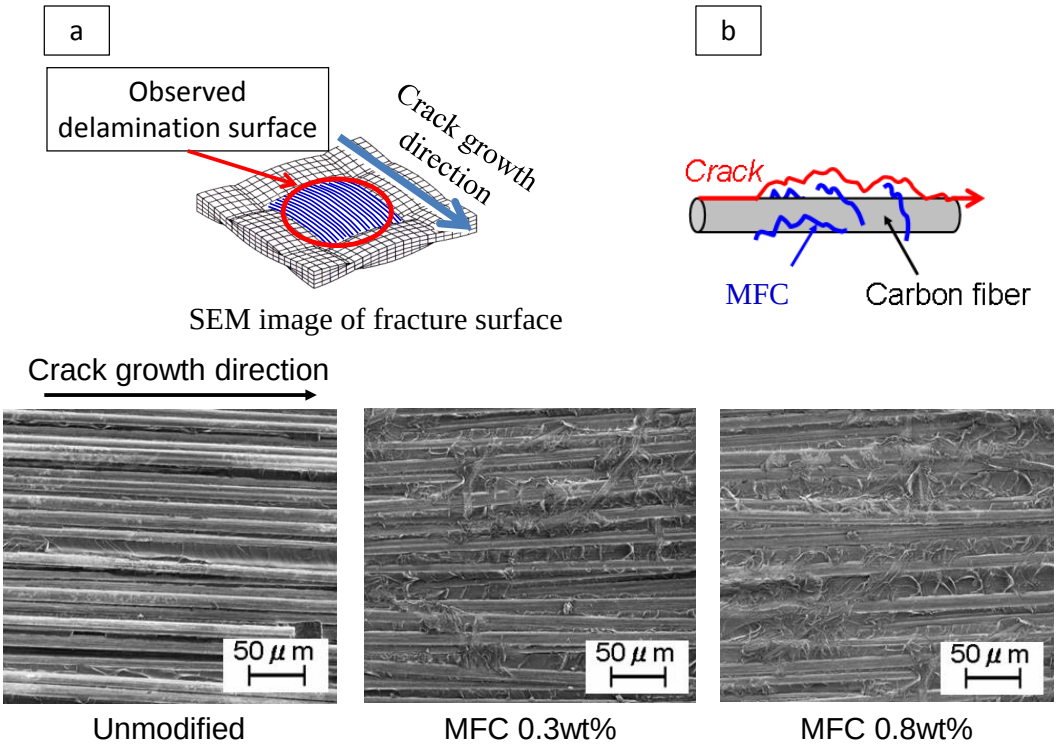

Fig.3-22. Fracture surface after fatigue DCB test of each specimen.

Furthermore, the fracture surface of specimens after fatigue DCB test at propagation areas was observed by SEM (Fig.3-22). It is clear that the fracture mode of unmodified

CFRP is interfacial failure that delamination propagate along weak CF/EP interface accompanying with a small amount of CF breakage. The surfaces of CFs are smooth reflecting a weak CF/EP adhesion. On the other hand, the dominant failure behavior is matrix cohesive failure in CF/EP/$MFC_{0.3}$ composite, where many resin contained MFC remain on the fracture surface. More residual resin containing nano fillers are found on the fracture surface of CF/EP/$MFC_{0.8}$ composite reflecting a stronger CF/matrix adhesion. The toughened EP by MFC remained on the fracture surface causes cracks to deflect accompanying with nano fiber bridging and propagating along tougher matrix that consume more energy (Fig.3-22-b). The effect of MFC on resistance to initiation and propagation of delamination of CFRP contributes to extended fatigue life of CFRP.

Furthermore, micro CT-scan was used to investigate the delamination state in CFRP at expected fatigue cycles. The density and length of delamination crack can be clearly observed by CT-scan. Herein, unmodified CF/VE and CF/VE containing 0.03wt% nano PVA fiber are characterized (Fig.3-23). At 1000 cycles, meta-delamination between warp and weft yarns has already occurred in all the CF/VE composites due to earlier initiation of transverse cracks. The length of meta-delamination is almost 2mm which is the width of weft or warp bundle. Therefore, the meta-delaminations are localized at CF bundle cells at ～1000 cycles. Lower density of delamination is found in modified CF/VE composites compared to unmodified composites. The density of delamination of CF/VE/$PVA_{0.03}$ and CF/VE/$PVA_{0.1}$ are almost same. As number of fatigue cycles increasing, the density of meta-delamination increases. The adjacent local delamination links together through matrix crack at gap between CF layers or transverse cracks to form long interlaminar delaminations. The interlaminar delamination propagating along interface between weft and resin also occurs and progresses due to redistribution of stress. More severe delamination occurs in unmodified CF/VE composites, which causes each CF laminate isolated and stress concentration to increase to accelerate the breakage of CFs resulting in final failure of composites. For the modified CF/VE composites, severe delamination happen after ～100000 cycles. With addition of nano PVA fibers, the effect on resistance to growth of delamination was found which reduced the stress concentration to slow down the breakage of CF, and finally extended the fatigue life.

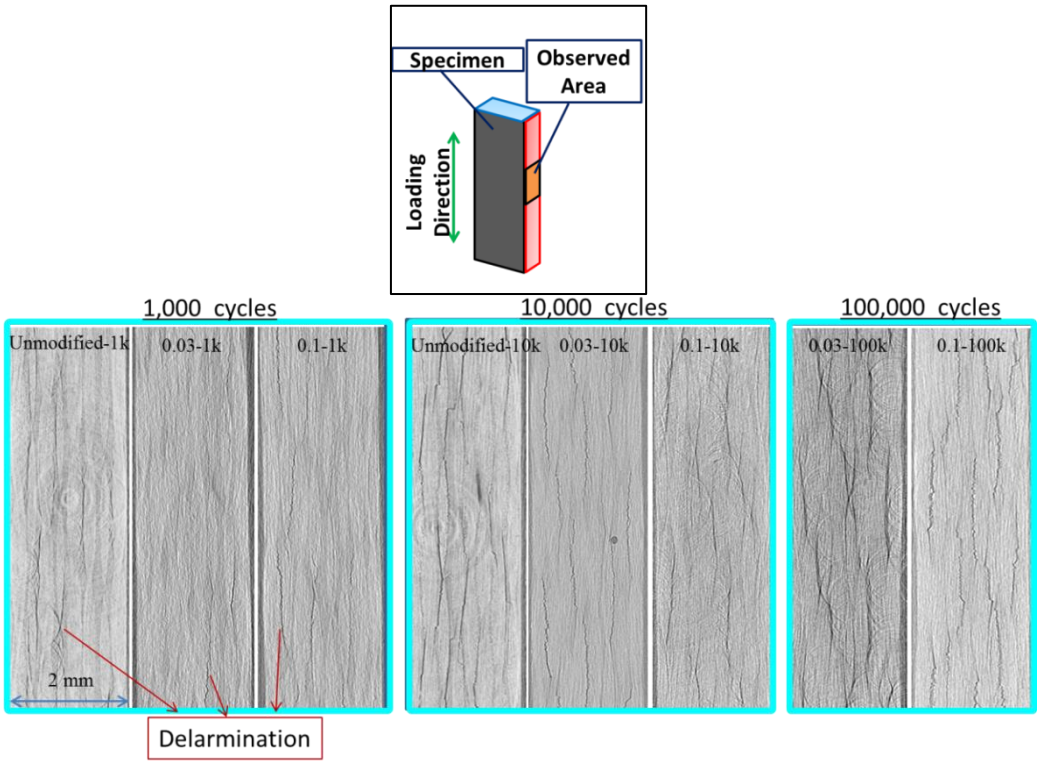

Fig.3-23. CF-scan images of nano PVA modified CF/VE composites at certain cycles

3.3.6.5 Discussion

Based on above observation and discussion, the fatigue damage progression of CFRP under effect of the addition of nano fiber is described in Fig.3-24. Matrix cracks initiate early in the unmodified composite at CF/resin interface due to weak CF/matrix adhesion, and resin rich area due to stress concentration at fatigue early stage (a). With addition of nano fiber, a late initiation and slower growth of matrix cracks including transverse cracks compared to unmodified composite was achieved. Nano fibers/matrix debonding is also progressing. The density of transverse cracks in unmodified CFRP increases fast and cracks spacing becomes smaller. After transverse cracks propagating to warp bundle, they can be arrested by the interface between warp and weft bundles, and propagated along these interfaces to form meta-delamination. A slower growth of transverse crack and delay of initiation and growth of meta-delamination can be obtained by incorporation of nano fillers in modified composites (b). The formation of meta-delamination and growth of matrix at interlaminar interface cause the stress to redistribute between CF layers inhomogeneously, and subsequently process to cause

final failure of specimens. The interlaminar delamination occurs fast and relate to final failure of specimen (c). However, addition of nano fibers can provide an effect on resistance to propagation of interlaminar delamination due to improve CF/matrix adhesion and matrix toughness, and crack deflection, interfacial debonding, bridging, or crack pinning at the micro scale. It delays the CFs breakage in warp bundles caused by the inhomogeneous stress redistribution and extends fatigue life of CFRP (d,e) finally.

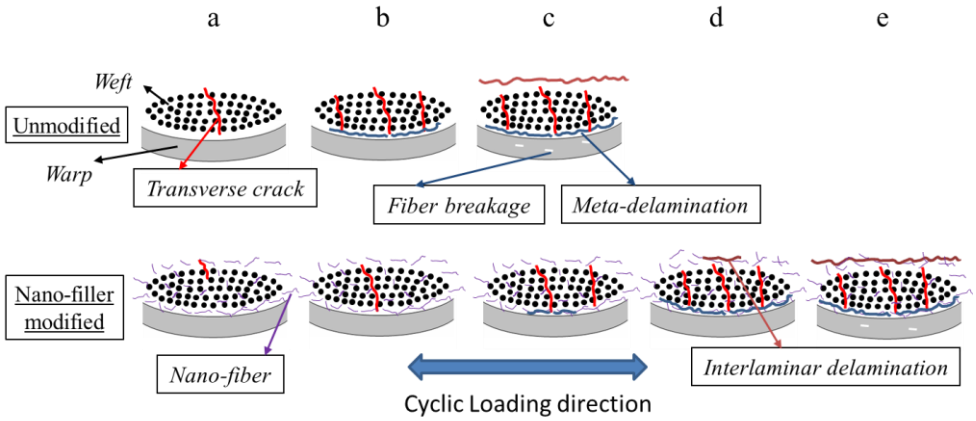

Fig.3-24. Fatigue damage progression of unmodified and modified CFRP

3.3.7 Reinforcing mechanism at micro scale

The fractography can often reflect the detailed information about the fracture mechanism. The delaminatin region of inside CF layer of fatigue specimens after test was further observed by SEM (Fig.3-25,3-26). Most of nano fibers are found at resin rich area or interlaminar interfaces. Only a small amount of nano fiber are found in the warp or weft bundles. Broken single cellulose fiber or nano PVA fiber fragment is observed in Fig.3-25-c and Fig.3-26-a (white circled region). Nano voids in the matrix or at tips of nano fiber are in Fig.3-25-c,d and Fig.3-26-a,b(white circled region). Debonding and pull-out of cellulose microfibrils consisting of single cellulose fibers or nano PVA fiber or PET fibers are found in Fig.3-25-a,b and Fig.3-26-c,d. Broken or pulled-out single cellulose fiber fragments was observed on the wall of cellulose microfibrils (Fig.3-25-a, inserted). Many cracks indicating crack deflection and matrix deformation also are found around the debonded nano fibers in Fig.3-25-b and Fig.3-26-c,d (red circled regions). In addition, crack pinning is found by nano voids at matrix or at tips of nano fiber broken areas in Fig3-.25-d and Fig.3-26-b (blue circled regions).

Due to contrained space by carbon fibers, the effect of the matrix deformation in CFRPs is limited. The energy absorption such as crack pinning, deflection, bridging, debonding, void nucleation and growth by addition of nano fiber becomes significant. When cracks propagate perpendicuar to the axis of nano fibers, fiber bridging by nano PVA fibers or MFC or single cellulose fibers accompany with fiber pull-out can be considered main energy absorption mechanisms. It depends on strength of nano fiber and nano fiber/matrix adhesive strength. It is interesting to note that when the cellulose microfibrils are pulled out from matrix, the single cellulose fibers that constituting the microfibrils break and pull out comprehensively (Fig.3-25-a-inerted). It also can be considered to contribute the total energy absorption.

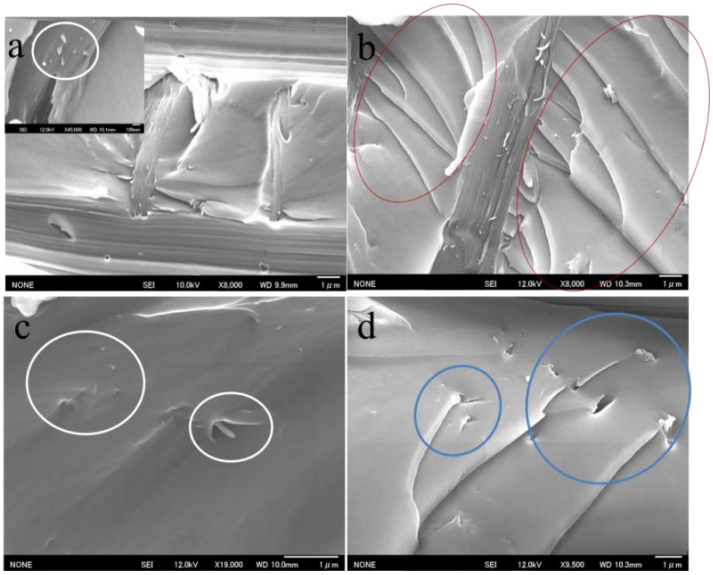

Fig.3-25. SEM images of the delaminated surface of CF/EP/MFC composites after fatigue test

Nano filler debonding and pull-out and fracture are considered most improtant energy absorption mechanims. Nano fiber/matrix debonding occurs easily due to the weak interfacial adhesion and difference of stiffness. Especially when crack propagates parallel to nano fiber direction, it can be considered that crack prefers to propagate along the interface between nano fiber and matrix as evidences that many debonded nano fibers can be found on the fracture surface. Models have been used to describe the energy absorption contributed by fiber debonding and pull-out [39-40]. During crack propagating alond nano fiber/matrix interface to form 3D pathway, many micro crack can be initiated at interface and radiate to matrix around this pathway, resulting in

increasing the ture fracture surface and more matrix deformation (red circled regions). The average surface roughness of the fracture surface can be used to characterize the contributed absorption energy. The rougher fracture surface is the main feature of fracture surface of composite containing nano fiber or other shape of nano fillers. Nano voids nucleation and growth in the matrix or at tips of broken nano fiber, and following crack pinning by nano voids are considered to be another reinforcing mechanism causing energy dissipation at a micrometre scale during cyclic loading.

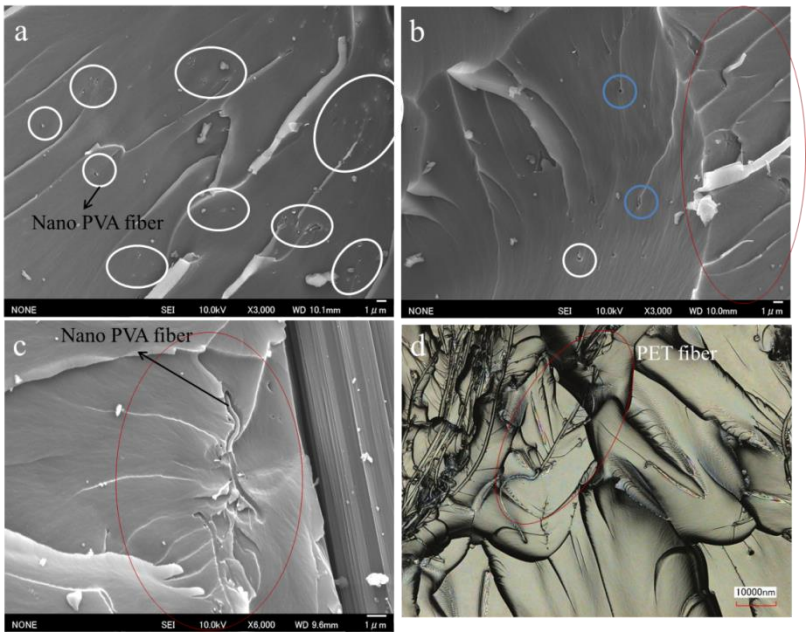

Fig.3-26. SEM images of the delaminated surface of CF/EP/PVA (a,b,c) and CF/EP/PET (d) composites after fatigue test

3.3.8 Optimum of modification volume of nano materials

The viscosity of matrix increases with increasing volume fraction of nano filler and as a result, it probably reduces the quality of impregnation of the reinforcement. Moreover, the increased viscosity causes more difficulty in fabrication process of CFRP and the cost increases accordingly. The aggregation of nano filler becomes obvious when the volume fraction is high. The existence of aggregation of nano filler could cause the stress concentration resulting in adverse effect on mechanical properties of CFRP. Therefore, the optimum volume fraction of nano fillers exists to achieve optimum mechanical properties. Based on our previous study, the addition of 0.05wt% of nano PVA fibers can be considered as optimum weight fraction for CF/VE composite.

And in other study, 0.5wt% of PET fiber is considered as optimum incorporation volume for CF/EP composite [29]. And for CF/EP composite, 0.3wt% is suitable.

Instead of dispersion, the effect of addition volume of nano fibers on the CF/matrix adhesion and subsequently on mechanical properties of CFRP also needs to be considered. From macro fracture mode of CF/EP composites after fatigue (Fig.3-15), fracture of CF/EP/$MFC_{0.8}$ specimens behaved brittlely. Cracks propagate transversely and cause the failure of many warp CF bundles indicating the weak resistance of CF warps to transverse cracks. In order to investigate the resistance capability of warp CF breakage when encountering with transverse cracks (Fig.3-27-b), the single edge notched specimens of UD CF/EP composites (0°) containing various ratio of MFC under 3 points bending load was conducted to investigate the critical energy release rate (G_{IC}). Dimension of specimens are displayed in Fig.3-27-a. The pre-crack was made by a fresh razor blade. It was found that when incorporation volume of MFC was 0.3wt%, G_{IC} value was almost unchanged (Fig.3-27-c). The crack tends to propagate perpendicularly to CF direction (0°) accompanying with a large scale of CF/EP interfacial debonding along 0° [41]. However, G_{IC} value of CF/EP/$MFC_{0.8}$ composite decreased by ～20%. CF/EP interfacial debonding along 0° is hard to occur due to stronger CF/EP adhesion. It indicates that CFs in warp bundle of CF/EP/$MFC_{0.8}$ specimens are easier to break when transverse cracks approaching to warp bundles. When CF/EP adhesion becomes much strong, brittle fracture behavior appears due to lower efficiency of stress reduction caused by interfacial debonding.

Furthermore, a simple model can be considered to describe the fracture mechanism of CF/EP/MFC composites containing different ration of MFC (Fig.3-28). With addition of MFC, a slower growth of matrix cracks including transverse cracks compared to unmodified composite was achieved. After transverse cracks propagating to warp bundle, they stopped and propagated along interface between weft and warp bundles to form meta-delamination when content of MFC was 0.3%, without causing the fracture of CFs in warp bundles due to lower stress concentration. A delay of initiation and growth of meta-delamination was obtained in modified composites. Furthermore, addition of MFC has provided an effect on resistance to propagation of interlaminar delamination due to improved CF/matrix adhesion, and finally contributed to improved

fatigue performance of composite. However, when weight fraction of MFC increased to 0.8wt%, the achieved much stronger CF/matrix caused CFs in warp bundles more easily to break due to insignificant efficiency of reduction of the stress concentration by interfacial debonding, resulting in a negative effect on fatigue properties. It is worth noting that fatigue life of CF/EP composites increases with the increase of interfacial IFSS provided by addition of MFC, but the optimum IFSS exists.

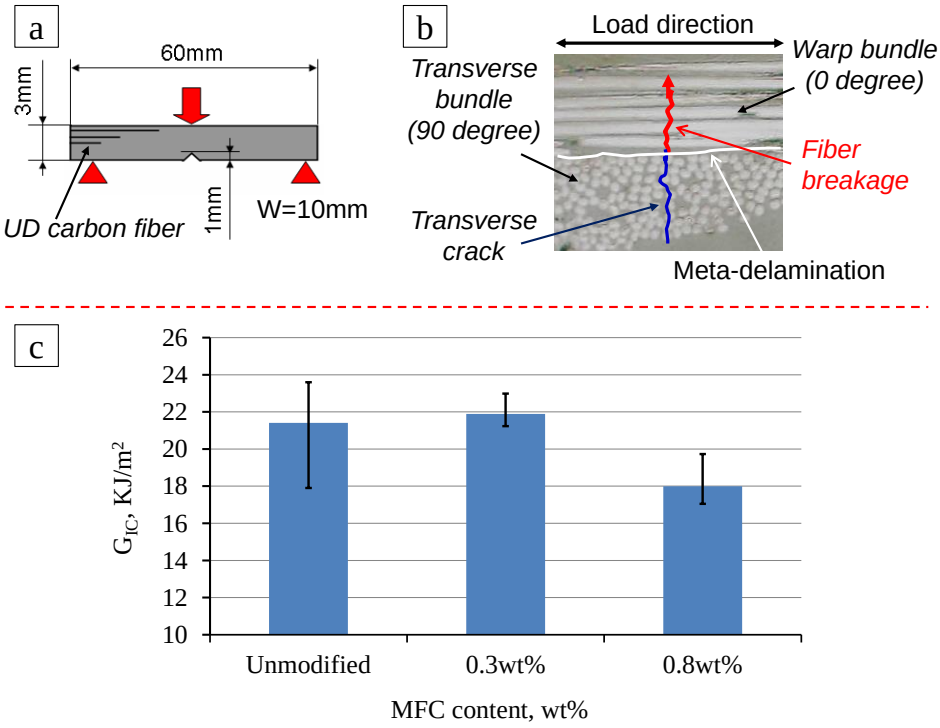

Fig.3-27. G_{IC} value according to the notched 3 points bending test of UD CF/EP composites (0°) with various MFC content

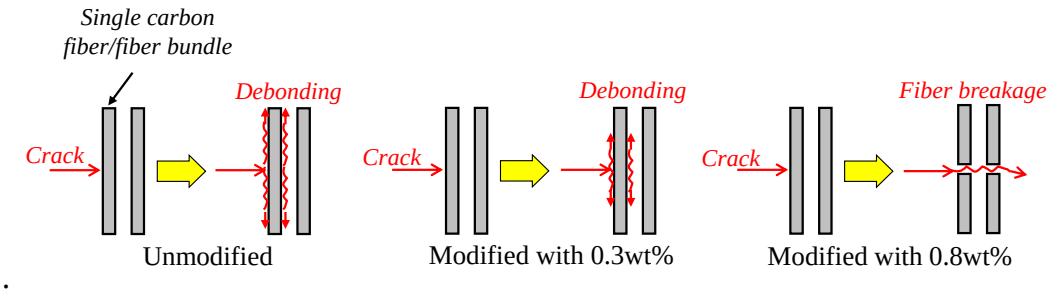

Fig.3-28. A model to describe the effect of IFSS on warp CFs fracture behavior under the effect of MFC

3.4 Conclusions

The effect of modification of nano fiber with different ratio on the mechanical properties of matrix and CFRP composites has been investigated. Incorporation of nano fillers such as nano PVA or MFC can improve the fracture toughness of polymer matrix slightly. The fracture toughness of modified resin increased with increasing the nano filler content. The addition of nano PVA showed almost no influence on CF/VE interfacial properties while MFC displayed obvious effect on improvement of CF/EP adhesion. Although nano filler performed a slight effect on improvement of static tensile properties of CFRP, the fatigue performance can be improved significantly by only incorporating a small amount of nano filler. With addition of MFC or nano PVA, a resistance to initiation and propagation of matrix crack including transverse crack, subsequent meta- and interlaminar- delamination was found according to corresponding mechanical test, and contributed to improvement of fatigue life. The reinforcing mechanism at micro scale was discussed. However, there exists an appropriate incorporation content for nano filler which makes the fatigue life longest. For nano PVA, the aggregation of nano filler becomes obvious when the volume fraction is high. When MFC content increased to 0.8wt%, the CF/matrix adhesion became much stronger, which caused CFs in warp easier to break due to ineffective stress reduction and subsequently reduced the fatigue life of CF/EP composites. It is necessary to adjust the CF/matrix adhesion to obtain a suitable value by a suitable content of nano filler for achieving optimum mechanical of CFRP.

References

1. Mouritz AP, Bannister MK, Falzon PJ, Leong KH. Review of applications for advanced three-dimensional fibre textile composites. Compos Part A: Appl Sci Manuf 1999;30:1445-1461.
2. Manjunatha CM, Taylor AC, Kinloch AJ, Sprenger S. The tensile fatigue behaviour of a silica nanoparticle-modified glass fibre reinforced epoxy composite. Compos Sci Technol 2010;70:193-199.
3. Higashino M, Takemura K, Fujii T. Strength and damage accumulation of carbon fabric composites with a cross-linked NBR modified epoxy under static and cyclic loadings. Compos Struct 1995;32: 357-366.
4. Khan SU, Munir A, Hussain R, Kim JK. Fatigue damage behaviors of carbon

fiber-reinforced epoxy composites containing nanoclay. Compos Sci Technol 2010;70:2077-2085.

5. Grimmer CS, Dharan CKH. High-cycle fatigue of hybrid carbon nanotube/glass fiber/polymer composites. J Mater Sci 2008;43:4487-4492.
6. Phong NT, Gabr MH, Okubo K, Chuong B, Fujii T. Improvement in the mechanical performances of carbon fiber/epoxy composite with addition of nano (Polyvinyl alcohol) fibers. Compos Struct 2013;99: 380-387.
7. Zhou YX, Pervin F, Jeelani S, Mallick PK. Improvement in mechanical properties of carbon fabric–epoxy composite using carbon nanofibers. J Mater Process Technol 2008;198:445-453.
8. Goda K. The role of interfacial debonding in increasing the strength and reliability of unidirectional fibrous composites. Compos Sci Technol 1999;59:1871-1879.
9. Oya N, Hamada H. Mechanical properties and failure mechanisms of carbon fibre reinforced thermoplastic laminates. Compos Part A: Appl Sci Manuf 1997;28:823-832.
10. Takemura K, Fujii T. JSME Int J. A, 43, 2 (2000) 186-195.
11. Zhang W, Srivastava I, Zhu YF, Picu RC, Koratkar N. Small,2009;12:1403-1407.
12. Arguelles A, vina J, Canteli AF, Castrillo MA, Bonhomme J. Compos Sci Technol 2008;68:2325-2331.
13. Haque A, Ramasetty A. Compos Struct 2005;71:68-77.
14. Lu J, Wang T, Drzal LT. Preparation and properties of microfibrillated cellulose polyvinyl alcohol composite materials. Compos Part A: Appl Sci Manuf 2008;39:738-46.
15. Nakagaito AN, Yano H. The effect of fiber content on the mechanical and thermal expansion properties of biocomposites based on microfibrillated cellulose. Cellulose 2008;15:555-9.
16. Okubo K, Fujii T, Yamashita N. Improvement of interfacial adhesion in bamboo polymer composite enhanced with micro-fibrillated cellulose. JSME Int J, Ser A 2005;48:199-204.
17. Gabr MH, Elrahman MA, Okubo K, Fujii T. Compos Struct 2010;92:1999-2006.
18. Takagaki N, Okubo K, Fujii T. Improvement of fatigue strength and impact properties of plain-woven CFRP modified with micro fibrillated cellulose. Adv

Mater Res 2008;47-50:133-6.

19. Siro I, Plackett D. Microfibrillated cellulose and new nanocomposite materials:a review. Cellulose. 2010;17(3): 459-494.
20. Fu Q, Jin Y, Song X, Gao J, Han X, Jiang X, Zhao Q, Yu D. Size-dependent mechanical properties of PVA nanofibers reduced via air plasma treatment. Nanotechnology, 2010;21(9):1-5.
21. Reifsnider KL, Talug A. Int. J. Fatigue. 1980;2(1): 3-11.
22. Gojny FH, Wichmann MHG, Kopke U, Fiedler B, Schulte K. Carbon nanotube reinforced epoxy-composites: enhanced stiffness and fracture toughness at low nanotube content. Compos Sci Technol 2004;64(15):2363-2371.
23. Liu WP, Hoa SV, Pugh M. Fracture toughness and water uptake of high performance epoxy/nanoclay nanocomposites. Compos Sci Technol 2005;65:2364-73.
24. Kim BC, Park SW, Lee DG. Fracture toughness of the nano particle reinforced epoxy composite. Compos Struct 2008;86: 69-77.
25. Tang YH, Ye L, Zhang Z, Friedrich K. Interlaminar fracture toughness and CAI strength of fibre-reinforced composites with nanoparticles-A review. Compos Sci Technol 86 (2013) 26-37.
26. Sun LY, Gibson RF, Gordaninejad F, Suhr J. Energy absorption capability of nanocomposites: A review. Compos Sci Technol 69 (2009) 2392-2409.
27. Liu LQ, Li LY, Gao Y, Tang LC, Zhang Z. Single carbon fiber fracture embedded in an epoxy matrix modified by nanoparticles. Compos Sci Technol 2013;77:101-9.
28. Rausch J, Zhuang RC, Mader E. Application of nanomaterials in sizings for glass fibre/polypropylene hybrid yarn spinning. Adv Perform Mater 2009;24(1):29-35.
29. Kawai E, Okubo K, Fujii T, Improvement of fatigue fatigue property of carbon fiber reinforced plastics enhanced with nano sized synthetic polymer fiber. Kathmandu Symposia on Advanced Materials 2012, pp.88-89.
30. Gabr MH, Elrahman MA, Okubo K, Fujii T. A study on mechanical properties of bacterial cellulose/epoxy reinforced by plain woven carbon fiber modified with liquid rubber. Compos Part A: Appl Sci Manuf 2010;9:1263-1271.
31. Ye YP, Chen HB, Wu JS, Chan CM. Interlaminar properties of carbon fiber composites with halloysite nanotube-toughened epoxy matrix. Compos Sci Technol

71 (2011) 717-723.

32. Yokozeki T, Iwahori Y, Ishiwata S, Enomoto K. Mechanical properties of CFRP laminates manufactured from unidirectional prepregs using CSCNT-dispersed epoxy. Compos Part A- Appl S 2007;38(10):2121-30.
33. Wichmann MHG, Sumfleth J, Gojny FH, Quaresimin M, Fiedler B, Schulte K. Glass-fibre-reinforced composites with enhanced mechanical and electrical properties-benefits and limitations of a nanoparticles modified matrix. Eng Fract Mech 2006;73(16):2346-59.
34. Seyhan AT, Tanoglu M, Schulte K. Mode I and mode II fracture toughness of Eglass non-crimp fabric/carbon nanotube (CNT) modified polymer based composites. Eng Fract Mech 2008;75(18):5151-62.
35. Reifsnider KL, Talug A. Analysis of fatigue damage in composite laminates. Int. J. Fatigue. 1980;2(1): 3-11.
36. Uenoya T, Fujii T. Influence of Matrix Toughness on Damage Initiation and Growth in Carbon Fiber Fabric Composites. J Reinf Plast Compos 2000;19(1) :83-94.
37. Nishikawa Y, Okubo K, Fujii T, Uenoya T. Fatigue Damage Evaluation of Plain-Woven Carbon/Epoxy Composites Using Thermo-Elastic Technique. J Soc Mat Sci 2005; 54(5):494-499 (In Japanese).
38. a. Makiko Toyota. Crack propagation crossing carbon fibers embedded in modified epoxy with nano sized polymer fibers. Master thesis. 2014. Doshisha University. b. Tubasa Kondo, Study on prevention of fatigue crack propagation of plain-woven CFRP due to addition of micro and nano sized glass fibers. Master thesis. 2014. Doshisha University.
39. Arakawa K, Takahashi K.Relationships between fracture parameters and fracture surface roughness of brittle polymers Int J Frac 1995;48:103-14
40. Hull D. Fractography: observing, measuring, and interpreting fracture surface topography. Cambridge: Cambridge University Press; 1999.
41. Tomita Y, Yamaki T, Morioka K. Effect of Fiber Strength on Notch Bending Fracture of Unidirectional Long Carbon Fiber-Reinforced. Materials Characterization. Materials Characterization. 1998;41:123-135.

Chapter IV

Effect of different thermosetting resin on the mechanical performance of carbon fiber reinforced plastic composite vessels

4.1 Introduction

The fiber reinforced composite pressure vessels have attracted more and more attention because of their potential application on aerospace, automobiles, chemical industries and marine due to excellent mechanical properties and low weight [1]. The most effective thermosetting plastic matrix is epoxy because of the relative high strength and good compatibility with carbon fiber (CF). Recently carbon fiber reinforced plastic composites (CFRP) using vinylester (VE) resin as matrix have attracted more attention due to relatively low cost, easy formation processing (such as resin transfer molding) because of relatively lower viscosity, and good corrosion resistance in comparison with epoxy [2-5]. Moreover, it is easy to improve the mechanical properties of VE resin by modifying the properties of monomer to obtain better durability of CF/VE composites, such as, adjusting the toughness of VE or the adhesion between carbon fiber and resin. Consequently, it is possible to reduce the cost significantly by improving the efficiency of fabricating and curing process compared to epoxy based composite vessel.

For the safety and cost reasons, it is essential to understand the damage initiation and propagation mechanism, subsequently the effect on leakage failure and final load-bearing failure of composite pipes or vessel under internal pressure loading. Due to anisotropy of composite structure, the damage inside of composite vessels including defect, matrix cracks, fiber/matrix debonding, delamination and final fiber failure are complicated. Many researches have been carried out to investigate the effect of damage on mechanical properties of vessels or pipes. Tarakcioglu et al. [6] have investigated the effect of surface cracks on strength theoretically and experimentally for glass/epoxy filament wound pipes. Jones et al. [7] found leakage of filament wound pipes governed by occurrence and intersection of transsverse cracks and damage was related to the

stresses and strains acting on the fibers. They proposed leakage behavior could be improved by inhibiting the initiation and propagation of transverse cracks. The dominated failure mechanism of pipe such as delamination or transverse cracking was related to stress ratio between the longitudinal and hoop direction [8]. The microstructural defects such as the voids produced during fabrication process also have an effect on the initiation of damage and failure mechanism [9]. However, there are not so many works about the damage behavior inside the vessel under effect of different matrix resin.

As one of non-destructive evaluation method, digital image correlation (DIC) method has been widely used for measuring the global strain of CFRP specimens [10-12], but there are few works have been focused on strain measurement of composite pressure vessel using DIC method during the mechanical test. The full field strain map at different stress level obtained by this method can supply much important information about the strain development, strain concentration, onset of damage, crack propagation, delamination and so on. Yao et al. [13] have applied digital speckle correlation method to obtain the full field deformation and strain distribution of a composite vessel. They found DIC method was suitable for deformation measurement of composite pressure vessels in real engineering practice base on comparison with results obtained by strain gauges measurement. Duane et al. used 3D DIC method to successfully provided accurate measurements of strain of a composite overwrapped pressure vessel, from which principal strain growth and strain concentration has been discussed [14].

In this study, the carbon fiber reinforced vinylester and epoxy composite pressure vessels with simple structure (90/15°) have been prepared. The DIC method has been used for the measurement of the strain distribution during burst pressure test. The initiation of crack and crack accumulation inside each kind of composite vessels under effect of different matrix resin has been discussed by the strain distribution maps, further observation by CT-scan and optical microscopy.

4.2 Experimental

4.2.1 Materials

Carbon fiber tow (Mitsubishi Rayon TR50S 12K) with the tensile strength of 4.9 GPa and Young’s modulus of 240 GPa was used as reinforcement. Modified vinyl ester resin

(AF, described at Chapter 2) and epoxy (Epiclon 850) supplied by DH Materials Inc. were used as matrix. 328E (Kayaku akzo corporation) and 8%CoOCt was used as curing agent and promoter for VE resin respectively. Acid anhydride as curing agent and the catalyzer also supplied by DH materials Inc. were used for epoxy.

4.2.2 Preparation of composite specimens

The CF/VE or CF/EP composite vessels (2.5L) consisted of an aluminum liner (~1.43 in thickness), longitudinal and hoop CF/VE or CF/EP layers which filament wound by Maruhati company (Japan). The wind angle of longitudinal layer was 15 degree with a thickness of ~1 mm and the thickness of hoop layer was ~1.5mm, as shown in Table.4-1. After filament wound, the CF/VE vessels were cured at 80℃ for 1h and post cured at 120℃ for 2h, while CF/EP vessels were cured at 80℃ for 1.5h and post cured at 130℃ for 1.5h. The carbon fiber volume of CF/VE and CF/EP vessels were about 53% and 60% respectively. The unidirectional (UD) CF/VE and CF/EP composites was filament wound at room temperature using the same VE or EP resins and then cured at same condition with former pressure vessels.

Table.4-1. Winding structure and layer thickness of vessels.

No. of vessel	Winding structure	Internal diameter, mm	Thickness, mm
CF/EP	$90^0/15^0$	99.36	1.53/0.94
CF/VE	$90^0/15^0$	99.36	1.52/1.09

4.2.3 Burst pressure test of vessels

First spraying the white paint to the surface of vessels, the spraying the black paint on the white painted area with a width of 30mm and an almost same length with vessels cylinder to form a speckle pattern before test [15-16]. During test, a cold light source was used to illuminate the speckle pattern region, while a CCD camera recorded the speckle image and stored by a computer as shown in Fig.4-1. After test, the digital images were analyzed by Vic-2D to obtain the global deformation information of vessels under different internal pressure. The vessels were fixed tightly by a strap to prevent movement during loading and a water pump was used to create pressure during

test. Two vessels of each type of matrix were conducted to test burst pressure. In addition, strain gauges were also used to measure the strain at head, center and back area at cylinder of vessel to obtain strain information for a comparison with results obtained by DIC method later.

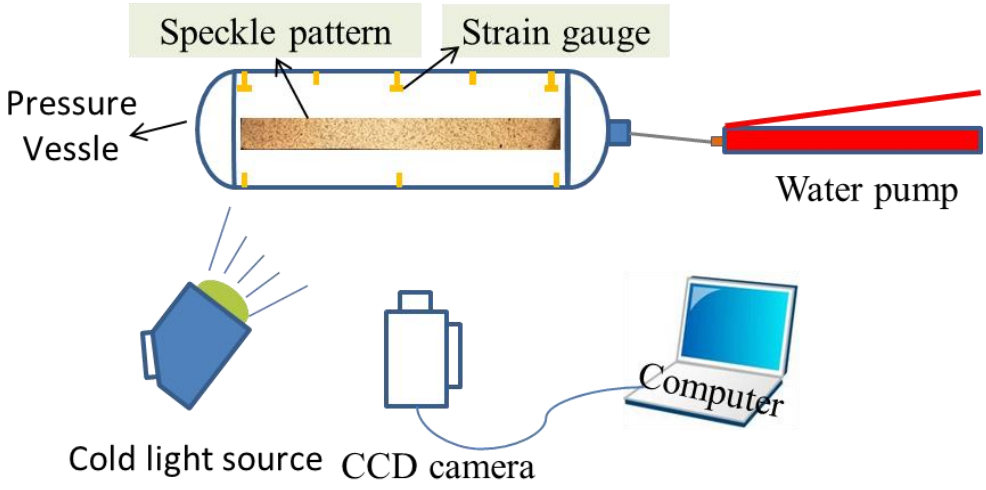

Fig.4-1. Burst pressure test of vessels.

4.2.4 Mechanical test of UD CF/VE and EP composites

The tensile properties of UD CFRP fabricated by using VE and EP as matrix were investigated by using a Shimadzu autograph universal testing machine according to ASTM D3039-08. The testing speed was set to 2 mm/min. The specimen dimension was 200 x 15 x 1 mm with a gage length of 100mm. The taps were made by Aluminum with 50 x 25 x 1 mm in dimension. At least 5 specimens were conducted to test.

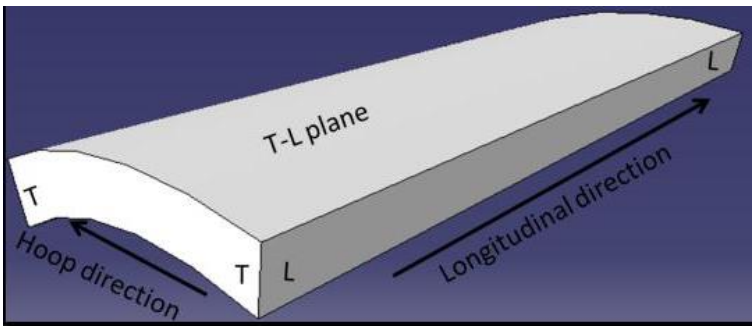

Fig.4-2. The cutting planes for observing damage of vessels by CT-scan or microscopy.

4.2.5 Damage observation

After failure, the longitudinal section (L-L) and cross-section (T-T) of the failure area, close to failure area and away from failure area at cylinder of vessel, were characterized by CT-scan (Skyscan1172Micro-CT), laser microscopy (VK-X200K) and scanning electron microscopy (SEM) observations (JSM-7001FD). During CT-scan observation, T-L plane observation also was conducted (Fig.4-2).

4.3 Results and discussion

4.3.1 Tensile properties of UD CF/VE and CF/EP composite

In order to obtained the modulus and strain at failure, DIC method was conducted during tensile test. The white and black paint was sprayed successively on the surface of tensile specimens to form a speckle pattern before test (Fig.4-3). A high resolution camera was used to record the speckle image deformation information every second during tensile loading and the obtained photos were stored by a computer. After test, the digital images were analyzed by Vic-2D to obtain the global deformation information of tensile specimens. As shown in Fig.4-3-right, the full field strain distribution can be obtained at different stress level. The palette represents the different strain. The inhomogeneity of strain distributions can reflect the different stress distribution in the composite at different loading level. The stress concentration areas at full field of specimens can be reflected based on this strain distribution map. It is possible to predict the potential failure area before final failure especially for textile specimens. The inhomogeneity is not so obvious in UD CFRP during tensile loading, but still shows the stress concentration areas. The stress concentration areas can be considered as the potential failure areas. The stress-strain curve can be plotted based on above strain information. The modulus was obtained according to stress-strain curve. The tensile properties of CF/EP and CF/VE UD composites are shown in Fig.4-4. It was found that CF/VE UD composites performed a comparable tensile strength and young’s modulus obtained by DIC method with CF/EP UD composite revealing the unobvious effect of different matrix on tensile properties of UD CDRP.

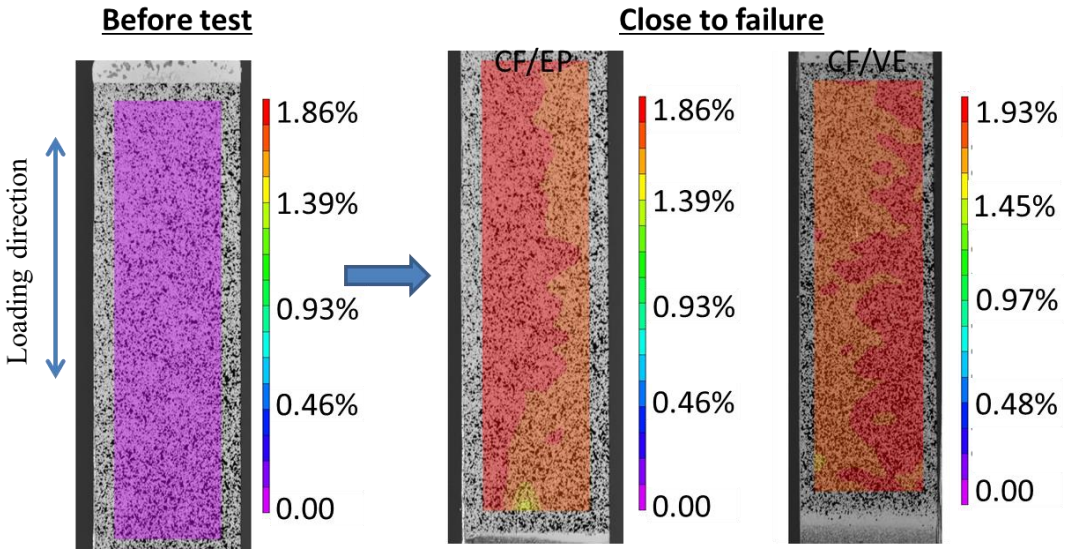

Fig.4-3. Speckle pattern on the tensile specimen before test and strain distribution map of specimen close to failure

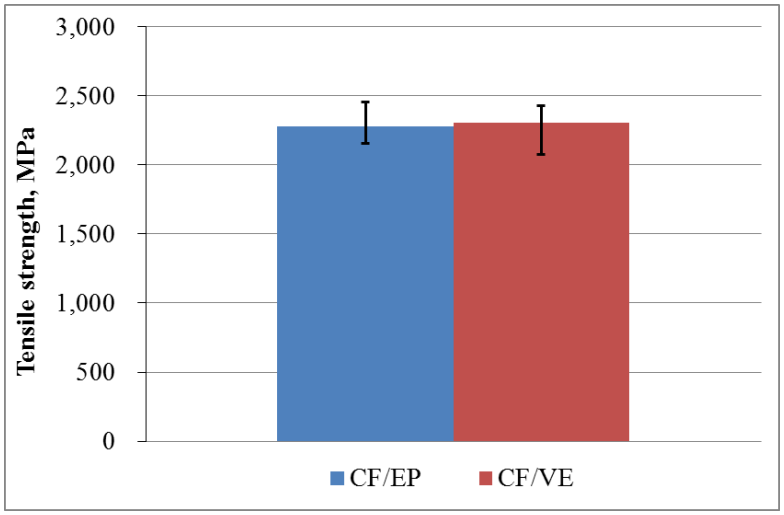

Fig.4-4. Tensile properties of unidirectional CF/VE and CF/EP composites.

4.3.2 Burst pressure of composite vessels

The burst pressure of CF/EP and CF/VE composite vessels are shown in Table.4-2. Two vessels of each type of composite vessels were conducted. The burst pressure of CF/EP vessel shows some distributed values (70 and 76 MPa), while burst pressure of CF/VE vessel shows almost constant value of about 76 MPa. Namely the burst pressure of type CF/VE vessel is even a little higher by ~5% than that of CF/EP vessel. The macroscopic failure modes of two types of composite vessel are shown in Fig.4-5, all

the vessels failed at the cylinder that was center or close to doom but not fixed. The CF failed at hoop layer firstly, following failure of longitudinal layer and liner occurred. The scatter of burst pressure and failure location might be caused by the non-uniform of thickness, fiber volume or existence of flaws in of CFs and defects inside composites layers due to materials properties and preparing conditions. The fracture features of CF/EP and CF/VE vessel are similar that carbon fibers break suddenly. It is a brittle failure mode where clusters of CFs fail adjacent to each other and approximately in same transverse plane can be observed. However, some CFs for hoop layer remained on the interlaminar interface between hoop and longitudinal layer of CF/VE vessel is found while the surface in CF/EP vessel is clean. It indicates the interfacial adhesion between hoop and longitudinal layer in CF/VE vessel performs strongly than CF/EP vessel, but further confirmation is necessary. Furthermore, the fracture surface was observed by SEM, as shown in Fig.4-6, hackle pattern indicating large scale plastic deformation of matrix were found in both CF/EP and CF/VE vessel.

Table.4-2. The burst pressure of CF/EP and CF/VE composite vessels.

Type of vessel	CF/EP		CF/VE	
	No.1	No.2	No.1	No.2
Burst pressure, MPa	76	70	76	77

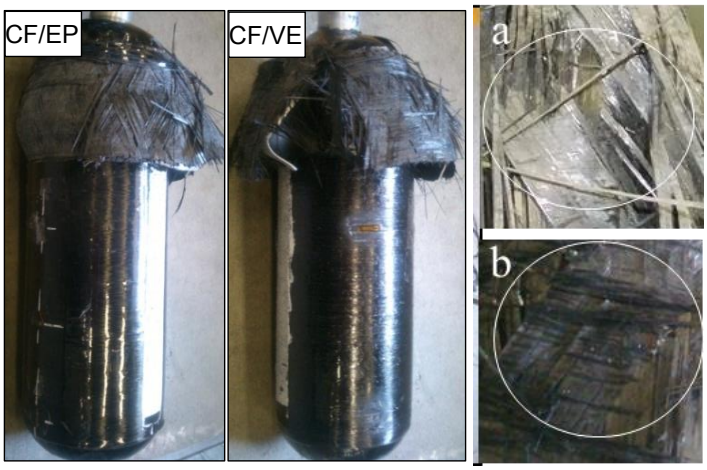

Fig.4-5. CF/EP and CF/VE composite vessels after failure. a: CF/EP; b: CF/VE.

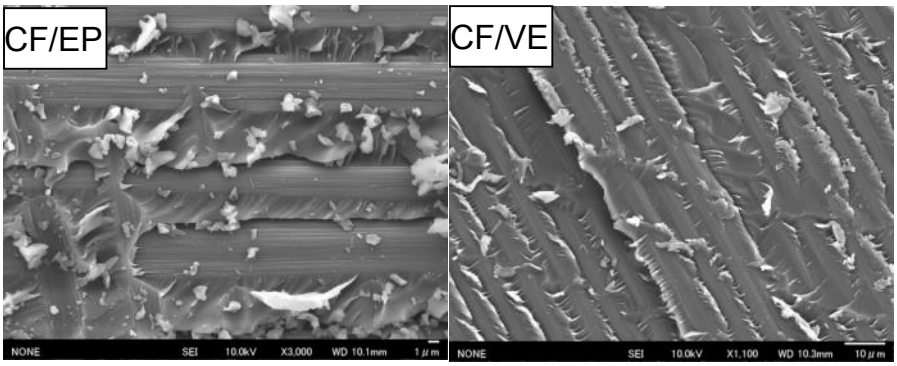

Fig.4-6. SEM images of fracture surface of CF/EP and CF/VE composite vessels.

4.3.3 Damage investigation in different composite vessels by DIC analysis

4.3.3.1 Damage initiation in different composite vessels

DIC method was used during the burst test of vessels, the strain distribution maps at damage initiation stage along longitudinal direction and hoop direction are shown in Fig.4-7 and 4-8. The strain distributions are inhomogeneous that some strain concentration areas exist (green areas in Fig.4-7 and 4-8). The strain concentration suggests the initiation of damage at the surface or inside the wall of pressure vessel under internal pressure loading. The damage in the composite layers was investigated by CT-scan (Fig.4-10), optical microscopy (Fig.4-11) and SEM (Fig.4-12) though the observation at non-failure areas after failure. The first damage mechanism mainly is matrix cracks initiated from fiber debonding due to weak CF/matrix interface or voids produced during fabrication process [9]. Then with the increase of internal pressure loading, the matrix cracks propagate or link together, subsequently form transverse cracks in the hoop layer or longitudinal layer (Fig.4-10 and 12). It is found that long transverse cracks in CF/EP vessel initiate early at a low average strain state when the internal pressure is only ~20MPa. On the other hand, CF/VE vessel initiates early damage at a higher average strain state when the internal pressure is ~35MPa. Moreover, at damage initiation stage, the morphology of strain concentration areas in CF/VE vessel is different to CF/EP vessel according to strain distribution map. Based on microscopy observation and CT-scan observation, CF/VE performs different damage morphology which is short cracks as well as tiny pore shape damage instead of long transverse cracks (Fig.4-10, 11 and 12). The higher toughness of VE resin can be considered to contribute to higher damage initiation pressure of CF/VE vessel than

CF/EP vessel due to provision of more resistance to crack initiation and propagation. The fracture toughness of bulk VE (AF) resin was ～1.027 MPa·$m^{1/2}$ while that of bulk EP was about 0.639 MPa·$m^{1/2}$ according to the previous studies. The higher damage initiation pressure of CF/VE vessel indicates a higher stress tolerance and more reliable.

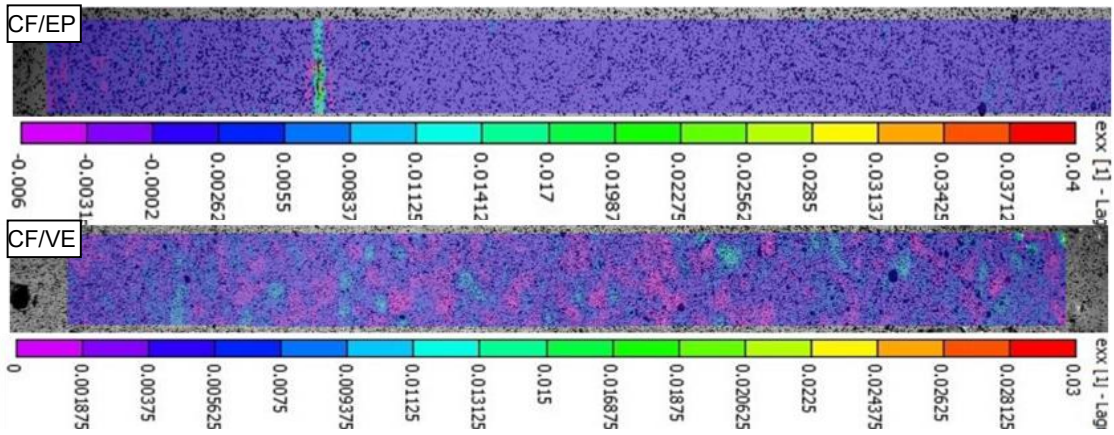

Fig.4-7. Initiation of cracks (xx direction) inside the composite vessels according to strain distribution map during burst pressure test.

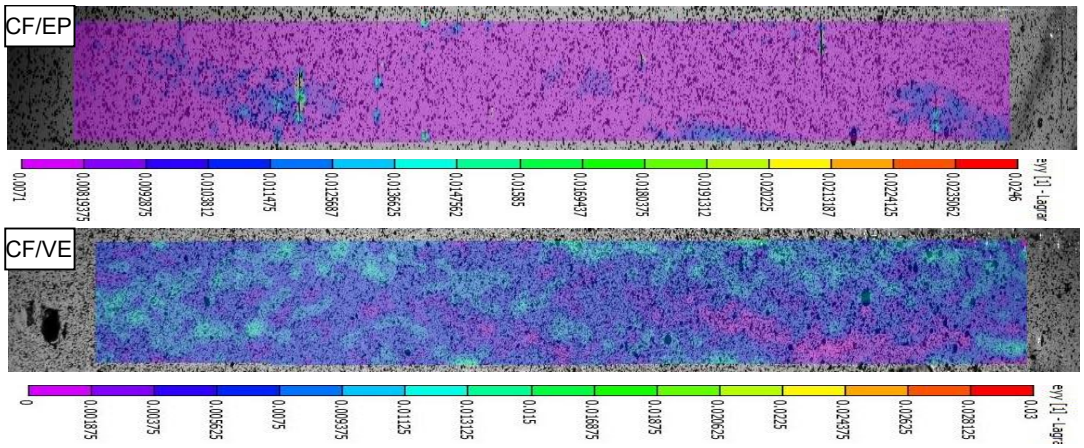

Fig.4-8. Initiation of cracks (yy direction) inside the composite vessels according to strain distribution map during burst pressure test.

At yy direction (hoop, Fig.4-8), the strain concentration area appears parallel to the winding direction of longitudinal layer (15°). The deformation of out-skin can be influenced by transverse cracks occurred in the longitudinal layer as confirmed by CT-scan (Fig.4-10.a-3 and b-3, region B). CF/EP and CF/VE initiate the damage in the longitudinal layer at almost the same internal pressure of about 35 MPa. The

morphology of the strain concentration area at yy direction also shows differently in different composite vessels. It is confirmed by internal damage observation that short transverse cracks are found in CF/EP vessel while the tiny pore shape damages are observed in CF/VE vessel. For the composite structural products such as pipers and pressure vessels without liner, the fluid leakage could occur through a path of transverse or delamination cracks when internal pressure comes to leakage pressure [18]. The delayed initiation and propagation of damage of CF/VE vessels can provide a positive effect on preventing the fluid leakage during their application.

4.3.3.2 Damage accumulation in different composite vessels

The strain distribution maps at the final stage just before final failure of each type of vessel are shown in Fig.4-9. With increasing the internal pressure, the density of strain concentration areas increase indicating that more damage are accumulated in the vessels. At xx direction (longitudinal), the strain concentration areas in CF/EP vessel are inhomogeneous. Dense strain concentration areas in the form of the long transverse cracks are observed which is confirmed by CT-scan image (Fig.4-10.a-1) and optical microscopy images based on longitudinal section (L-L) observation (Fig.4-11.a). The space between neighboring transverse cracks become smaller and the length of crack become longer as the strain of vessel increases. The transverse cracks occur firstly at the surface layer due to highest stress at surface, then propagate from surface to internal layer and coalesce with voids or other matrix cracks or delamination (Fig.4-12-a,b). At the same time, transverse cracks also occur in longitudinal layer (region B in Fig.4-10.a-3) especially at misaligned area of CFs such as cross-points of CF yarns due to stress concentration under internal pressure loading as shown in Fig.4-12-c. With increasing internal pressure, the cracks tend to link together to form through-out thickness cracks which might be the main path of leakage [19]. In addition, some cracks occur and propagate to form delamination along longitudinal direction at hoop layer particularly at resin rich area between two yarns of carbon fiber (Fig.4-11) [9]. CF/VE vessel performs more homogeneous strain distribution except a small amount of serious pore shape strain concentration areas which might be potential failure area. Less and shorter transverse cracks in both hoop and longitudinal layers than CF/EP vessels are observed as well, which is confirmed by following slide observation by CT-scan Fig.4-10-b and Fig.4-11-b.

At yy direction (hoop), the increase of number of strain concentration areas indicates the growth of transverse cracks especially at cross-points of two yarns in longitudinal layer. The strain distribution map of CF/VE vessel is more homogeneous except the existence of several red spots. As show in Fig.4-10.a-1,3 and b-1,3 (region B), dominated serious damage in longitudinal layer of CF/VE vessel is porosity accompanying with some short cracks formed by coalescence of voids or propagation of the transverse cracks. A large number of voids produce during fabrication process due to high viscosity of VE resin. On the other hand, the larger and longer cracks along longitudinal direction of longitudinal layer happen inside CF/EP vessel which might due to lower toughness of EP than VE.

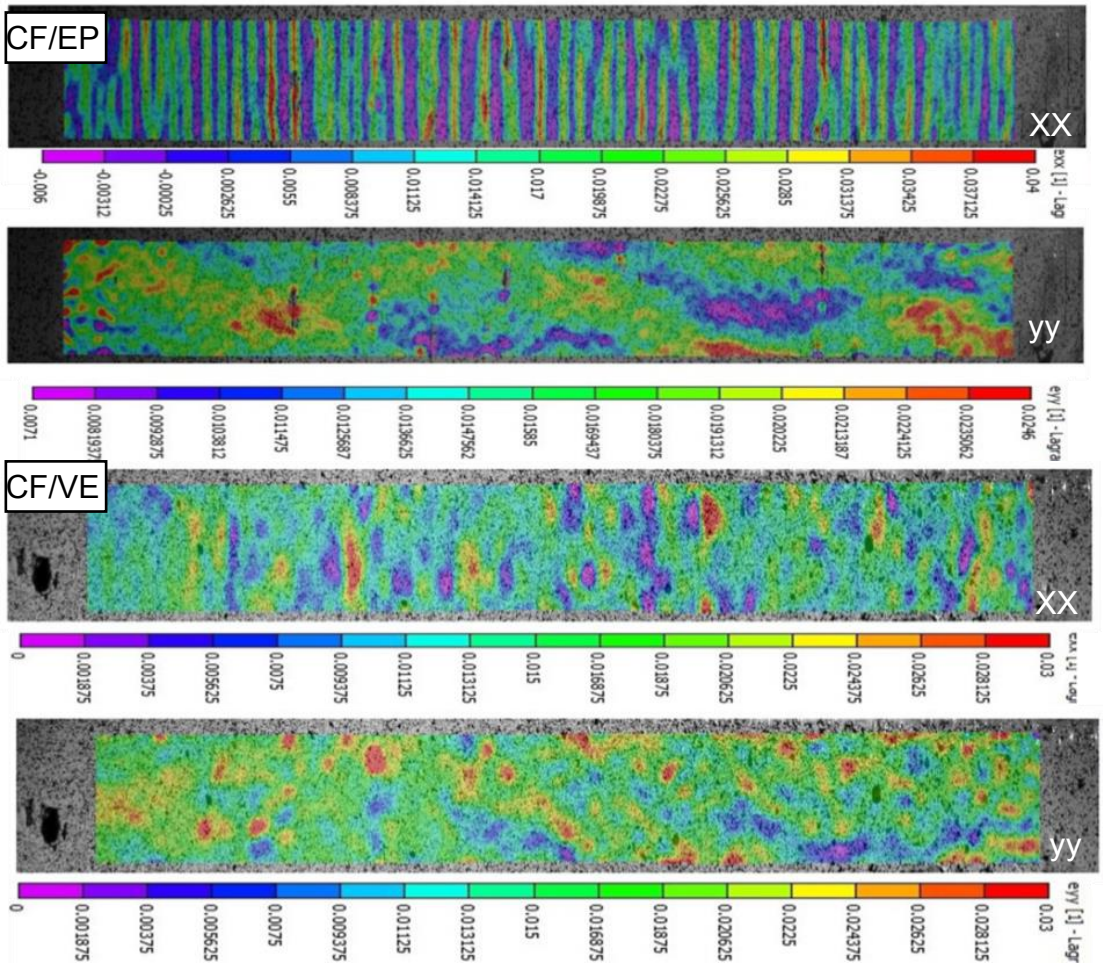

Fig.4-9. The strain distribution map of composite vessels at final stage just before bursting

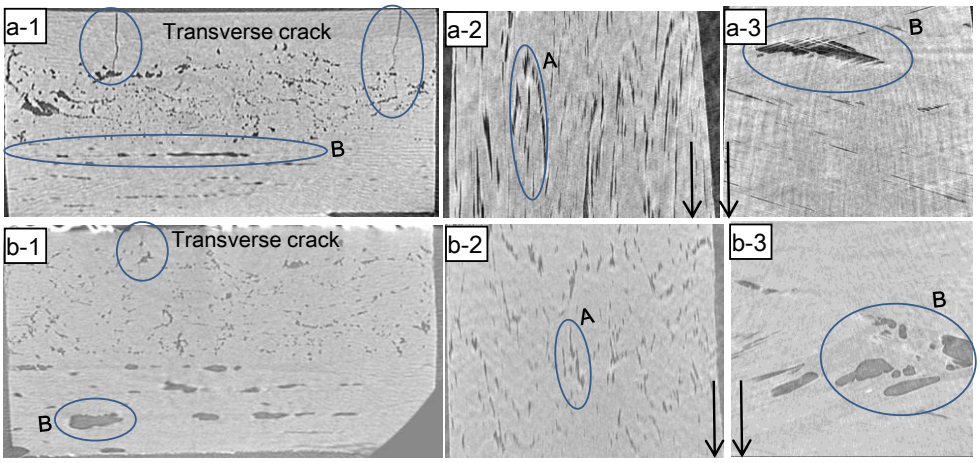

Fig.4-10. CT-scan images of center area of CF/EP (a) and CF/VE vessel (b) after failure (1: longitudinal section fragment; 2: T-L plane of hoop layer; 3: T-L plane of longitudinal layer). Arrow represents hoop direction.

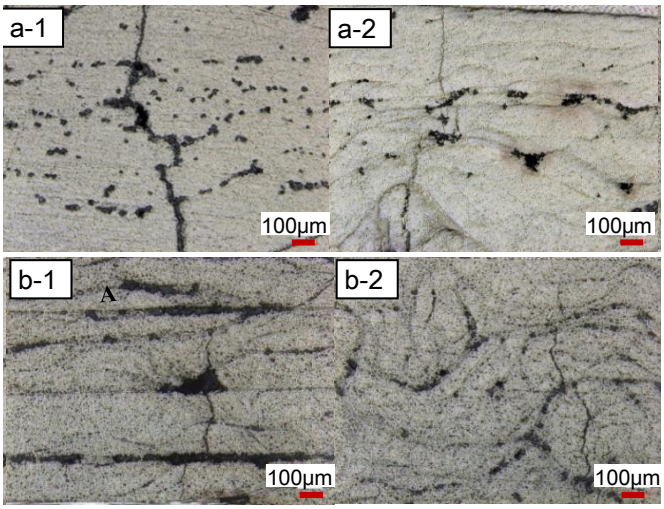

Fig.4-11. Optical microscopy images of longitudinal section L-L (hoop layer) of CF/EP (a) and CF/VE vessels (b) after failure (1: close to failure area; 2: away from failure area).

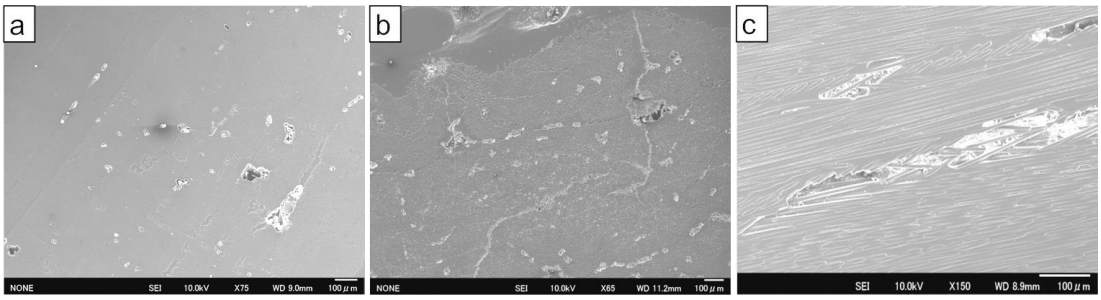

Fig.4-12. SEM image of the cross-section of CF/VE (a) and CF/EP (b, c) vessel.

4.3.4 S-S curves of different composite vessels

It has been noted that the strain gauge can only reflect the point information of deformation, while more comprehensive information can be obtained by DIC method. Herein, three regions were divided to characterize the stress and strain relations of each type of vessels via DIC method and strain gauges, which were front (F), center (C) and back (B) as well as failure, close to failure, away from failure area, as shown in Fig.4-13-A. The solid line of Fig.4-13 and 14 shows the stress-strain (s-s) curves of all the vessels obtained by DIC method and the dotted line shows the s-s curves obtained by strain gauges. The blue solid line of Fig.4-13-B reflects the stress-strain relation of the failure area of CF/EP vessel at yy direction. All the curves are almost linear indicating that almost no degradation of stiffness happens until final failure of vessels. It is found that the failure area (F) shows a faster increase of strain than non-failure area (C and B) and performs a higher strain at failure. A little more damages and longer cracks at regions closed to failure area are found in Fig.4-12. The modulus of the failure area is lower than non-failure area indicating the vessel finally broken at weaker area. But CF/VE vessel didn't burst at weakest area (F) which might due to faster crack propagation at failure area initiated from larger voids or coalescence of voids. From Fig.4-12-b, cracks initiated at voids could be found as discussed by Bai et al. [9]. According to s-s curves obtained by strain gauges, strain of failure area of all the vessels grew faster and burst at weak area.

The non-failure area exhibit a same modulus in CF/VE and CF/EP vessel based on both DIC and strain gauge result (Fig.4-14). However, at failure area, the modulus is different according to results obtained by both of DIC and strain gauge. They show the same trend that CF/VE performs a high modulus than CF/EP, which contributes a higher burst pressure of CF/VE vessel. The strain at failure of failure area of CF/EP vessel is 1.73% according to DIC result, and CF/VE vessel has a comparable strain at failure with a value of 1.62%. Stiffness of hoop layer obtained by DIC method is a litter lower than that from strain gauges due to influence of deformation of longitudinal layer. In general, the results of deformation obtained by DIC and strain gauges are almost same [13]. It is very convenient to investigate the deformation and damage initiation or

propagation of vessel by DIC method.

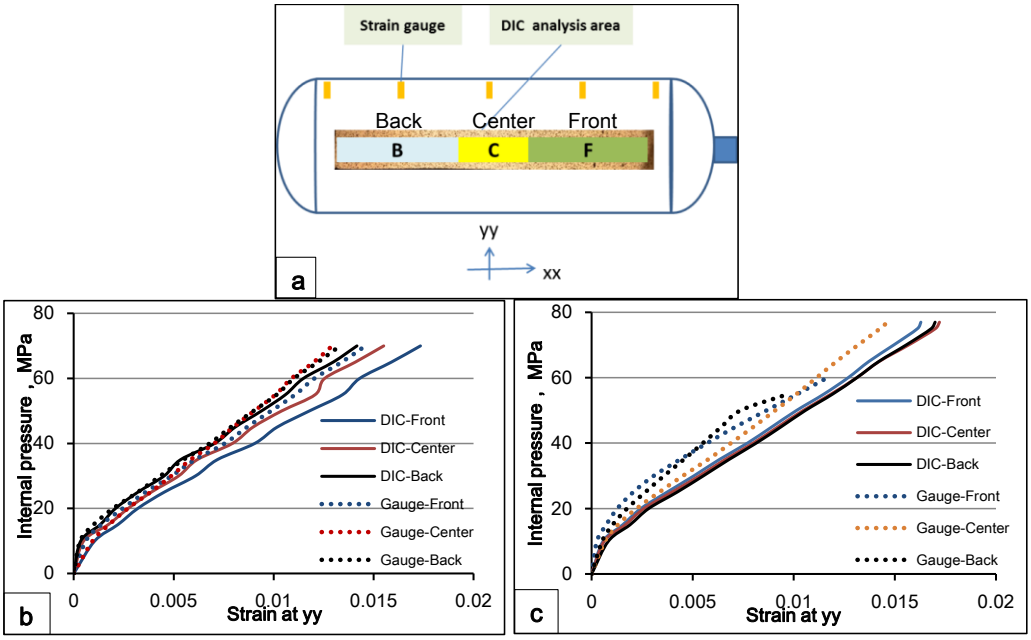

Fig.4-13. Stress-strain curves of vessels obtained by DIC method and strain gauges (a. measurement position of strain gauge and DIC method; b. CF/EP vessel; c.CF/VE vessel).

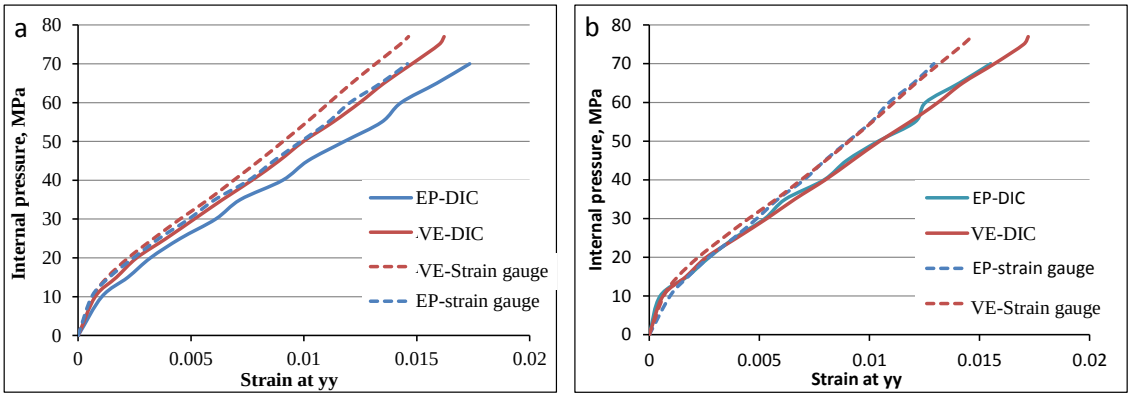

Fig.4-14. Stress-strain curves of different vessels at failure area (a) and away from failure area (b).

4.4 Conclusions

It was found that CF/VE UD composites performed a comparable tensile strength and young's modulus obtained by DIC method with CF/EP UD composite. Then, the carbon fiber reinforced vinylester and epoxy composite pressure vessels with a simple structure (90/15°) have been prepared and conducted by burst pressure test with speckle pattern

on cylinder region of vessel. The CF/VE composite vessel has performed a little higher burst pressure by ~5% than CF/EP vessel. According to the DIC method, the delayed initiation and propagation of cracks in CF/VE vessels was found which can provide a positive effect on preventing the fluid leakage during their application. CF/VE vessel performed more homogeneous strain distribution in the form of less and shorter transverse cracks than CF/EP vessels were observed at hoop layer. In addition, dominated damage in longitudinal layer of CF/VE vessel was relatively huge porosity accompanying with some short cracks while larger and longer crack along longitudinal direction of longitudinal layer happened inside CF/EP vessel which might due to lower toughness of EP than VE. The results of deformation obtained by DIC and strain gauges were almost same indicated that DIC method is a useful and convenient non-destructive evaluation method to investigate the damage initiation and propagation of composite vessel.

References

1. Frank C. Shen. A filament-wound structure technology overview. Materials Chemistry and Physics 42 (1995) 96-100.
2. Daniels WE. Vinyl Ester Polymers. In Encyclopedia of Polymer Science and Engineering, 2nd ed.; Mark, H. F., Ed. Wiley: New York, 1985;17: 393.
3. Kootsookos A, Burchill PJ. The effect of the degree of cure on the corrosion resistance of vinyl ester/glass fibre composites. Compos Part A: Appl Sci Manuf. 2004;35(4):501-508.
4. Zhu J, Imam A, Crane R, Lozano K, Khabashesku V, Barrera E. Processing a glass fiber reinforced vinyl ester composite with nanotube enhancement of interlaminar shear strength. Compos. Sci. Technol. 2007;67(7-8):1509-1517.
5. Buarque EN, Almeida JRM. The effect of cylindrical defects on the tensile strength of glass fiber/vinyl-ester matrix reinforced composite pipes, Compos. Struct. 2007;79(2):270-279.
6. Tarakcioglu N, Akdemir A, Avci A. Strength of filament wound GRP pipes with surface crack. Compos Part B.2001; 32 (2): 131-138.
7. Jones MLC, Hull D. Microscopy of failure mechanisms in filament-wound pipe. J

Mater Sci.1979; 14(1):165-174.

8. Martens M, Ellyin F. Biaxial monotonic behaviour of a multidirectional glass fiber epoxy pipe. Compos Part A: Appl Sci Manuf. 2000;31(9):1001-14.
9. Bai J, Seeleuthner P, Bompard P. Mechanical behaviour of ±55° filament-wound glass-fibre/epoxy-resin tubes: I. Microstructural analyses, mechanical behaviour and damage mechanisms of composite tubes under pure tensile loading, pure internal pressure, and combined loading. Compos Sci Technol. 1997;57(2):141-153.
10. Behrad Koohbor, Silas Mallon, Addis Kidane, Michael A. Sutton. A DIC-based study of in-plane mechanical response and fracture of orthotropic carbon fiber reinforced composite. Composites: Part B 66 (2014) 388-399.
11. Tomasz Brynk, Rafal M. Molak, Miroslawa Janiszewska, Zbigniew Pakiela. Digital Image Correlation measurements as a tool of composites deformation description. Computational Materials Science 64 (2012) 157-161
12. Andrew Makeev. Interlaminar shear fatigue behavior of glass/epoxy and carbon/epoxy composites. Composites Science and Technology, 2013;80(17):93-100
13. Yao XF, Meng LB, Jin JC, Yeh HY. Full-field deformation measurement of fiber composite pressure vessel using digital speckle correlation method. Polymer Testing 2005; 24(2):245-251.
14. Duane M. 3D Digital Image Correlation of a Composite Overwrapped Pressure Vessel During Hydrostatic Pressure Tests. 2007 SEM Annual Conference & Exposition on Experimental and Applied Mechanics. pp.487
15. Nicoletto, G, Anzelotti G, Riva E. Mesoscopic strain fields in woven composites: Experiments vs. finite element modeling. Optics and Lasers in Engineering. 2009;47(3-4):352-359.
16. Vieille B, Taleb L. About the influence of temperature and matrix ductility on the behavior of carbon woven-ply PPS or epoxy laminates: Notched and unnotched laminates. Compos. Sci. Technol. 2011;71(7): 998-1007
17. Fuwa M, Bunsell AR, Harris B. Tensile failure mechanisms in carbon fibre reinforced plastics. J Mater Sci.1975;10(12):2062-2070
18. Sjogren BA, Berglund LA. The effects of matrix and interface on damage in GRP cross-ply laminates. Compos. Sci. Technol. 2000;60(1): 9-21.

19. Karayaka, M., Srinivasan, S., Miyase, A, Wang, S. Leakage damage and failure of glass-fibre reinforced composite tubular vessels under combined internal pressure and axial loading. Proceedings of the 10th International Conference on Composite Materials (ICCM), Whistler, Be, Canada, August 1995;1:747-754.

Chapter 5

Final Remarks

In this thesis, the investigation of the effects of the matrix properties on the mechanical properties of carbon fiber reinforced plastic composites (CFRPs) has been conducted.

Some major conclusions obtained from this work are presented as follows:

1. The influence of matrix properties including the fracture toughness and carbon fiber (CF)/vinylester (VE) adhesion on the static tensile or flexural, interlaminar and fatigue properties of CF/VE composites was investigated. An appropriate chemical modification of VE resin was conducted to alter the matrix properties. An improvement by up to 37.3% of tensile strength and up to 37.1% of flexural strength of CF/VE composites was achieved. CF/VE composites performed different failure mode and strain at failure due to the effect of matrix properties under the static tensile or flexural loading. On the contrary, the interlaminar fracture toughness as well as impact resistance capability of CF/VE composites decreased compared to CF/A composite. It was found that the different fracture mode dominated the energy absorption during fracture of specimens. Tension-tension fatigue life of CF/modified VE composites was improved by several ten times compared to control resin composite. Based on TSA method and further SEM observation, the fracture toughness of resin affected the initiation and growth of matrix cracks especially transverse cracks dominantly because cracks tended to initiate at matrix and propagate along matrix due to high IFSS. At middle stage of fatigue test, delamination tended to initiate early in composites made by matrix resin with lower fracture toughness due to earlier initiation of transverse crack. High CF/VE adhesive strength performed a positive effect on the resistance to delamination growth to extend fatigue life of composites finally. A simple model has been used to characterize the relationship between matrix properties and fatigue life of CF/VE composites to show how to design matrix. The positive hybrid effect of matrix toughness and CF/VE adhesion on the static tensile strength and fatigue life of CF/VE composites was found.

2. The effect of modification of nano fiber with different size or mechanical properties on the mechanical properties of matrix and CFRP composites was investigated. The

fracture toughness of modified resin can be improved by addition of environment-friendly nano fillers such as nano PVA or MFC, and increased with increasing their content. The addition of nano PVA showed almost no influence on CF/VE interfacial properties while MFC displayed obvious effect on improvement of CF/EP adhesion. Although nano filler performed just a slight effect on improvement of static tensile properties of CFRP, the fatigue performance can be improved significantly by only incorporating a small amount of nano filler. With addition of MFC or nano PVA, a resistance to initiation and propagation of matrix crack including transverse crack, subsequent meta- and interlaminar- delamination was found according to corresponding mechanical test, and contributed to improvement of fatigue life. The reinforcing mechanism at micro scale was discussed as well. However, there existed an appropriate incorporation content for nano filler which made the fatigue life longest. For nano PVA, the aggregation of nano filler became obvious when the volume fraction was high. When MFC content increased to 0.8 wt%, the CF/matrix adhesion became much stronger, which caused CFs in warp easier to break due to ineffective stress reduction and subsequently reduced the fatigue life of CF/EP composites. It is necessary to adjust the CF/matrix adhesion to obtain a suitable value by a suitable content of nano filler for achieving optimum mechanical of CFRP.

3. The effect of different matrix on mechanical properties of carbon fiber reinforced composite pressure vessels was investigated. The CF/VE composite vessel has performed a little higher burst pressure by ~5% than CF/EP vessel. According to the DIC method, the delayed initiation and propagation of cracks in CF/VE vessels was found. CF/VE vessel performed more homogeneous strain distribution in the form of less and shorter transverse cracks than CF/EP were observed at hoop or longitudinal layer which might due to lower toughness of EP than VE. The results of deformation obtained by DIC and strain gauges were almost same indicating that DIC method is a useful and convenient non-destructive evaluation method to investigate the damage initiation and propagation of composite vessel.

ACKNOWLEDGMENT

First of all, I would like to express my deepest gratitude to my supervisor, Professor Toru Fujii for giving me the opportunity to study at AMSEL and take on a very interesting subject. He has taught me many basic mechanical engineering knowledge and always guided me in the right research direction. He also has given me very inspirational advice and careful revision on my papers and thesis. He has given me several chances to attend several seminars, exhibitions and international conferences to enrich my knowledge and experiences. Moreover, he helped me to get rid of many troubles so that I could focus on my research. I am deeply grateful of his help in the completion of this thesis. I also would like to give my sincere gratitude to Professor Kazuya Okubo, for his instructive advice for my papers and his significant support for my study and experiments. He made me feel warm and free that I carried on my study and research smoothly. He also supported me to join several conferences and seminars, and always encouraged me.

I am very grateful to Prof. Matsuoka, Prof. Hirayama, Prof. Tanaka and Prof. Miyamoto, for their encouragement and kindly supporting for experiments or tests and encouragement. Also thanks to the DHM for their support of experimental materials.

I would like to express grateful to Dr. Mohamed H. Gabr, Dr. N.T.Phong, Mr. Gibeop Nam, Andrea Betti (exchange student), Max, Bas, Onno and Rob (internship student), Kondo, Maehada, Kimura, Umeki, Kosai, Moriuchi, Nagata, Akeshiro, Nishikiori, NQ Wu and other undergraduate students in AMSEL for great collaborations and kind supports during the period of my doctor course. Thanks to Hieda and Okumura (undergraduate student) for the assistant of my experiments. Thanks to Mr. Matusima and Mr. Aoki from machine shop for the help of making necessary parts for my testing, Ms. Morita and Ms. Toda from SEM room for the help of SEM observation. Thanks to my friends, K. Zeng, Lili, and L. Ma for revising and polishing my papers.

Special thanks to my wife (N. Shan) and my parents for their continuous support and encouragement without a word of complaint.

November 21, 2014

Mechanical Engineering Doshisha University

YONGZHENG SHAO